Department of Mathematics and Statistics

Optimal guidance and control in space technology

Jingyang Zhou

This thesis is presented for the Degree of
Doctor of Philosophy
of
Curtin University

February 2011

Declaration

I affirm that the material in this thesis is the result of my own original research and has not been submitted for any other degree, diploma, or award.

.....
Jingyang Zhou
February 2011

Abstract

In this thesis, we deal with several optimal guidance and control problems of the spacecrafts arising from the study of lunar exploration. The research is composed of three parts: 1. Optimal guidance for the lunar module soft landing, 2. Spacecraft attitude control system design basing on double gimbal control moment gyroscopes (DGCMGs), and 3. Synchronization motion control for a class of nonlinear system.

To achieve a precise pinpoint lunar module soft landing, we first derive a three dimensional dynamics to describe the motion of the module for the powered descent part by introducing three coordinate frames with consideration of the moon rotation. Then, we move on to construct an optimal guidance law to achieve the lunar module soft landing which is treated as a continuously powered descent process with a constraint on the angle of the module between its longitudinal axis and the moon surface. When the module reaches the landing target, the terminal attitude of the module should be within an allowable small deviation from being vertical with reference to lunar surface. The fuel consumption and the terminal time should also be minimized. The optimal descent trajectory of the lunar module is calculated by using the control parameterization technique in conjunction with a time scaling transform. By these two methods, the optimal control problem is approximated by a sequence of optimal parameter selection problems which can be solved by existing gradient-based optimization methods. MISER 3.3, a general purpose optimal control software package, was developed based on these methods. We make use of this optimal control software package to solve our problem. The optimal trajectory tracking problem, where a desired trajectory is to be tracked with the least fuel consumption in the minimum time, is also considered and solved.

With the consideration of some unpredicted situations, such as initial point perturbations, we move on to construct a nonlinear optimal feedback control law for the powered deceleration phase of the lunar module soft landing. The motion of the lunar module is described in the three dimensional coordinate system. Based on the nonlinear dynamics of the module, we obtain the form of an optimal closed loop control law, where a feedback gain matrix is involved. It is then shown that this feedback gain matrix satisfies a Riccati-like matrix differential equation. The optimal control problem is first solved as an open loop optimal control problem by using the time scaling transform and the control parameterization method. By virtue of the relationship between the optimal open loop control and the optimal closed loop control along the optimal trajectory, we present a practical

method to calculate an approximate optimal feedback gain matrix, without having to solve an optimal control problem involving the complex Riccati-like matrix differential equation coupled with the original system dynamics.

To realize the spacecraft large angle attitude maneuvers, we derive an exact general mathematical description of spacecraft attitude motion driven by DGCMGs system. Then, a nonlinear control law is designed based on the second method of Lyapunov and the stability of the attitude control system is established during the design process. A singularity robustness plus null motion steering law is designed to realize the control law. Principle of DGCMGs' singularity is proved, and the singularity analysis of the orthogonally mounted three DGCMGs system and that of the parallel mounted four DGCMGs system are presented.

Finally, we consider a new class of nonlinear optimal tracking and synchronizing control problems subject to control constraints, where the motions of two distinct objects are required to achieve synchronization at the minimum time while achieving the optimal tracking of a reference target. We first provide a rigorous mathematical formulation for this class of optimal control problems. A new result ensuring the synchronization of the two distinct objects is obtained. On this basis, a computational method is developed for constructing an optimal switching control law under which the motions of the two distinct objects will achieve synchronization at the minimum time while achieving the optimal tracking of a reference target. This computational method is developed based on novel applications of the control parameterization method and a time scaling transform. A practical problem arising from the study of the angular velocity tracking and synchronization of two spacecrafts during their formation flight is formulated and solved by the method proposed.

List of publications

The following papers (which have been published or accepted for publication) were completed during PhD candidature:

- D. Zhou, and J. Y. Zhou, "Nonlinear attitude control of spacecraft based on double-gimbaled control moment gyroscopes," *Journal of Astronautics*, vol. 30, no. 1, pp. 179-187, 2009.
- J. Y. Zhou, and D. Zhou, "Robust nonlinear slewing motion control of spacecraft truss with scissored pair of CMGs," *Journal of Astronautics*, vol. 30, no. 2, pp. 579-584, 2009.
- J. Y. Zhou, K. L. Teo, D. Zhou, and G. H. Zhao, "Optimal guidance for lunar module soft landing," *Nonlinear Dynamics and Systems Theory*, vol. 10, no. 2, pp. 189–201, 2010.
- J. Y. Zhou, K. L. Teo, D. Zhou, and G. H. Zhao, "Nonlinear optimal feedback control for lunar module soft landing," *Journal of Global Optimization*, to appear.
- J. Y. Zhou, and K. L. Teo, "On a class of nonlinear optimal synchronization and tracking control problems," *International Journal of Innovative Computing, Information and Control*, to appear.

The following papers were completed during PhD candidature and are currently under review:

- S. Sun, D. Zhou, J. Y. Zhou and K. L. Teo, "Backstepping design of three dimensional guidance laws considering autopilot lag," *IEEE Transactions on Aerospace and Electronic Systems*, conditionally accepted.
- D. Zhou, S. Sun, B. Zhou, J. Y. Zhou and K. L. Teo, "Discrete sliding-mode guidance laws of a homing missile," *AIAA Journal of GuidanceControl and Dynamics*, submitted.

Acknowledgements

The research reported in this thesis was carried out between September 2008 and October 2010, while I was a PhD student in the Department of Mathematics and Statistics, Curtin University. I am very grateful for the help I received from friends, family, teachers, and colleagues during this time. Without it, this thesis could not be completed.

I am especially indebted to my supervisors, Prof. Kok Lay Teo and A/Prof. Volker Rehbock. They have guided my research during the past two years with remarkable patience and enthusiasm. Prof. Teo, in particular, should be commended for supporting me for so long in both my study and my life: he has been the supervisor of my study and a wise guider of my life since the first time we met in Harbin 2007! During the two years of my stay in Australia, he gave me so much unselfish help. I would also thank Prof. Teo for sponsoring me to attend the conference in China.

I also thank Prof. Yong Hong Wu, the postgraduate coordinator in the Department of Mathematics and Statistics. Prof. Wu was the chairman of my thesis committee and he helped me on many occasions.

I would particularly thank my wife for her encouragement and numerous help during my PhD study.

I am grateful to my good friend – A/Prof. Guohui Zhao who gave me so much help and advise in my papers.

I thank all of the staff in the Department of Mathematics and Statistics for contributing to a friendly work environment. The administrative staff – Joyce Yang, Shuie Liu, Lisa Holling, and Shally Wang—deserve special thanks for providing kind and professional help on numerous occasions.

I have really enjoyed working with other PhD students in the Department of Mathematics and Statistics, especially Lin Qun, Xu Honglei, Wang Lingyun, Li Bin, Yu Changjun and Liu Xia. I thank each of them for being a wonderful friend and colleague. Additionally, I thank each of the department's academic visitors that I had the opportunity to meet. Dr. Jiang Canghua, in particular, has been an excellent friend and mentor.

I also thank the good friends I met in Perth: Li Binghui and Wen Shuqin.

Finally, on a more personal note, I sincerely thank everyone in my family for their support and encouragement during my PhD candidature.

Contents

CHAPTER 1

Introduction

1.1 Motivation and background

The moon is the nearest celestial body to our home planet — the earth. Exploration of the lunar environments and recourses is of much importance and is the very first step that mankind could reach out of the earth to the unknown deep space. Lunar exploration is a tremendous system engineering whose benefits could promote the development of our human society in many aspects such as science and technology, economy, military affairs and politics.

Researches on the moon could improve the knowledge of human about the universe, the formation, evolvement and characters of the solar system and the relationship between space environment and the nature system of the earth. Such kind of outer space research activities could also lead to a great development of many other kinds of science areas such as artificial intelligence, robots, remote control, automation, ultrasonic flight, space material, space life science and so on. It has been proved through investigation that the moon contains many special kinds of recourses that could be utilized by human. The lunar mineral reserve will be a very important supplement for the earth recourses. A clean and efficient nuclear fusion recourse — He3 — stored abundantly in the lunar regolith — could fulfill the demand for electricity of the human society for ten thousand years which would be of great importance for the sustainable development of the human civilization. Due to the stability and periodicity property of the lunar orbit, permanent lunar base could be set up on the moon surface as an observation platform for the artificial satellites. The lunar base could also be used as a relay station for the investigations of the Mars or other planets. In general, lunar exploration will definitely speed up the development of science and technology which would have a deep influence on the human civilization.

Since the late fifties, former Soviet Union and now Russia, America, China, Japan, India and European Union have set out to explore the moon. Various projects have been proposed. Satellites and probes have been sent out to the moon for investigations. The unique recourses and strategic position of the moon have made it a focus of the modern science.

Since the first unmanned lunar probe was lunched by the former Soviet Union on 2nd January 1959, by now, more than fifty lunar probes have been sent to the moon. Seven manned lunar explorations were carried out by the American (the Apollo Program), six of them were successfully accomplished and twelve astronauts reached the moon. Generally speaking, the flight motions of all these lunar probes can be divided into three categories, i.e., flying over, circling or landing on the moon. Those missions aiming to land the lunar module safely on the surface of the moon are the most important ones.

There are two main approaches to the landing of the lunar module on the moon surface — the hard landing approach and the soft landing approach. For the hard landing approach, the lunar module flies to the moon from the earth in an elliptical transfer orbit. The terminal velocity of the module is not constrained and the module will crash on the moon surface with a high speed. Investigation information can be sent back to the earth only during the phase that the module is approaching the moon. If the terminal velocity of the module with respect to the moon is decelerated to a relatively safe value, the soft landing approach can be achieved. The lunar module could perform ground experiments on the moon surface and much more information can be acquired when compared with the hard landing approach. It is obvious that the soft landing approach has more practical uses against the hard landing approach.

There are also two main manners to achieve the lunar module soft landing. The first one is the vertical soft landing method. The lunar module first speeds up and flies to the moon from the parking orbit of the earth. Velocity and trajectory are modified during the flight. When approaching the moon, the module is reoriented against the moon surface vertically and a main thruster begins to work to reduce the velocity of the module. When the module is close to the moon surface, the main thruster will be shut down and a set of small thrusters start to work to achieve the soft landing. The vertical soft landing method were adopted by the 'Lunar 9', 'Lunar 13' landing capsules of the former Soviet Union and the 'Lunar Prospector' missions of NASA. The second method of soft landing starts from a circular parking orbit of the moon (see Figure 1.1). The lunar module is composed of two parts — an orbital module and a landing module. To achieve soft landing, the landing module is first detached from the orbital module which will stay on the parking orbit for other experiments and activities. Then, the soft landing procedure of the landing module begins. According to the preselected landing target, the lunar module is decelerated and enters into a lower energy elliptical orbit, i.e., the Hohmann transfer orbit, which is coplanar with the parking orbit. The elliptical Hohmann transfer orbit has the aposelene and the perilune which are, respectively, 100km and 15km distance away from the moon surface. When the module reaches the perilune, the powered descent soft landing begins. Normally, the lunar soft landing process from the perilune to the moon surface can be divided into three phases (see Figure 1.2). The first part is the powered deceleration phase, from 15km to 2km above the lunar surface, the module velocity is

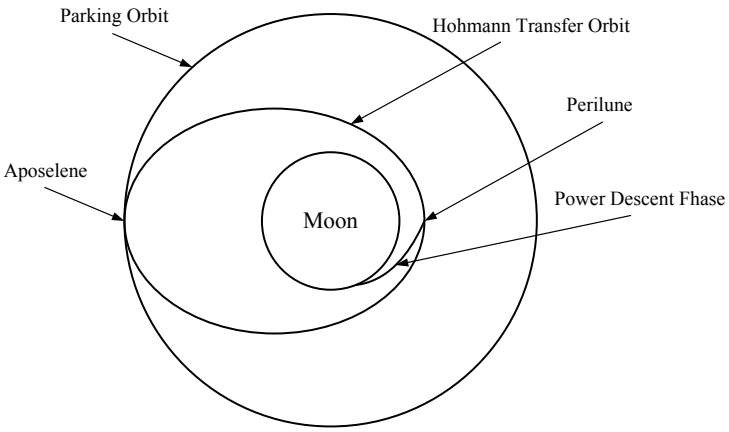

Figure 1.1: The general view of sequence for lunar soft landing.

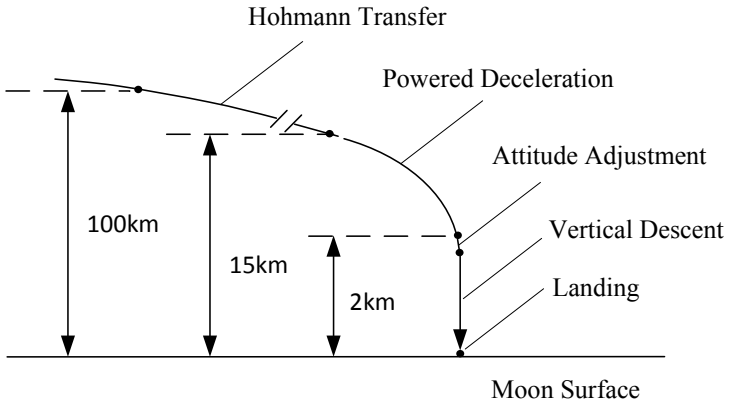

Figure 1.2: The procedure of powered descent soft landing.

reduced to 0m/s by the propellant of the main thruster. The second part, from 2km to 100m above the lunar surface, is the attitude adjustment phase, with the help of the attitude control unit (thrusters or control moment gyros) the module attitude is adjusted so that it is vertical to the moon surface. The last part is the vertical descent phase, a set of small thrusters is employed to cancel the moon gravity to ensure the module soft landing on the lunar surface vertically. The second soft landing method was adopted by the Apollo Program.

Since there is negligible atmosphere surrounding the moon to be used by the lunar module for deceleration, the lunar soft landing can not be performed in the same way as landing on the earth or Mars. Thus, to realize the task of soft landing, one way is to use the reverse force thruster to decelerate the velocity of the landing module starting from the perilune. This together with the attitude control unit will guide the module to reach the landing target with a small and safe final velocity. However, the fuel of the landing module will be consumed substantially during this process. As the mass of the lunar module is always limited, it is extremely important that the fuel consumption is minimized. In this way, more payloads can be equipped (see, for example, [21, 79, 82, 84, 95]). From the

open literature, we note that James S. Meditch [50] is one of the pioneers who studied the fuel optimization problem of the lunar module soft landing as an optimal control problem. He derived the optimal control law for the thrusters by using the Pontryagin Maximum Principle. He then pointed out that, during the last phase of the soft landing, the fuel consumption minimization is equivalent to the time optimal control. Christopher N. D'Souza et al [11] studied the optimal guidance law of a planetary probe soft landing. The guidance law is composed of a linear function of the system states and a nonlinear function of the flight time. The flight time can be obtained through solving a quadratic equation analytically. The advantage of this approach is that it gives rise to an explicit solution and does not need iterations. Wang et al [89] designed a time and fuel optimal descent trajectory for a lunar module with a constant thrust force. By comparing the Kepler descent phase and the continuously powered descent phase, they pointed out that choosing a point before the perilune as the initial point of the powered descent phase rather than the perilune could further reduce the fuel consumption. But the difference is insignificant. For the probe soft landing on a planet surface, Ma et al [47] proposed a robust control law by using the sliding mode control method which is easy for real applications. Based on the optimal guidance approach of a carrier rocket, Wang et al [83] obtained a suboptimal guidance law for achieving the soft landing of a lunar module under the assumption that the gravitational field on the moon surface is uniform. The guidance law is expressed as a function of time-to-go. Hebertt [20] proposed a feedback regulation scheme based on an off-line trajectory for a vertically controlled spacecraft to achieve the soft landing on a planet without atmosphere. Ruan [64] developed a nonlinear neurocontrol method based on the linearized system dynamics for the soft landing of a lunar module. Xi et al [94] designed an optimal control law for the soft landing of a lunar module by using the Pontryagin Maximum Principle. Liu et al [44] obtained an optimal open loop control strategy for the soft landing of a lunar module with a pre-specified terminal time by using the control parameterization technique in conjunction with a time scaling transform. In most relevant papers in the literature, including those mentioned above, the system of differential equations describing the motion of the lunar module is in a two-dimensional polar coordinate system and the effect of the moon rotation is not taken into account. That is, the module is assumed to descend along a vertical plane in the Lunar Central Inertial Coordinate system. Because of the moon rotation, this assumption is not realistic. A lunar module does not necessarily descend along such a vertical plane. Hence, to perform a successful lunar soft landing, a three-dimensional dynamic model that could precisely describe the motion of the module together with an optimal fuel consumption control strategy are desirable.

For spacecrafts, attitude control system is of extreme importance among all the control systems. The result of the mission is directly related to the performance of the attitude control system. In the lunar exploration, the orbital module and the landing module both

need a precise and reliable attitude control unit. The spacecraft attitude control system is composed mainly of three parts, i.e., attitude sensors, controllers and actuators. There are many different types of attitude sensors such as gyroscope, earth sensor, sun sensor, star sensor and so on. Controller is the spacecraft onboard computer whose mission is to receive information from the attitude sensors and output commands for the actuators. The spacecraft attitude actuators normally include spin stabilizer, environment torque stabilizer, magnetic torque controller, thruster and fly wheel system. Fly wheel system consists of reaction wheel, momentum biased wheel, gimballed momentum wheel and control moment gyros (CMGs). With the development of deep space exploration, higher quality attitude control systems are expected for spacecraft. Reliability and precision are the most important indexes for spacecraft attitude control systems.

Among all these attitude actuators, the spin stabilizer, environment torque stabilizer and magnetic torque controller could generate small control torques which are suitable for attitude stabilization, but not enough for the requirements of rapid attitude maneuver of large spacecraft. The thruster is the most commonly used attitude control device due to its simplicity in the design process. However, it is not effective for a long duration mission because of the high fuel consumption. It is also unsuitable for a high accuracy attitude control mission because the torque output is nonsmooth.

Fly wheel system could exchange the momentum stored in the wheel system with the spacecraft body, so as to change the angular momentum of the spacecraft and realize the attitude maneuver. The advantages of the fly wheel system are that it could output smooth control torques and it only needs the electric power which can be supplied by the solar array system. So the fly wheel system is suitable for long duration flight missions. Reaction wheel, momentum biased wheel, gimballed momentum wheel are those that the spin velocities of the wheels can be adjusted. The attitude stabilization and maneuver are achieved by adjusting the velocities of the spin rotors. By this manner, from the mechanical point of view, the system output torque is equal to the effort inputted into the system. So the efficiency of the control is low and it's hard to increase the spin velocity to gain large control torques. The fly wheels with constant velocity spin rotors are called control moment gyros. The CMGs are usually classified by the number of gimbals, i.e., single gimbal CMGs (SGCMGs) or double gimbal CMGs (DGCMGs) (see Figure 1.3 and Figure 1.4). The control torques are acquired by rotation of the gyro gimbals. For the rotors with high spin velocities, the CMGs system could output a large control torque by only a small torque exerted on the gyro gimbals. Hence, the control efficiency of the CMGs system is much higher when compared with the other fly wheel systems. Due to their superior properties such as large torque amplification, momentum exchange capacity and less power consumption, CMG-based attitude control systems are very attractive for space applications. The CMGs systems are adopted as the main attitude control devices not only for large spacecrafts but also for small agile satellites and space robots.

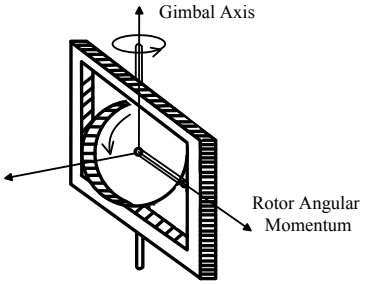

Figure 1.3: Configuration of SGCMG.

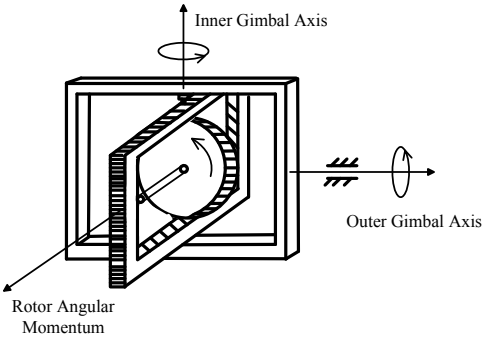

Figure 1.4: Configuration of DGCMG.

A single SGCMG could provide the control torque for one axis of a spacecraft and one DGCMG could control the rotation motions of two axes of a spacecraft. Hence, to realize the three axes maneuver of a spacecraft, at least three SGCMGs or two DGCMGs are needed. In practice, for the three axes attitude maneuver of a spacecraft, more SGCMGs or DGCMGs are equipped to provide redundancy and improve system stability. For instance, 'Sky Lab' utilized a three DGCMGs system as its attitude actuator and a six SGCMGs system were adopted by the 'Mir space station'. The 'international space station' are using four DGCMGs to realize a Zero-Propellant Maneuver (ZPM).

The SGCMGs based spacecraft attitude control systems have been extensively studied during the past four decades. Oh and Vadali [55] proposed the dynamic equations for large angle rotational motion of spacecraft equipped with SGCMGs using Newton-Euler approach, and derived a feedback control law based on Lyapunov stability theory. The control inputs are gyro torques which can be acquired by gimbal angle velocity steering law. The feedback control law and the angular velocity steering law could work well even in the presence of a short time singularity. Singularity is one of the most severe problems existed in the CMG-based control systems. They would significantly depress the performance of the attitude control system. The singularity situation occurs when all individual CMG torque output vectors are perpendicular to the commanded torque direction. It means that no control torque is generated for the commanded gimbal rates and the spacecraft attitude will lose controllability along the singularity direction. The

singularity situations can be divided into two basic types – the external singularity and the internal singularity. The external singularity is the simplest singular state which is also named saturation singularity characterized by the momentum envelope. The momentum envelope is a three dimensional surface representing the maximum available angular momentum of CMGs along any given direction. Any singular status for which the total CMG angular momentum is inside the momentum envelope is called the internal singularity. Margulies [48] detailed the singularity situations for arbitrary SGCMGs clusters by discussing the geometric properties of the singular surface and the algorithms for the parametric construction of the angular momentum envelope. Vadali, Oh, and Walker [81] discussed how to find the initial gimbal angles to avoid the system from entering into singularity states and presented a feedback control strategy based on null motion to move the gimbal angles to their preferred positions. Paradiso [56] proposed a guided depth-first search that could manage null motions about torque producing trajectories which can avoid singular states in the minimally redundant SGCMGs systems. Bedrossian et al [6] proposed a steering law by using Moore-Penrose (MP) pseudo inverse and null motion to realize the control command for SGCMGs system. When system approaches singularity, the MP pseudo inverse is replaced by robust singularity steering law and the geometric singularity could be transmitted. By replacing the pseudo inverse of Jacobian matrix with its transpose, Wu [91] proposed a steering law that can make the steering error converge to zero exponentially. Concerning the servo characters and parameter uncertainties of the SGCMGs system, Wu and Chou [92] designed a robust steering law by estimating the uncertain parameters. Under such a steering law, the steering error converges to zero exponentially. With the assumptions that the system parameters and disturbances are not exactly known, Zhou [103] proposed an adaptive nonlinear control law that could drive a scissored pair of CMGs to achieve the synchronization precession so as to realize the slewing motion of a space structure. Based on the singularity robust steering law, Wei [90] presented a simple steering method which could transmit or escape from the singular status efficiently. A non-diagonal weighting matrix is employed in solving the least square solutions of a mixed norm. However, this steering law can not achieve precise attitude maneuver in the presence of internal singularities. Vadali [80] proposed a suboptimal method for choosing the gimbal angles of the SGCMGs system, the cost function is the singularity measure of the system Jacobian Matrix. Zhang and Li [101] studied the singularity measure of the CMGs system by utilizing the fuzzy decision method and designed a steering law which could avoid singular status through searching the gradients of the singularity measure. Bedrossian et al [5] compared the singularity problems that exist in the robots and the CMGs system. They found that both systems have similar singularity configurations.

It has been proved that the configuration of the SGCMGs clusters will directly influence the complexity of the singular status and the efficiency of the steering laws. Pyramid

mounting arrangement of four SGCMGs is a typical configuration adopted by researchers, see, for example, [32]. Jia and Xu [24] studied the singular status of a dual parallel configured SGCMGs cluster. Zhang [100] stated that the regular pentagonal pyramid arrangement is the optimal configuration. Concerning the index of the configuration efficiency and the complexity of the singular surface, Wu [93] pointed out that the regular dodecahedron is an ideal configuration for the SGCMGs system.

Variable speed control moment gyroscope (VSCMG) is a promising alternative to eliminate the singular statues of the CMGs system due to its extra freedom provided by the variable speed rotor. Schaub and Junkins [65] presented a steering law with null motion based on the VSCMG system. The steering law could continuously optimize the condition number of the Jacobian matrix and drive the gimbal angles away from the singular status without producing any torques. By virtue of the variable speed, VSCMG system could reconfigure the momentum distribution of the whole CMG system with only a small control torque input. VSCMG could serve as CMG as well as reaction wheel for spacecraft attitude stabilization and maneuver. Schaub et al [66] proposed a steering law which could realize both attitude missions simultaneously. Based on VSCMG system, Avanzini and Guido [4] presented a feedforward steering law by utilizing a constraint optimization method. The steering law could avoid singularities and deal with gimbal failures. But it is rather complicated for real applications. Lappas et al [33] applied the robust singularity method on VSCMGs system and designed a steering law which could avoid singularities. Romano and Agrawal [63] studied the attitude dynamics and control method for a spacecraft equipped with VSCMGs system.

Combined application of CMGs and reaction wheels could realize the integrated power and attitude control of a spacecraft. Roithmayr [62] proposed a control law that could achieve earth orientation and power management simultaneously. The reaction wheels are rotated reversely to store the power. The angular momenta of the reaction wheels and the CMGs are utilized to control the attitude of the spacecraft. Utilization of the VSCMG could also realize the integrated power and attitude control. In Richie et al [60], the variable speed SCMGs were used as the attitude control actuators as well as the power management devices. Yoon and Tsiotras [99] proposed to realize the attitude and energy tracking by accelerating the rotors of the VSCMGs system.

The SGCMG based spacecraft attitude control schemes have been studied extensively in recent years. However, due to the complicated nature of the singular surfaces, it is difficult to design the SGCMGs steering law. Hence, the application of the SGCMGs system is restricted. For its extra gimbal, each DGCMG has one more degree of freedom than a SGCMG. So the singular configuration of the DGCMGs system is much more simple than the SGCMGs system. Studies on the use of DGCMGs system as the attitude stabilization and control devices can be found in some literatures. Ahmed and Bernstein [1] derived the dynamic equations of a single DGCMG by using the Lagrange method and designed

an adaptive feedback control law which could follow the gyro command. By comparing the abilities of the SGCMG and the DGCMG on suppressing the vibrations of a space beam, Muise et al [53] found that, under the same circumstances, the performance of the DGCMG is 2-3 times better than that of the SGCMG and can not be influenced by the directions of the disturbances. Liu et al [43] proposed an optimal attitude control law for a spacecraft equipped with a variable speed DGCMGs system. As the explicit solutions can not be obtained directly, they used the variational method to estimate the cost index and obtained the optimal solutions by using the conjugate gradient method [10]. Dzielski et al [13] linearized the attitude dynamics of the spacecraft driven by DGCMGs system, and derived the attitude control law and the CMGs steering law. Several problems such as redistribution of the rotors, bounds of the gimbal velocities, and how to ensure the performance of the system when singularity occurs, are considered during the design procedure. Boyarski and Ben-Asher [9] studied the time optimal reorientation problem for the inner gimbal of a DGCMG mounted on an immobilized platform. An explicit solution was obtained which satisfies the Maximum Principle and the sufficient condition of the Hamilton-Jacobi-Bellman equation. Tsuneo [78] proposed a steering law involving a gradient null motion method for the DGCMGs system. Under this steering law, the DGCMGs could avoid or escape from the internal singularities. However, the computational effort is very heavy. Kennel [27] designed a steering law which can be applied to parallel mounted DGCMGs systems. The advantage of the steering law is that it considers all the DGCMGs as a cluster. When the requirement of the DGCMGs angular momentum is increasing, it only needs to add a few more DGCMGs to the original system, and the redesign of the control system is avoided. He also proposed an isogonal distribution method for the three DGCMGs system which could reduce the cross coupling effects, avoid antiparallel distribution and enlarge the gain of the control law [28]. Although studies on DGCMGs system can be found in many published papers, a precise three dimensional spacecraft attitude dynamics based on DGCMGs system has not yet been found in the open literature.

There are mainly two methods for the landing module to ascend from the moon surface and fly back to the earth. The first return method corresponds to the vertical landing mode. The main thruster is ignited and the landing module ascends vertically from the moon surface. When the velocity of the module reaches 3km/s, the thruster will be shut down and the module flies directly back to the earth. At the moment when the module escapes from the lunar gravitational field, the relative speed of the module with respect to the earth is about 1km/s which will increase to 11km/s when reaching the border of the earth atmosphere. The second return method corresponds to the soft landing mode starting from the lunar parking orbit. When the investigations have been accomplished, the landing module ascends vertically from the moon surface back to the parking orbit and docks with the orbital module. Then, the entire module will speed up and return to the earth.

To realize the second return strategy, either in manned or unmanned missions, a crucial step is to dock the landing module with the orbital module. When the two modules are close enough, their attitudes and attitude velocities should achieve synchronization within a limited time so as to ensure the safety of the modules to perform a successful docking. Therefore, synchronization control technique plays a very important role in the rendezvous and docking missions of the spacecrafts.

Synchronization control of different objects aims at achieving the synchronized motions of the objects with reference to desired target motions. These objects can be mechanical systems, robots, electrical motors, precision optical instruments, or spacecrafts [37, 40, 54, 69, 96], just to name a few. It has attracted an increasing attention in recent years. There are two main approaches to the synchronization control – the master-slave mode approach and the equal-status mode approach. For objects with distinct characteristics in their dynamics, it is more suitable to use the master-slave mode approach, where the object with a slower dynamics is taken as the master, while the object with a faster dynamics is taken as the slave. Its objective is to ensure that the motion of the slave will synchronize with that of the master. If the dynamic characteristics of the two objects are close, it is more suitable to use the equal-status mode approach. In this approach, the cross coupling terms for measuring the synchronization errors are introduced. Both these approaches are well studied in the literature.

Arimoto et al [3] developed a cooperative motion control scheme for the synchronization of a set of robot arms or fingers with tele-operation of the master-slave robotic systems, where the second method of Lyapunov was utilized to show the asymptotic stability. Tao et al [73] proposed a compliant coordination control method for two moving industrial robots by using the master-slave mode approach. A computational scheme was then presented. Miyazaki et al [51] presented a bilateral servo controller for a master-slave robot system through the stability analysis based on the Lyapunov theory. This controller is easily implementable and assures the asymptotic stability even if the arms of the master and the slave have complex nonlinear dynamics with different structures.

Adaptive control methods have been widely implemented for solving the cross-coupling synchronization problems. An early application was proposed by Tomizuka et al [76] in which an adaptive cross-coupling control law was utilized to synchronize the motions of two DC motors whose models can be described by a first order linear dynamics. This control law consists of a proportional feedback controller, an adaptive disturbance compensator and an adaptive feedforward controller. A cross-coupling term is introduced to deal with the synchronization errors. Due to the cross-coupling effect, the disturbances on one motor will also appear on the other motor. However, the system synchronization is achieved. Kamano et al [26] extended the adaptive feedforward control law to the position synchronization problem of two objects. The model of each object is described by a second order linear dynamics. In the two articles mentioned above, the stability of each

system is established by Popov stability criterion [8]. It is, however, a very complicated task to verify the positive definite property of the transfer function matrix. Thus, these methods are only suitable for solving problems with first or second order linear dynamics.

Adaptive cross-coupling synchronization control can also be extended to higher order linear or nonlinear systems. Based on Tomizuka's work, Yang and Chang [96] designed an adaptive synchronization control law for a scissored pair of CMGs which can be used to control the slewing motion of a spacecraft structure. Both the synchronization problems of the positions and velocities are considered. Tsao et al [77] applied the adaptive method to the velocity synchronization control problem of two or four magnetic suspension motors. However, they did not provide system stability analysis in their works. In fact, for high order linear or nonlinear systems, Lyapunov theory is a powerful tool for control system design. System stability can be guaranteed during the design stage. Based on the Lyapunov method, Sun [70] proposed an adaptive cross-coupling synchronization control law which could be used for the synchronous manipulations of multi objects. Under the presence of constant external disturbances, this control law could make the tracking error of each object converge to zero as well as achieve the synchronization between different objects. Sun [71] also applied this control method to the assembling system carried by multi robots, and the punching and cutting synchronization control problems of the numerical control machines. Liu and Sun [41] proposed a uniform synchronization strategy for a multi-axis control problem. Under the uniform framework, the asymptotic convergence of both tracking and synchronization errors are achieved and the performance of the transient motion is improved by selecting proper position synchronization errors.

Applications of adaptive cross-coupling synchronization control also appear in the research works on multi robots coordinate control problems. Namvar and Aghili [54] studied the coordinate control problem of multi robots for grasping an object with an unknown shape. Based on Lyapunov theory, they proposed an adaptive mixed force motion controller to achieve robust stability against environmental frictions and nonparametric uncertainties. By studying the assembly tasks performed by coordinate multiple robots, Zhu [105] proposed an adaptive synchronization control algorithm, and pointed out that the contact force at the end-effector of each robot should be a function of the states of all the robots and also be a function of the control inputs when subject to rigid constraints. The algorithm was applied to a dual-arm case subject to both flexible and rigid constraints, and was also extended to a multiple-arm case. Rodriguez-Angeles and Nijmeijer [61] addressed the synchronization control problem of multiple-robots under the circumstance that only the positions of the robots can be measured. The control algorithm proposed consists of a feedback controller and a nonlinear observer which could estimate the angular velocity information of each joint. The convergence properties of the synchronization errors and the estimation errors were proved. They also presented a master-slave synchronization method for the robot with flexible joints. With the feed-

back linearization technique, the synchronization controller and the nonlinear observer were designed based on Lyapunov theory. Koren [31] improved the performance of a conventional biaxial system by introducing a symmetrical cross-coupling control, where the whole system is considered as a single unit. Srinivasan and Kulkarni [68] designed a cross-coupling controller to improve the accuracy of a high-speed contour that is independent of the tracking accuracy in a biaxial machine tool feed driver.

Robust control theory could also be applied to synchronization control system designs. By researching the motion synchronization problem for a dual-cylinder electro hydraulic (EH) lift system, Sun and Chiu [72] designed an outer-loop motion synchronization controller utilizing the linear multiple input/multiple output (MIMO) robust control technique. A cross-coupling controller using a H_∞ control scheme was proposed by Fang and Chen [14] to reduce the contouring error for a two-axis, direct-drive robot in tracking linear and circular contours. To achieve tracking and synchronization control of two n-dimensional linear systems with reference to given commands, Zhou [102] designed a H_∞ control law by constructing a dual-input/dual-output system using the difference between the output of the two original systems. The method was further extended to the case in which the control objects have dual inputs and was applied to the synchronization control problem of the Wafer-Retical Stage. Wang and Liu [88] designed a sliding mode variable structure control law for the synchronization control of a chaotic system in the presence of nonlinear inputs, parameter uncertainties and external disturbances. Gao et al [17] proposed a robust finite time fast sliding mode controller and pointed out that, by this controller, many chaotic systems can achieve synchronization with identical system response through state transformation. Yau et al [98] studied the synchronization control method for a class of chaotic systems with uncertainties.

Feedback linearization technique, backstepping method, fuzzy control and neural network can also be utilized to solve the synchronization control problems of nonlinear systems. Moore and Chen [52] proposed a fuzzy coupling synchronization method. With the synchronization errors and their derivatives, compensations for each loop are calculated based on fuzzy rules. The method was verified by simulations. The stability analysis was, however, not provided. Lee and Jeon [34] presented a neural network approach to the synchronization of two motion axes. The weights of the neural network can be adjusted by a learning law derived from the gradient algorithm.

Synchronization control has also been widely used in the areas of aeronautical engineering and aerospace engineering such as aircraft/spacecraft formation flight, rendezvous and docking, space arm coordinate operations, attitude actuators synchronization control and so on. For instances, Liu et al [40] presented an adaptive synchronization control law for the angular velocity synchronization problem of multiple aircrafts. Shan et al [67] proposed a synchronized trajectory-tracking control strategy for multiple experimental three-degrees-of-freedom helicopters. Asymptotic convergence is achieved by using Lya-

punov theory. Zhou [103] proposed a synchronization approach to a scissored pair of CMGs to manipulating the attitude motion of spacecrafts. During the missions of spacecraft rendezvous and docking (for example, space shuttle docks with the space station, lunar landing module docks with the orbital module), synchronization control also plays a very important role. A precise, reliable and fast synchronization strategy is always highly in demand.

Optimal control, also named as Dynamic Optimization or Process Optimization, is an important branch of modern control theory. The central issue of the optimal control problem can be stated as: For a given dynamical system, find an admissible control law which could bring the system from an initial state to a desired terminal state such that a performance index is minimized/maximized subject to constraints on the control and state. Applications of optimal control can be found in a wide range of disciplines, such as space technology, life science, economics, social science and engineering. For example, in the mission of lunar module soft landing, it is required that the module reaches the moon surface with the least fuel consumption. For the synchronization motion control of multiple objects, it aims to achieve the synchronization in minimum time. In supply chain management, various raw materials are bringed into a finished product which will be delivered to the end customer. The objective is to minimize the cost and maximize the profit during the accomplishment of the whole process. To solve an optimal control problem arising from practice, we need to construct a mathematical model to describe the physical problem.

For an optimal control problem, it normally consists of four parts as described below.

1. Mathematical model expressed as a system of dynamic equations. It describes the behaviors of the system, and is called system dynamics. One such system dynamics is:

$$\dot{\boldsymbol{x}}(t) = \boldsymbol{f}\big(t, \boldsymbol{x}(t), \boldsymbol{u}(t)\big), \qquad t \in [t_0, t_f], \tag{1.1}$$

where $\boldsymbol{x}(t) \in \mathbb{R}^n$ is the state vector at time t, $\boldsymbol{u}(t) \in \mathbb{R}^r$ is the control vector at time t, and $\boldsymbol{f} : \mathbb{R} \times \mathbb{R}^n \times \mathbb{R}^r \to \mathbb{R}^n$ is a given function, while the time t_0 and t_f in (1.1) are called the initial and terminal time, respectively, and the interval $[t_0, t_f]$ is called the time horizon. Thus, the change rate of the state vector is a function of the time, the current state and the control.

2. Conditions on the initial and terminal state, called the boundary conditions of the system dynamic. In an optimal control problem, the initial time t_0 and the initial state vector $\boldsymbol{x}(t_0) \in \mathbb{R}^n$ are normally given. However, the situations for the terminal state $\boldsymbol{x}(t_f)$ at the terminal time t_f vary from problem to problem. The terminal time could be free or pre-determined. A terminal state constraint may be a fixed point or a manifold in the state space. Sometimes, parts of the state elements are free while others are fixed. All

these situations can be described as:

$$\boldsymbol{x}(t_f) \in \boldsymbol{M} \tag{1.2}$$

where $\boldsymbol{M}$ is a target set.

3. Admissible controls. For a physical control problem, any measurable function $\boldsymbol{u}$ such that $\boldsymbol{u}(t) \in U$ for almost all $t \in [t_0, t_f]$ is called an admissible control, where $U \in \mathbb{R}^r$ is a specified control constraint set, which is often a compact subset of $\mathbb{R}^r$. Let $\mathcal{U}$ be the class of all such admissible controls. An optimal control must be an admissible control.

4. Objective function. Suppose there are many controls which could transfer the initial state $\boldsymbol{x}(t_0)$ to a target set $\boldsymbol{M}$, i.e., $\boldsymbol{x}(t_f) \in \boldsymbol{M}$. Then, an important question arises: which one is the best/optimal? To assess the quality of these controls, we need to construct a function to describe the performance of the system under various controls. This function is called an objective function or performance index. If the objective function is to be maximized, then it is called a profit function. On the other hand, if it is to be minimized, then it is called a cost function.

There are two classic theorems that can be used to deal with the optimal control problems – Pontryagin's minimum principle and Bellman's principle of optimality. We shall introduce them briefly.

Pontryagin's minimum principle was proposed by Pontryagin and his colleagues in 1956, and it is probably the most famous theory in optimal control area. The basic idea of Pontryagin's minimum principle is to construct a Hamiltonian function by introducing a new costate vector [10]. Then, the optimal control problem can be solved by minimizing the Hamiltonian function which yields a two-point boundary-value problem (TPBVP) in terms of the optimal state and the costate. Because the minimum principle is a necessary condition for optimality, the solution of the TPBVP is a candidate solution of the original optimal control problem [97].

Belleman's principle of dynamic programming was derived during 1953 to 1957. The solution to the well-known Hamilton-Jacobi-Bellman equation, if it exists, can be utilized to construct an optimal controller for the optimal control problem. Belleman's principle of dynamic programming offers a sufficient condition for optimality.

The minimum principle and the dynamic programming are powerful tools. However, it is often difficult to solve them analytically. Consequently, numerical methods for solving optimal control problems are extensively studied. Many methods can be found in the literature [2, 18, 30, 86, 87]. For example, the shooting method which is used to solve the two-pint boundary-value problem is derived from the maximum principle. However, the shooting method needs an accurate estimation of the costate initial value, which is often difficult to obtain. An new alternative method is presented in [12, 15], where the initial value of the costate is determined in advance and the state and costate equations

are calculated forward in time simultaneously. However, if the problem only has a few number of constraints, this approach would be more time consuming than the traditional method.

The control parameterization method [15, 45, 74, 85] is another numerical approach to solve various optimal control problems. The main idea of the control parameterization method is to approximate the control variables by a linear combination of some basic functions. The coefficients of these functions are chosen as decision variables. Then, the original optimal control problem is approximated by a sequence of optimal parameter selection problems, each of which can be viewed as a mathematical programming problem. Thus, standard mathematical programming techniques can be applied to solve each of these optimal parameter selection problems.

To apply the control parameterization technique described above we need to partition the time horizon in advance. The partition points, also named switching times, are fixed. A better approach is to regard these points as variables and choose them optimally. However, it has been proved [19, 74] that the gradient formulas of the cost function and the constraint functions with respect to the variable partition points are discontinuous. Thus, they are very difficult to implement. To overcome this difficulty, a time scaling transform is introduced. The main idea is to map all these variable time points into fixed time points in a new time horizon, such that the gradient formulas are continuous and easy to calculate.

For the optimal control problems involving infinite many inequality constraints, the conventional constrained optimization methods are not capable to solve such problems. Hence, a constrained transcription method [23] is introduced, where the continuous inequality constraints are first transformed into equivalent equality constraints in integral form. However, the integrands are nonsmooth. Thus, a local smoothing technique is used to approximate these nonsmooth integrands by smooth functions. In this way, the original problem is approximated by a sequence of optimization problems involving inequality constraints in integral form, where each of which can be solved by using conventional constrained optimization methods.

There are several software packages available for solving optimal control problems. One of which is known as MISER 3.3 [22]. It was developed based on the control parameterization technique, a time scaling transform, and the control transcription method. This software has been successfully applied to a variety of optimal control problems (see, for example, [16, 35, 38, 39, 49, 58]).

1.2 Overview of this thesis

In the previous section, we briefly introduced the backgrounds of several kinds of spacecraft missions and the control methods used therein. In particular, three problems were

discussed: (1) Lunar module soft landing with optimal fuel consumption control strategy; (2) Spacecraft attitude control devices and the control methods utilized; and (3) Synchronization control approaches to realize spacecraft formation flight, rendezvous and docking, which could also be applied to relevant problems in industry and engineering. Thereafter, the development and applications of optimal control methods are briefly discussed. In this thesis, we will deal with all the three problems mentioned above. The rest of the thesis is briefly described below.

In Chapter 2, we consider the optimal control problem of a lunar module soft landing, starting from the perilune to the moon surface. In this problem, the motion of the module is described in a three dimensional coordinate system and the control inputs are bounded. By using the control parameterization technique and the time scaling transform, we design an optimal control strategy to realize the soft landing of the lunar module such that the fuel consumption and the terminal time are minimized. The terminal attitude of the module is kept to be within an allowable small deviation from being vertical with respect to lunar surface so as to ensure that the module could stand on the moon vertically. Then, the optimal descent trajectory is obtained. We then move on to consider an optimal trajectory tracking problem, where a desired trajectory is tracked such that the fuel consumption and the flying time are minimized. This optimal tracking problem is solved using the same approach to the first optimal control problem.

In Chapter 3, based on the same background of lunar module soft landing, we consider the optimal control problem in which the system initial states are perturbed from the prespecified positions. To deal with such situations, an optimal closed loop control law is designed for the powered deceleration phase. The proposed control law involves a feedback gain matrix which satisfies a Riccati-like matrix differential equation. Then, a practical method is presented to calculate an approximate optimal feedback gain matrix, without having to solve an optimal control problem involving the complex Riccati-like matrix differential equation coupled with the original system dynamics.

In Chapter 4, the control problem of spacecraft attitude maneuver is considered. Here, we utilize the DGCMGs system as the attitude actuator of the spacecraft. First, an exact mathematical description of the spacecraft attitude motion driven by DGCMGs is derived. Then, a nonlinear feedback control law is proposed based on the second theorem of Lyapunov and the system stability is proved during the design procedure. A singularity robust plus null motion steering law is also presented which could avoid and escape from the internal singularities of the DGCMGs system. Singularity situations that exist in two kinds of DGCMG configurations, i.e., orthogonally mounted three DGCMGs and parallel mounted four DGCMGs, are detailed.

In Chapter 5, a class of nonlinear optimal tracking and synchronization control problems are considered, where the motions of two distinct objects are required to achieve synchronization at the minimum time while achieving the optimal tracking of a reference

target. We develop a computational method to construct an optimal switching law to realize such an optimal tracking and synchronization mission. The method proposed is then used to solve a practical problem, which arises from the study of the angular velocity tracking and synchronization of two spacecrafts during their formation flight.

Chapter 6 concludes the thesis with some concluding remarks and suggestions for further research.

CHAPTER 2

Optimal guidance for lunar module soft landing

2.1 Introduction

In this chapter, we consider an optimal control problem arising from the optimal guidance of a lunar module to achieving soft landing during the powered descent part, i.e., from 15km height to the moon surface.

In most of the relevant papers in the literature, the descriptions of the system dynamics of the lunar module soft landing are in a two-dimensional polar coordinate system. The descent trajectory of the lunar module is assumed to remain in a vertical plane without consideration of the lateral movement. Neither the influence of the moon rotation is taken into account. However, the lunar module does not, in practice, descend along such a vertical plane. To realize a precise pinpoint soft landing, we first derive a three-dimensional dynamics for the motion of the lunar module. Then, we move on to construct an optimal guidance law to achieve the soft landing of the module. In this chapter, we assume that only the main reverse force thruster is equipped on board for deceleration, and that all the three phases of the powered descent (powered deceleration phase, attitude adjustment phase and vertical descent phase) are considered as a whole piece. The lunar soft landing is treated as a continuously powered descent process with a constraint on the angle of the module between its longitudinal axis and the moon surface. When the module touches down on the moon surface, the terminal attitude of the module should be within an allowable small deviation from being vertical with respect to lunar surface. The aim is to achieve these goals in such a way that the fuel consumption and the terminal time are minimized. The optimal descent trajectory of the lunar module is calculated by using the control parameterization technique in conjunction with a time scaling transform [75]. By these two methods, the optimal control problem is approximated by a sequence of optimal parameter selection problems. Each of which is basically a mathematical programming problem and hence can be solved by existing gradient-based optimization methods [22, 25, 29]. A general purpose optimal control software package, called MISER

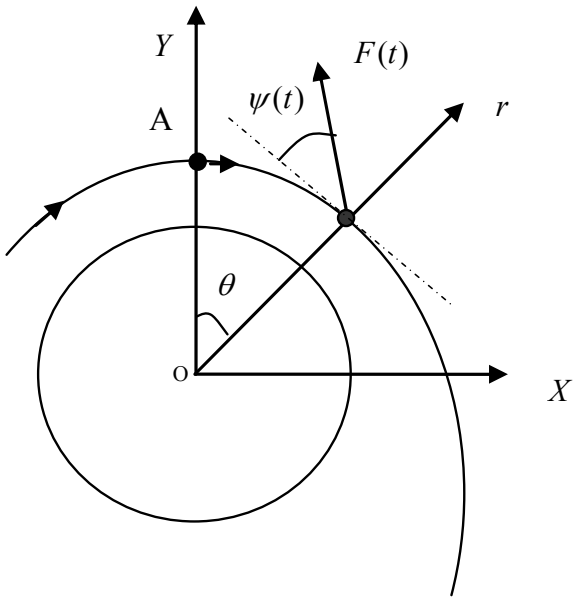

Figure 2.1: Polar coordinate system of lunar soft landing.

3.3, was developed based on these methods. We make use of this optimal control software package to solve our problem in this chapter.

The optimal trajectory tracking problem, where a desired trajectory is to be tracked with the least fuel consumption in the minimum time, is also considered and the same approach to the first optimal control problem is utilized to solve this optimal trajectory tracking problem.

2.2 Two-dimensional coordinate system of lunar soft landing

In this section, we will briefly introduce the commonly used polar coordinate system for the lunar module soft landing (see Figure 2.1).

In Figure 2.1, o represents the origin of the coordinate system which is coincide with the moon center. oY is from the center of the moon to the perilune which is orthogonal to oX. r is the distance between the module and the center of the moon. θ is the angle between oY and or. $F(t)$ is the thrust force of the engine, satisfying $0 \leq F(t) \leq F_{\max}$. $\psi(t)$ is the angle between the perpendicular of or and the direction of the thrust force, satisfying $0 \leq \psi(t) \leq \pi/2$.

With reference to the above coordinate system, the dynamic equations of the lunar module are:

$$\begin{cases} \dot{r} = v \\ \dot{v} = F\sin\psi/m - \mu/r^2 + r\omega^2 \\ \dot{\theta} = \omega \\ \dot{\omega} = -(F\cos\psi/m + 2v\omega)/r \\ \dot{m} = -F/C \end{cases} \tag{2.1}$$

where $v \in R$ is the velocity along the direction of or, μ is the gravitational force of the moon, C represents the specific impulse of the thruster, $m \in R$ is the mass of the module and $\omega \in R$ is the angular velocity of the module with reference to the center of the moon.

From Figure 2.1, it is seen that (2.1) could only describe the motion of the module in oXY plane, while the motion orthogonal to this plane is not considered. So, the application of (2.1) is based on the assumption that the velocity of the module always lies in the oXY plane, and the specified landing site is also in the same plane. However, such an assumption can not always be satisfied in practice. For instance, if the initial velocity of the module is not in the oXY plane, then the module will never reach the landing target precisely, no matter what control policies are used. Thus, the limitation of the two-dimensional polar coordinate system is obvious. In the next section, we will derive a precise three-dimensional coordinate system to describe the motion of the lunar module soft landing.

2.3 Three-dimensional coordinate system of lunar soft landing

The moon is not a perfect sphere, and its shape is distorted slightly because of the tidal effects caused by the gravitation of the earth. In the study of the lunar module soft landing, we normally take the moon as a sphere with a mean radius which is about 1738km. The spin angular velocity of the moon is $\omega_L = 2.661699 \times 10^{-6}$ rad/s, which will influence the guidance accuracy of the lunar soft landing, and the influence will increase as the module approaches the moon equator. So, in this section, we will derive a three-dimensional dynamics for the lunar soft landing, where the moon rotation will be taken into consideration. The optimal guidance law to achieve the soft landing will be discussed in next section.

As the influences of other celestial bodies on the lunar module are small when compared with the moon gravity, the lunar module soft landing can be treated as a two-body system [94]. The motion of the lunar module soft landing is described in a three-dimensional coordinate system (Figure 2.2). Let $oxyz$ and $ox_Ly_Lz_L$ be, respectively, the Lunar Central Inertial Coordinate and Lunar Fixed Coordinate with the moon equator as the reference plane. $Ax_1y_1z_1$ is the orbit coordinate, A is the position of the lunar module. The three-

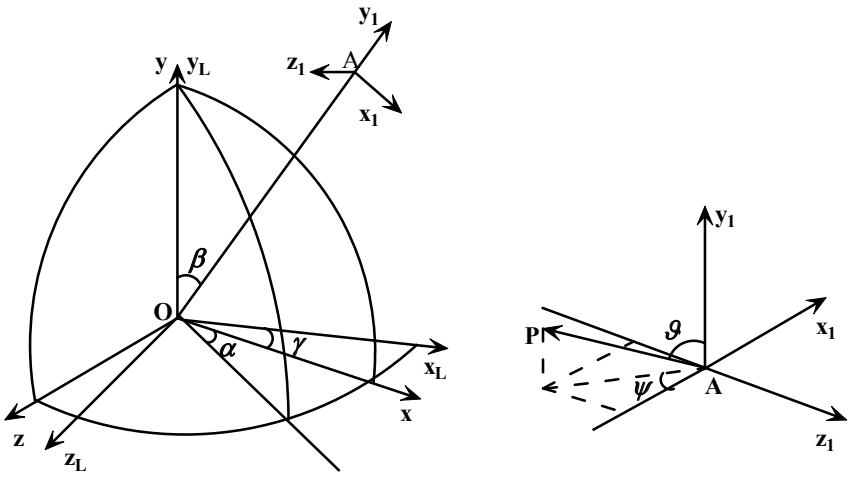

Figure 2.2: Three-dimensional coordinate systems.

dimensional coordinate forms a right handed system. α and β represent, respectively, the rotational angles between $oxyz$ and $Ax_1y_1z_1$. ϑ is the separation angle between $\boldsymbol{P}$ (the thrust force) and Ay_1. ψ is the separation angle of the projection of $\boldsymbol{P}$ onto the plane Ax_1z_1 with reference to the negative direction of Ax_1. So the direction of $\boldsymbol{P}$ in the coordinate $Ax_1y_1z_1$ can be expressed in terms of ϑ and ψ. γ is the rotational angle between $oxyz$ and $ox_Ly_Lz_L$. Without loss of generality, we can assume that $oxyz$ and $ox_Ly_Lz_L$ coincide with each other at the time when the process of the soft landing begins.

Based on the above definitions, the coordinate transformation matrix from $Ax_1y_1z_1$ to $oxyz$ can be easily obtained as follows:

$$\boldsymbol{T}_1 = \begin{bmatrix} \cos\alpha\cos\beta & \sin\beta & -\sin\alpha\cos\beta \\ -\cos\alpha\sin\beta & \cos\beta & \sin\alpha\sin\beta \\ \sin\alpha & 0 & \cos\alpha \end{bmatrix}. \tag{2.2}$$

The coordinate transformation matrix from $oxyz$ to $ox_Ly_Lz_L$ is

$$\boldsymbol{T}_2 = \begin{bmatrix} \cos\gamma & 0 & -\sin\gamma \\ 0 & 1 & 0 \\ \sin\gamma & 0 & \cos\gamma \end{bmatrix}. \tag{2.3}$$

Based on Newton's second law, the dynamic equations of the module in the Lunar Central Inertial Coordinate can be derived as:

$$\left[\frac{d\vec{\boldsymbol{V}}_I}{dt}\right]_I = \boldsymbol{T}_1 \cdot \begin{bmatrix} QV_r\sin\vartheta\cos\psi/m \\ QV_r\cos\vartheta/m \\ QV_r\sin\vartheta\sin\psi/m \end{bmatrix} + \frac{\vec{\boldsymbol{G}}_1}{m} \tag{2.4}$$

where $\vec{\boldsymbol{V}}_I$ and $\vec{\boldsymbol{G}}_1$ are, respectively, the module velocity vector and the lunar attraction

force vector in the Lunar Central Inertial Coordinate, m is the mass of the lunar module, Q and V_r represent, respectively, the fuel consumption rate and the specific impulse of the thruster. The product of Q and V_r is the magnitude of the thrust force $\boldsymbol{P}$ whose direction is defined as positive, while the direction of $\vec{\boldsymbol{G}}_1$ is defined as negative.

Let $\vec{\boldsymbol{R}}$ be the position vector of the module, and let $\vec{\boldsymbol{V}}_L$ be the velocity vector of the module in the Lunar Fixed Coordinate, $\vec{\boldsymbol{\omega}}$ is the angular velocity vector of the Lunar Fixed Coordinate with reference to the Lunar Central Inertial Coordinate. From Coriolis Principle [7], we have

$$\vec{\boldsymbol{V}}_I = \vec{\boldsymbol{V}}_L + \vec{\boldsymbol{\omega}} \times \vec{\boldsymbol{R}} \tag{2.5}$$

Differentiate (2.5), we obtain the acceleration vector of the module with reference to the Lunar Central Inertial Coordinate given below.

$$\left[\frac{d\vec{\boldsymbol{V}}_I}{dt}\right]_I = \left[\frac{d\vec{\boldsymbol{V}}_L}{dt}\right]_I + \vec{\boldsymbol{\omega}} \times \left[\frac{d\vec{\boldsymbol{R}}}{dt}\right]_I + \left[\frac{d\vec{\boldsymbol{\omega}}}{dt}\right]_I \times \vec{\boldsymbol{R}} \tag{2.6}$$

According to Coriolis Principle, we have the following equations.

$$\left[\frac{d\vec{\boldsymbol{V}}_L}{dt}\right]_I = \left[\frac{d\vec{\boldsymbol{V}}_L}{dt}\right]_L + \vec{\boldsymbol{\omega}} \times \vec{\boldsymbol{V}}_L \tag{2.7}$$

$$\left[\frac{d\vec{\boldsymbol{R}}}{dt}\right]_I = \vec{\boldsymbol{V}}_L + \vec{\boldsymbol{\omega}} \times \vec{\boldsymbol{R}} \tag{2.8}$$

As the lunar spin velocity is constant, it follows that

$$\left[\frac{d\vec{\boldsymbol{\omega}}}{dt}\right]_I = 0 \tag{2.9}$$

Substitute (2.7), (2.8) and (2.9) into (2.6), we obtain

$$\left[\frac{d\vec{\boldsymbol{V}}_L}{dt}\right]_L = \left[\frac{d\vec{\boldsymbol{V}}_I}{dt}\right]_I - 2\vec{\boldsymbol{\omega}} \times \vec{\boldsymbol{V}}_L - \vec{\boldsymbol{\omega}} \times (\vec{\boldsymbol{\omega}} \times \vec{\boldsymbol{R}}) \tag{2.10}$$

Thus, the dynamics of the module expressed in the Lunar Fixed Coordinate can be written as:

$$\begin{aligned}\begin{bmatrix} \dot{V}_{xL} \\ \dot{V}_{yL} \\ \dot{V}_{zL} \end{bmatrix} = \boldsymbol{T}_2 \cdot \boldsymbol{T}_1 \cdot \begin{bmatrix} QV_r \sin\vartheta \cos\psi/m \\ QV_r \cos\vartheta/m \\ QV_r \sin\vartheta \sin\psi/m \end{bmatrix} + \frac{\vec{\boldsymbol{G}}_{1L}}{m} \\ - 2\vec{\boldsymbol{\omega}} \times \vec{\boldsymbol{V}}_L - \vec{\boldsymbol{\omega}} \times (\vec{\boldsymbol{\omega}} \times \vec{\boldsymbol{R}})\end{aligned} \tag{2.11}$$

where $\dot{V}_{xL}$, $\dot{V}_{yL}$ and $\dot{V}_{zL}$ are the components of the module acceleration vector on each axis of the Lunar Fixed Coordinate, and $\vec{\boldsymbol{G}}_{1L}$ represents the projection of $\vec{\boldsymbol{G}}_1$ in the Lunar Fixed Coordinate. The lunar gravitational force $\vec{\boldsymbol{g}}$ consists of the attraction force and the centrifugal force which can be written in the Lunar Fixed Coordinate as

$$\vec{\boldsymbol{g}}_L = \frac{\vec{\boldsymbol{G}}_{1L}}{m} - \vec{\boldsymbol{\omega}} \times (\vec{\boldsymbol{\omega}} \times \vec{\boldsymbol{R}}) \tag{2.12}$$

Substitute (2.12) into (2.11), we have

$$\begin{bmatrix} \dot{V}_{xL} \\ \dot{V}_{yL} \\ \dot{V}_{zL} \end{bmatrix} = \boldsymbol{T}_2 \cdot \boldsymbol{T}_1 \cdot \begin{bmatrix} QV_r \sin\vartheta \cos\psi/m \\ QV_r \cos\vartheta/m \\ QV_r \sin\vartheta \sin\psi/m \end{bmatrix} + \vec{\boldsymbol{g}}_L - 2\vec{\boldsymbol{\omega}} \times \vec{\boldsymbol{V}}_L \tag{2.13}$$

Let x_L, y_L and z_L be, respectively, the coordinates of the module in the Lunar Fixed Coordinate. Then, by choosing the state vector as

$$\boldsymbol{x}_L = [x_L, y_L, z_L, V_{xL}, V_{yL}, V_{zL}, m]^T,$$

the system dynamic equations can be derived as:

$$\begin{cases} \dot{x}_L = V_{xL} \\ \dot{y}_L = V_{yL} \\ \dot{z}_L = V_{zL} \\ \dot{V}_{xL} = BQV_r/m - g_{xL} - 2\omega_L V_{zL} \\ \dot{V}_{yL} = CQV_r/m - g_{yL} \\ \dot{V}_{zL} = DQV_r/m - g_{zL} + 2\omega_L V_{xL} \\ \dot{m} = -Q \end{cases} \tag{2.14}$$

where

$$\begin{aligned} B &= (\cos\alpha\cos\beta\cos\gamma - \sin\alpha\sin\gamma)\sin\vartheta\cos\psi \\ &\quad -(\sin\alpha\cos\beta\cos\gamma + \cos\alpha\sin\gamma)\sin\vartheta\sin\psi + \sin\beta\cos\gamma\cos\vartheta \\ C &= -\cos\alpha\sin\beta\sin\vartheta\cos\psi + \cos\beta\cos\vartheta + \sin\alpha\sin\beta\sin\vartheta\sin\psi \\ D &= (\cos\alpha\cos\beta\sin\gamma + \sin\alpha\cos\gamma)\sin\vartheta\cos\psi \\ &\quad -(\sin\alpha\cos\beta\sin\gamma - \cos\alpha\cos\gamma)\sin\vartheta\sin\psi + \sin\beta\sin\gamma\cos\vartheta, \end{aligned}$$

while g_{xL}, g_{yL} and g_{zL} denote the respective components of the lunar gravitation in the Lunar Fixed Coordinate.

2.4 Problem formulation

For continuously powered descent soft landing, the reverse force thruster begins to work, starting from the perilune to decelerate the initial velocity of the module. With the cooperation of the attitude control devices, the module is guided to reach the landing target vertically with an allowable small and safe final velocity. This is achieved under the control constraints such that the fuel consumption and the flight time are minimized.

For (2.14), we introduce two new state equations

$$\dot{\vartheta} = v \tag{2.15}$$

$$\dot{\psi} = w \tag{2.16}$$

Let

$$\begin{aligned} \boldsymbol{x} &= [x_L, y_L, z_L, V_{xL}, V_{yL}, V_{zL}, \vartheta, \psi, m]^T \\ &= [x_1, x_2, x_3, x_4, x_5, x_6, x_7, x_8, x_9]^T \end{aligned} \tag{2.17}$$

and

$$\boldsymbol{u} = [Q, v, w]^T = [u_1, u_2, u_3]^T \tag{2.18}$$

The original system dynamics (2.14) can be rewritten in the form of an affine nonlinear system given below.

$$\dot{\boldsymbol{x}}(t) = \boldsymbol{f}(\boldsymbol{x}(t)) + \boldsymbol{B}(\boldsymbol{x}(t))\boldsymbol{u}(t) \tag{2.19}$$

where

$$\boldsymbol{f}(\boldsymbol{x}) = [x_4, x_5, x_6, -g_{xL} - 2\omega_L x_6, -g_{yL}, -g_{zL} + 2\omega_L x_4, 0, 0, 0]^T, \tag{2.20}$$

$$\boldsymbol{B}(\boldsymbol{x}) = \begin{bmatrix} 0 & 0 & 0 & M_1 & M_2 & M_3 & 0 & 0 & -1 \\ 0 & 0 & 0 & 0 & 0 & 0 & 1 & 0 & 0 \\ 0 & 0 & 0 & 0 & 0 & 0 & 0 & 1 & 0 \end{bmatrix}^T, \tag{2.21}$$

while

$$\begin{aligned} M_1 = {} & [(\cos\alpha\cos\beta\cos\gamma - \sin\alpha\sin\gamma)\sin x_7\cos x_8 \\ & -(\sin\alpha\cos\beta\cos\gamma + \cos\alpha\sin\gamma)\sin x_7\sin x_8 + \sin\beta\cos\gamma\cos x_7]V_r/x_9, \\ M_2 = {} & [-\cos\alpha\sin\beta\sin x_7\cos x_8 + \cos\beta\cos x_7 + \sin\alpha\sin\beta\sin x_7\sin x_8]V_r/x_9, \end{aligned}$$

and

$$M_3 = [(\cos\alpha\cos\beta\sin\gamma + \sin\alpha\cos\gamma)\sin x_7\cos x_8 \\ -(\sin\alpha\cos\beta\sin\gamma - \cos\alpha\cos\gamma)\sin x_7\sin x_8 + \sin\beta\sin\gamma\cos x_7]V_r/x_9.$$

The boundedness constraints on the control vector $\boldsymbol{u} = [u_1, u_2, u_3]^T$ are specified below:

$$\boldsymbol{\alpha} \leq \boldsymbol{u}(t) \leq \boldsymbol{\beta},\ \forall\ t \geq 0, \tag{2.22}$$

where $\boldsymbol{\alpha} = [\alpha_1, \alpha_2, \alpha_3]^T$ and $\boldsymbol{\beta} = [\beta_1, \beta_2, \beta_3]^T$, while $\alpha_i,\ i = 1, 2, 3$, and $\beta_i,\ i = 1, 2, 3$, are given constants. Let $\mathcal{U}$ be the set of all such controls. Elements from $\mathcal{U}$ are called admissible controls and $\mathcal{U}$ is referred to as the class of admissible controls.

The initial conditions of the soft landing are determined by the state of the lunar module in the perilune at the initial time $t_0 = 0$. The terminal constraints are specified by the requirement of the soft landing, i.e., when the lunar module reaches the target at the terminal time t_f which is free, its velocity should be close to zero and its longitudinal axis should be close to vertical to the moon surface. So the initial conditions and terminal state constraints can be expressed as:

$$\boldsymbol{x}(t_0) = [x_{L0}, y_{L0}, z_{L0}, V_{xL0}, V_{yL0}, V_{zL0}, \vartheta_0, \psi_0, m_0]^T \tag{2.23}$$

and

$$\boldsymbol{\Phi} = \begin{bmatrix} x_L(t_f) - x_{Lr} \\ y_L(t_f) - y_{Lr} \\ z_L(t_f) - z_{Lr} \\ V_{xL}(t_f) - 0 \\ V_{yL}(t_f) - 0 \\ V_{zL}(t_f) - 0 \end{bmatrix} = 0 \tag{2.24}$$

$$\vartheta_{t_f} \leq x_7(t_f) \leq 0 \tag{2.25}$$

where $(x_{Lr},\ y_{Lr},\ z_{Lr})$ represents the position of the landing target in the Lunar Fixed Coordinate, ϑ_{t_f} is the terminal separation angle of the module between its longitudinal axis and the direction of the plumb line. Our aim is to design an optimal control strategy to achieve the task of soft landing of the lunar module such that conditions (2.24) and (2.25) are satisfied and the fuel consumption and the flying time are minimized. The task of minimizing the fuel consumption and the flying time is formulated as the task of minimizing the following cost function

$$J = m_0 - x_9(t_f) + t_f \tag{2.26}$$

We may now formally state our optimal control problem as follows.

Problem P. *Given system (2.19), find a control* $\boldsymbol{u} \in \mathcal{U}$ *such that the cost function (2.26) is minimized subject to the control constraint (2.22), the initial condition (2.23) and the terminal state constraints (2.24) and (2.25).*

2.5 Parameterization of the Control

To solve Problem P, we shall utilize the control parameterization technique to approximate the control vector $\boldsymbol{u}$ with piecewise constant functions over the time interval $[0, t_f]$ as:

$$u_1^p(t) = \sum_{k=1}^{n_p} \sigma_1^k \chi_{[\tau_{k-1}, \tau_k)}(t) \tag{2.27a}$$

$$u_2^p(t) = \sum_{k=1}^{n_p} \sigma_2^k \chi_{[\tau_{k-1}, \tau_k)}(t) \tag{2.27b}$$

$$u_3^p(t) = \sum_{k=1}^{n_p} \sigma_3^k \chi_{[\tau_{k-1}, \tau_k)}(t) \tag{2.27c}$$

where

$$\tau_0, \tau_1, \ldots, \tau_{n_p},\ \tau_{k-1} < \tau_k,\ k = 1, 2, \ldots, n_p \tag{2.28}$$

(with $\tau_0 = 0$ and $\tau_{n_p} = t_f$) are partition points of the time interval $[0, t_f]$, and $\chi_I(t)$ denotes the indicator function of I defined by

$$\chi_I(t) = \begin{cases} 1, \ t \in I \\ 0, \ \text{elsewhere} \end{cases} \tag{2.29}$$

Let $\boldsymbol{\tau} = [\tau_1, \ldots, \tau_{n_p}]^T$ and let Υ^p be the set which consists of all such $\boldsymbol{\tau}$. For each $j = 1, 2, 3$, and $k = 1, 2, \ldots, n_p$, σ_j^k is a constant control parameter, and τ_k, $k = 1, \ldots, n_p - 1$, are the switching times. Let $\boldsymbol{\sigma}_j = [\sigma_j^1, \cdots, \sigma_j^{n_p}]^T$, $j = 1, 2, 3$, and let $\boldsymbol{\sigma} = [(\boldsymbol{\sigma}_1)^T, (\boldsymbol{\sigma}_2)^T, (\boldsymbol{\sigma}_3)^T]^T$. Define $\boldsymbol{u}^p = [u_1^p, u_2^p, u_3^p]^T$.

As $\boldsymbol{u}^p \in \mathcal{U}$, it is clear that

$$\alpha_j \le \sigma_j^k \le \beta_j \tag{2.30}$$

for $j = 1, 2, 3$, and $k = 1, 2, \ldots, n_p$. Let Ξ^p denote the set containing all such $\boldsymbol{\sigma}$. Here, for the soft landing of a lunar module, the terminal time $\tau_{n_p} = t_f$ is unknown and regarded as a decision variable. So, the original control vector (2.18) is approximated by (2.27), leading to an approximate optimal control problem to the optimal control Problem P given below.

Problem P$_p$. *Given system (2.19), find a control in the form of (2.27) such that the cost function (2.26) is minimized subject to the control constraints (2.30), the initial condition*

(2.23) and the terminal state constraints (2.24) and (2.25).

Thus, by solving Problem P_p, we obtain an approximate solution to Problem P. It is expected that this approximate solution will be closer to the optimal solution when the number of the partition points is increased.

To enhance the performance of the approximation, we should regard the partition points as decision variables to be selected optimally. However, it is known [19, 74] that the gradient formulas of the cost function and the constraint functions with respect to the variable partition points are discontinuous over $[0, t_f]$. Thus, they do not work well in practice. To overcome this obstacle, a time scaling transform [75] is introduced to map all these variable time points τ_k, $k = 1, \ldots, n_p$, into fixed time points ς_k, $k = 1, \ldots, n_p$, in a new time horizon $[0, 1]$, such that

$$0 = \varsigma_0 < \varsigma_1 < \cdots < \varsigma_{n_p-1} < \varsigma_{n_p} = 1 \tag{2.31}$$

For this, we introduce a new state equation defined on $[0, 1]$

$$\frac{dt(s)}{ds} = \mu^p(s) \tag{2.32}$$

where $t(0) = 0$, $t(1) = t_f$, and

$$\mu^p(s) = \sum_{k=1}^{n_p} \delta_k \chi_{[\varsigma_{k-1}, \varsigma_k)}(s) \tag{2.33}$$

Here,

$$\delta_k \geq 0, \ \ k = 1, \ldots, n_p \tag{2.34}$$

are decision variables. $\mu^p(s)$ is called the time scaling control. It is a nonnegative piecewise constant function with possible discontinuities at the pre-fixed knots ς_k, $k = 1, \ldots, n_p - 1$. Let $\boldsymbol{\delta} = [\delta_1, \cdots, \delta_{n_p}]^T$.

By applying the time scaling transform (2.32), system equations (2.19) and (2.32) are transformed into

$$\frac{d\tilde{\boldsymbol{x}}(s)}{ds} = \begin{bmatrix} \mu^p(s)[\boldsymbol{f}(t(s), \hat{\boldsymbol{x}}(s)) + \boldsymbol{B}(t(s), \hat{\boldsymbol{x}}(s))\hat{\boldsymbol{u}}^p(s)] \\ \mu^p(s) \end{bmatrix} = \tilde{\boldsymbol{f}}(s, \tilde{\boldsymbol{x}}, \boldsymbol{\sigma}, \boldsymbol{\delta}) \tag{2.35}$$

where $\tilde{\boldsymbol{x}} = [\tilde{x}_1, \cdots, \tilde{x}_9, \tilde{x}_{10}]^T = [(\hat{\boldsymbol{x}})^T, t]^T$, $\hat{\boldsymbol{x}}(s) = \boldsymbol{x}(t(s))$, and $\hat{\boldsymbol{u}}^p(s) = \boldsymbol{u}^p(t(s))$ given by

$$\hat{\boldsymbol{u}}^p(s) = \sum_{k=1}^{n_p} \boldsymbol{\sigma}^k \chi_{[\varsigma_{k-1}, \varsigma_k)}(s) \tag{2.36}$$

The initial condition is

$$\tilde{\boldsymbol{x}}(0) = [x_{L0}, y_{L0}, z_{L0}, V_{xL_0}, V_{yL_0}, V_{zL0}, \vartheta_0, \psi_0, m_0, 0]^T \tag{2.37}$$

The cost function (2.26) and the terminal constraints (2.24) and (2.25) become

$$\tilde{J} = m_0 - \tilde{x}_9(1) + \tilde{x}_{10}(1) \tag{2.38}$$

and

$$\tilde{\boldsymbol{\Phi}} = \begin{bmatrix} \tilde{x}_1(1) - x_{Lr} \\ \tilde{x}_2(1) - y_{Lr} \\ \tilde{x}_3(1) - z_{Lr} \\ \tilde{x}_4(1) - 0 \\ \tilde{x}_5(1) - 0 \\ \tilde{x}_6(1) - 0 \\ \tilde{x}_{10}(1) - t_f \end{bmatrix} = 0 \tag{2.39}$$

$$\vartheta_{t_f} \leq \tilde{x}_7(1) \leq 0 \tag{2.40}$$

respectively. They can be written in canonical form as:

$$\tilde{g}_0(\boldsymbol{\sigma}, \boldsymbol{\delta}) = \tilde{\Phi}_0(\tilde{x}(1|\boldsymbol{\sigma}, \boldsymbol{\delta}),\ \boldsymbol{\sigma}, \boldsymbol{\delta}) + \int_0^1 \tilde{\ell}_0(s,\ \tilde{x}(s|\boldsymbol{\sigma}, \boldsymbol{\delta}),\ \boldsymbol{\sigma}, \boldsymbol{\delta})ds \tag{2.41}$$

and

$$\tilde{g}_i(\boldsymbol{\sigma}, \boldsymbol{\delta}) = \tilde{\Phi}_i(\tilde{x}(1|\boldsymbol{\sigma}, \boldsymbol{\delta}),\ \boldsymbol{\sigma}, \boldsymbol{\delta}) + \int_0^1 \tilde{\ell}_i(s,\ \tilde{x}(s|\boldsymbol{\sigma}, \boldsymbol{\delta}),\ \boldsymbol{\sigma}, \boldsymbol{\delta})ds = 0, \quad i = 1, ..., 7, \tag{2.42}$$

$$\tilde{g}_i(\boldsymbol{\sigma}, \boldsymbol{\delta}) = \tilde{\Phi}_i(\tilde{x}(1|\boldsymbol{\sigma}, \boldsymbol{\delta}),\ \boldsymbol{\sigma}, \boldsymbol{\delta}) + \int_0^1 \tilde{\ell}_i(s,\ \tilde{x}(s|\boldsymbol{\sigma}, \boldsymbol{\delta}),\ \boldsymbol{\sigma}, \boldsymbol{\delta})ds \leq 0, \quad i = 8, 9, \tag{2.43}$$

where $\tilde{\ell}_i = 0$, for $i = 0, 1, ..., 9$, while $\tilde{\Phi}_i$, $i = 0, 1, ..., 9$, are defined by (2.38), (2.39) and (2.40), respectively.

The original optimal control problem is now approximated by a sequence of optimal parameter selection problems depending on n_p, the number of the partition points of the time horizon $[0, t_f]$, given below.

Problem $\tilde{\mathrm{P}}_p$. *Given system (2.35) with the initial condition (2.37) on the time interval $s \in [0, 1]$, find a control parameter vector $\boldsymbol{\sigma} \in \Xi^p$ and a switching time vector $\boldsymbol{\delta} \in \Upsilon^p$, such that the cost function (2.38) is minimized subject to the terminal constraints (2.39) and (2.40).*

For each n_p, Problem $\tilde{\mathrm{P}}_p$ can be solved as a nonlinear optimization problem where the cost function (2.38) is minimized subject to the terminal constraints (2.39) and (2.40)

and the constraints on the decision vectors $\boldsymbol{\sigma}$ and $\boldsymbol{\delta}$ given by (2.30) and (2.34), where the dynamical system (2.35) is used to generate the values of the cost function (2.38) and the constraint functions (2.39) and (2.40). Existing gradient-based optimization methods can be used to solve Problem $\tilde{\mathrm{P}}_{\mathrm{p}}$. For this, we need the gradient formulas of the objective function and the constraint functions. For the constraints (2.30) and (2.34), their gradient formulas are straightforward to derive. The gradient formulas of the objective function (2.38) and the constraint functions (2.39) and (2.40) are given bellow. The proof follows from a similar argument as that given for Theorem 5.2.1 Chapter 5 in [74].

Theorem 2.1. *For each $i = 0, 1, \ldots, 9$, the gradient of the function $\tilde{g}_i$ with respect to $\boldsymbol{\sigma}$ and $\boldsymbol{\delta}$ are given by*

$$\frac{\partial \tilde{g}_i(\boldsymbol{\sigma}, \boldsymbol{\delta})}{\partial \boldsymbol{\sigma}} = \int_0^1 \frac{\partial \tilde{H}_i(s, \tilde{\boldsymbol{x}}(s), \boldsymbol{\sigma}, \boldsymbol{\delta}, \tilde{\boldsymbol{\lambda}}^i(s|\boldsymbol{\sigma}, \boldsymbol{\delta}))}{\partial \boldsymbol{\sigma}} ds \tag{2.44}$$

and

$$\frac{\partial \tilde{g}_i(\boldsymbol{\sigma}, \boldsymbol{\delta})}{\partial \boldsymbol{\delta}} = \int_0^1 \frac{\partial \tilde{H}_i(s, \tilde{\boldsymbol{x}}(s), \boldsymbol{\sigma}, \boldsymbol{\delta}, \tilde{\boldsymbol{\lambda}}^i(s|\boldsymbol{\sigma}, \boldsymbol{\delta}))}{\partial \boldsymbol{\delta}} ds \tag{2.45}$$

where

$$\tilde{H}_i(s, \tilde{\boldsymbol{x}}, \boldsymbol{\sigma}, \boldsymbol{\delta}, \tilde{\boldsymbol{\lambda}}^i) = \tilde{\ell}_i(s, \tilde{\boldsymbol{x}}, \boldsymbol{\sigma}, \boldsymbol{\delta}) + (\tilde{\boldsymbol{\lambda}}^i)^T \tilde{\boldsymbol{f}}(s, \tilde{\boldsymbol{x}}, \boldsymbol{\sigma}, \boldsymbol{\delta}) \tag{2.46}$$

and, for each $i = 0, 1, \ldots, 9$, $\tilde{\boldsymbol{\lambda}}^i(s|\boldsymbol{\sigma}, \boldsymbol{\delta})$ is the solution of the following co-state system corresponding to $(\boldsymbol{\sigma}, \boldsymbol{\delta})$:

$$\frac{d(\tilde{\boldsymbol{\lambda}}(s))^T}{ds} = -\frac{\partial \tilde{H}_i(s, \tilde{\boldsymbol{x}}(s|\boldsymbol{\sigma}, \boldsymbol{\delta}), \boldsymbol{\sigma}, \boldsymbol{\delta}, \tilde{\boldsymbol{\lambda}}(s))}{\partial \tilde{\boldsymbol{x}}}, \ s \in [0, 1) \tag{2.47a}$$

with

$$(\tilde{\boldsymbol{\lambda}}(1))^T = \frac{\partial \tilde{\Phi}_i(\tilde{\boldsymbol{x}}(1|\boldsymbol{\sigma}, \boldsymbol{\delta}))}{\partial \tilde{\boldsymbol{x}}} \tag{2.47b}$$

Proof. Let $\boldsymbol{\sigma} \in \mathbb{R}^{n_p}$ be given and let $\boldsymbol{\rho} \in \mathbb{R}^{n_p}$ be arbitrary but fixed. Define

$$\boldsymbol{\sigma}(\varepsilon) = \boldsymbol{\sigma} + \varepsilon \boldsymbol{\rho} \tag{2.48}$$

where $\varepsilon > 0$ is an arbitrarily small real number. For brevity, let $\tilde{\boldsymbol{x}}(\bullet)$ and $\tilde{\boldsymbol{x}}(\bullet\,; \varepsilon)$ denote, respectively, the solution of the system (2.35) corresponding to $\boldsymbol{\sigma}$ and $\boldsymbol{\sigma}(\varepsilon)$. Clearly, from (2.35), we have

$$\tilde{\boldsymbol{x}}(s) = \tilde{\boldsymbol{x}}^0 + \int_0^s \tilde{\boldsymbol{f}}\left(\tau, \tilde{\boldsymbol{x}}\left(\tau\right), \boldsymbol{\sigma}, \boldsymbol{\delta}\right) d\tau \tag{2.49}$$

and

$$\tilde{\boldsymbol{x}}(s\,; \varepsilon) = \tilde{\boldsymbol{x}}^0 + \int_0^s \tilde{\boldsymbol{f}}\left(\tau, \tilde{\boldsymbol{x}}\left(\tau\,; \varepsilon\right), \boldsymbol{\sigma}\left(\varepsilon\right), \boldsymbol{\delta}\right) d\tau \tag{2.50}$$

Thus,

$$\Delta\tilde{\boldsymbol{x}}(s) = \left.\frac{d\tilde{\boldsymbol{x}}(s;\varepsilon)}{d\varepsilon}\right|_{\varepsilon=0} = \int_0^s \left\{ \frac{\partial\tilde{\boldsymbol{f}}(\tau,\tilde{\boldsymbol{x}}(\tau),\boldsymbol{\sigma},\boldsymbol{\delta})}{\partial\tilde{\boldsymbol{x}}}\Delta\tilde{\boldsymbol{x}}(\tau) + \frac{\partial\tilde{\boldsymbol{f}}(\tau,\tilde{\boldsymbol{x}}(\tau),\boldsymbol{\sigma},\boldsymbol{\delta})}{\partial\boldsymbol{\sigma}}\boldsymbol{\rho} \right\} d\tau \tag{2.51}$$

Clearly,

$$\Delta\dot{\tilde{\boldsymbol{x}}}(s) = \frac{\partial\tilde{\boldsymbol{f}}(s,\tilde{\boldsymbol{x}}(s),\boldsymbol{\sigma},\boldsymbol{\delta})}{\partial\tilde{\boldsymbol{x}}}\Delta\tilde{\boldsymbol{x}}(s) + \frac{\partial\tilde{\boldsymbol{f}}(s,\tilde{\boldsymbol{x}}(s),\boldsymbol{\sigma},\boldsymbol{\delta})}{\partial\boldsymbol{\sigma}}\boldsymbol{\rho} \tag{2.52a}$$

$$\Delta\tilde{\boldsymbol{x}}(0) = 0 \tag{2.52b}$$

Now, $\tilde{g}_i(\boldsymbol{\sigma}(\varepsilon),\boldsymbol{\delta})$ can be expressed as:

$$\begin{aligned}\tilde{g}_i(\boldsymbol{\sigma}(\varepsilon),\boldsymbol{\delta}) = {}& \tilde{\Phi}_i(\tilde{\boldsymbol{x}}(1;\varepsilon),\boldsymbol{\sigma}(\varepsilon),\boldsymbol{\delta}) \\ &+ \int_0^1 \left\{ \tilde{H}_i\left(s,\tilde{\boldsymbol{x}}(s;\varepsilon),\boldsymbol{\sigma}(\varepsilon),\boldsymbol{\delta},\tilde{\boldsymbol{\lambda}}^i(s)\right) - \left(\tilde{\boldsymbol{\lambda}}^i(s)\right)^T \tilde{\boldsymbol{f}}(s,\tilde{\boldsymbol{x}}(s;\varepsilon),\boldsymbol{\sigma}(\varepsilon),\boldsymbol{\delta}) \right\} ds\end{aligned} \tag{2.53}$$

where $\tilde{\boldsymbol{\lambda}}^i$ is yet arbitrary. Thus, it follows that

$$\begin{aligned}\Delta\tilde{g}_i(\boldsymbol{\sigma}(\varepsilon),\boldsymbol{\delta}) = \left.\frac{d\tilde{g}_i(\boldsymbol{\sigma}(\varepsilon),\boldsymbol{\delta})}{d\varepsilon}\right|_{\varepsilon=0} &= \frac{\partial\tilde{g}_i(\boldsymbol{\sigma},\boldsymbol{\delta})}{\partial\boldsymbol{\sigma}}\boldsymbol{\rho} \\ &= \Delta\tilde{\Phi}_i(\tilde{\boldsymbol{x}}(1),\boldsymbol{\sigma},\boldsymbol{\delta}) \\ &\quad + \int_0^1 \left\{ \Delta\tilde{H}_i\left(s,\tilde{\boldsymbol{x}}(s),\boldsymbol{\sigma},\boldsymbol{\delta},\tilde{\boldsymbol{\lambda}}^i(s)\right) - \left(\tilde{\boldsymbol{\lambda}}^i(s)\right)^T \tilde{\boldsymbol{f}}(s,\tilde{\boldsymbol{x}}(s),\boldsymbol{\sigma},\boldsymbol{\delta}) \right\} ds\end{aligned} \tag{2.54}$$

where

$$\Delta\tilde{\Phi}_i(\tilde{\boldsymbol{x}}(1),\boldsymbol{\sigma},\boldsymbol{\delta}) = \frac{\partial\tilde{\Phi}_i(\tilde{\boldsymbol{x}}(1),\boldsymbol{\sigma},\boldsymbol{\delta})}{\partial\tilde{\boldsymbol{x}}}\Delta\tilde{\boldsymbol{x}}(1) \tag{2.55}$$

$$\Delta\tilde{\boldsymbol{f}}(s,\tilde{\boldsymbol{x}}(s),\boldsymbol{\sigma},\boldsymbol{\delta}) = \Delta\dot{\tilde{\boldsymbol{x}}}(s) \tag{2.56}$$

and

$$\begin{aligned}\Delta\tilde{H}_i\left(s,\tilde{\boldsymbol{x}}(s),\boldsymbol{\sigma},\boldsymbol{\delta},\tilde{\boldsymbol{\lambda}}^i(s)\right) = {}& \frac{\partial\tilde{H}_i\left(s,\tilde{\boldsymbol{x}}(s),\boldsymbol{\sigma},\boldsymbol{\delta},\tilde{\boldsymbol{\lambda}}^i(s)\right)}{\partial\tilde{\boldsymbol{x}}}\Delta\tilde{\boldsymbol{x}}(s) \\ &+ \frac{\partial\tilde{H}_i\left(s,\tilde{\boldsymbol{x}}(s),\boldsymbol{\sigma},\boldsymbol{\delta},\tilde{\boldsymbol{\lambda}}^i(s)\right)}{\partial\boldsymbol{\sigma}}\boldsymbol{\rho}\end{aligned} \tag{2.57}$$

Choose $\tilde{\boldsymbol{\lambda}}^i$ to be the solution of the costate system (2.47) corresponding to $\boldsymbol{\sigma}$. Then, by substituting (2.47a) into (2.57), we obtain

$$\Delta\tilde{H}_i\left(s,\tilde{\boldsymbol{x}}(s),\boldsymbol{\sigma},\boldsymbol{\delta},\tilde{\boldsymbol{\lambda}}^i(s)\right) = -\left(\dot{\tilde{\boldsymbol{\lambda}}}^i(s)\right)^T \Delta\tilde{\boldsymbol{x}}(s) + \frac{\partial\tilde{H}_i\left(s,\tilde{\boldsymbol{x}}(s),\boldsymbol{\sigma},\boldsymbol{\delta},\tilde{\boldsymbol{\lambda}}^i(s)\right)}{\partial\boldsymbol{\sigma}}\boldsymbol{\rho} \tag{2.58}$$

Hence, (2.54) yields

$$\begin{aligned}\frac{\partial \tilde{g}_i(\boldsymbol{\sigma},\boldsymbol{\delta})}{\partial \boldsymbol{\sigma}}\boldsymbol{\rho} =& \frac{\partial \tilde{\Phi}_i(\tilde{\boldsymbol{x}}(1),\boldsymbol{\sigma},\boldsymbol{\delta})}{\partial \tilde{\boldsymbol{x}}}\Delta\tilde{\boldsymbol{x}}(1) \\ &+ \int_0^1 \left\{ -\frac{d}{ds}\left[\left(\tilde{\boldsymbol{\lambda}}^i(s)\right)^T \Delta\tilde{\boldsymbol{x}}(s)\right] + \frac{\partial \tilde{H}_i\left(s,\tilde{\boldsymbol{x}}(s),\boldsymbol{\sigma},\boldsymbol{\delta},\tilde{\boldsymbol{\lambda}}^i(s)\right)}{\partial \boldsymbol{\sigma}}\boldsymbol{\rho} \right\} ds \\ =& \frac{\partial \tilde{\Phi}_i(\tilde{\boldsymbol{x}}(1),\boldsymbol{\sigma},\boldsymbol{\delta})}{\partial \tilde{\boldsymbol{x}}}\Delta\tilde{\boldsymbol{x}}(1) - \left(\tilde{\boldsymbol{\lambda}}^i(1)\right)^T \Delta\tilde{\boldsymbol{x}}(1) + \left(\tilde{\boldsymbol{\lambda}}^i(0)\right)^T \Delta\tilde{\boldsymbol{x}}(0) \\ &+ \int_0^1 \left\{ \frac{\partial \tilde{H}_i\left(s,\tilde{\boldsymbol{x}}(s),\sigma,\boldsymbol{\delta},\tilde{\boldsymbol{\lambda}}^i(s)\right)}{\partial \boldsymbol{\sigma}}\boldsymbol{\rho} \right\} ds \end{aligned} \tag{2.59}$$

Substituting (2.47b) and (2.52b) into (2.59), we have

$$\frac{\partial \tilde{g}_i(\boldsymbol{\sigma},\boldsymbol{\delta})}{\partial \boldsymbol{\sigma}}\boldsymbol{\rho} = \int_0^1 \left\{ \frac{\partial \tilde{H}_i\left(s,\tilde{\boldsymbol{x}}(s),\boldsymbol{\sigma},\boldsymbol{\delta},\tilde{\boldsymbol{\lambda}}^i(s)\right)}{\partial \boldsymbol{\sigma}}\boldsymbol{\rho} \right\} ds \tag{2.60}$$

Since $\boldsymbol{\rho}$ is arbitrary, (2.44) follows readily from (2.60). We obtain the gradient formula (2.44). The proof of the validity of (2.45) is similar to that of (2.44). Thus, the proof is complete. □

For each n_p, Problem $\tilde{\mathrm{P}}_p$ is an optimal parameter selection problem, which can be viewed as a nonlinear optimization problem. The gradient formulas of the cost function (2.41) and the constraint functions (2.39) and (2.40) are given in Theorem 2.1, while the constraints (2.30) and (2.34) are just the bounds for the control parameter vector and the time scaling control vector.

At this stage, we see that Problem P is approximated by a sequence of optimal parameter selection problems, each of which can be viewed as a mathematical programming problem and hence can be solved by existing gradient-based optimization methods. The optimal control software MISER 3.3 was implemented based on these ideas, where the control is approximated by piecewise constant functions (i.e., in terms of zero order spline basis functions) or piecewise linear functions (i.e., in terms of first order spline basis functions). It is used here to solve our optimal control problem. Intuitively, the larger the n_p, the closer Problem $\tilde{\mathrm{P}}_p$ is to Problem P. This intuition is true. We shall briefly discuss the convergence issue as follows. Let $(\boldsymbol{\sigma}^{p,*}, \boldsymbol{\delta}^{p,*})$ be the optimal parameter vector of Problem $\tilde{\mathrm{P}}_p$, and let $\tilde{\boldsymbol{u}}^{p,*}$ be the corresponding piecewise constant control given by

$$\tilde{\boldsymbol{u}}^{p,*}(s) = \sum_{k=1}^{n_p} \boldsymbol{\sigma}^{p,*} \chi_{[\frac{k-1}{n_p},\frac{k}{n_p})}(s) \tag{2.61}$$

where

$$\tilde{\boldsymbol{u}}^{p,*} = [\tilde{u}_1^{p,*}, \tilde{u}_2^{p,*}, \tilde{u}_3^{p,*}]^T \tag{2.62}$$

$$\boldsymbol{\sigma}^{p,*} = [(\boldsymbol{\sigma}_1^{p,*})^T, (\boldsymbol{\sigma}_2^{p,*})^T, (\boldsymbol{\sigma}_3^{p,*})^T]^T \tag{2.63}$$

and

$$\boldsymbol{\delta}^{p,*} = [\delta_1^{p,*}, \ldots, \delta_{n_p}^{p,*}]^T \tag{2.64}$$

In the original time horizon $[0, t_f]$, we have

$$\boldsymbol{u}^{p,*}(t) = \sum_{k=1}^{n_p} \boldsymbol{\sigma}^{p,*} \chi_{[\tau_{k-1}^{p,*}, \tau_k^{p,*})}(t) \tag{2.65}$$

where

$$\tau_i^{p,*} = \sum_{k=1}^{i} \delta_k^{p,*}, \quad i = 1, \ldots, n_p \tag{2.66}$$

Furthermore, let $\boldsymbol{u}^*$ be the optimal control of Problem P. In the original time horizon, if the number of the partition points $n_p \to \infty$, then the objective value of the approximate Problem P_p will converge to that of the original Problem P [74], which gives

$$g_0(\boldsymbol{u}^{p,*}) \to g_0(\boldsymbol{u}^*) \tag{2.67}$$

With the time scaling transform (2.32), the partition points become decision variables. Thus, the search space is larger. The varying time points could capture the discontinuities of the optimal control if the number of partition points in the new time horizon is greater or equal to that in the original time horizon. Thus, the optimal value of the objective function of Problem $\tilde{\mathrm{P}}_p$ should be less than or equal to the optimal value of the objective function of Problem P_p. Since the convergence of Problem P_p has been established (see [75]), the convergence of Problem $\tilde{\mathrm{P}}_p$ is guaranteed by the squeeze theorem.

From our extensive simulation study, we observe that n_p does not need to be chosen to be too large. In fact, the difference in the cost values between $n_p = 20$ and those with larger n_p is, in general, very insignificant. Thus, $n_p = 20$ is chosen in our numerical simulation.

2.6 Optimal trajectory tracking

We now move on to consider a situation for which the spacecraft is required to track a desired trajectory, such that the fuel consumption and the terminal time are minimized. To realize such an optimal tracking control problem, we only need to modify the cost

function J of Problem P as:

$$J = m_0 - x_9(t_f) + t_f + \int_0^{t_f} [(x_1(t) - \bar{x}_r(t))^2 + (x_2(t) - \bar{y}_r(t))^2 + (x_3(t) - \bar{z}_r(t))^2]dt \quad (2.68)$$

where $(\bar{x}_r,\ \bar{y}_r,\ \bar{z}_r)$ denotes the desired reference trajectory. Let this optimal trajectory tracking problem be referred to as Problem T. Using the control parameterization technique and the time scaling transform as described in Section 3, Problem T is transformed into Problem $\tilde{\mathrm{T}}_p$, where the transformed cost function

$$\tilde{J} = m_0 - \tilde{x}_9(1) + \tilde{x}_{10}(1) + \int_0^1 [(\tilde{x}_1(s) - \hat{x}_r(s))^2 + (\tilde{x}_2(s) - \hat{y}_r(s))^2 + (\tilde{x}_3(s) - \hat{z}_r(s))^2]ds \quad (2.69)$$

is to be minimized over $\Xi^p \times \Upsilon^p$ subject to the system dynamic (2.35) with initial condition (2.37) and the terminal state constraints (2.39) and (2.40), where $\hat{x}_r(s) = \bar{x}_r(t(s))$, $\hat{y}_r(s) = \bar{y}_r(t(s))$, $\hat{z}_r(s) = \bar{z}_r(t(s))$.

The gradient formulas of the cost function (2.69) and constraint functions (2.39) and (2.40) can be derived in the same way as those given for the gradient formulas of the cost function and the constraint functions of Problem $\tilde{\mathrm{P}}_p$ given in Theorem 2.1. The optimal control parameter selection problem $\tilde{\mathrm{T}}_p$ is thus solved by utilizing the optimal control software MISER 3.3.

2.7 Numerical simulations

The initial conditions of the lunar module are given as: $x_{L0} = 8.19371 \times 10^5$m, $y_{L0} = 1.428867 \times 10^6$m, $z_{L0} = 5.996306 \times 10^5$m, $V_{xL0} = 1115$m/s, $V_{yL0} = -981.82$m/s, $V_{zL0} = 816$m/s, $m_0 = 600$kg. At the initial time of the soft landing, the rotational angle $\gamma(t_0) = 0°$. Specific impulse $V_r = 300 \times 9.8$m/s and the angular velocity of the moon rotation $\omega_L = 2.661699 \times 10^{-6}$rad/s.

We first consider the task of achieving the soft landing of the lunar module. The landing target is in Mare Imbrium on the moon surface, which is located at 38.628° North latitude and 36.806° West longitude. Control variables are chosen subject to the bounds: $0 \text{ kg/s} \le \sigma_1^k \le 0.51 \text{ kg/s}$, $\left|\sigma_2^k\right| \le 1\ °/\text{s}$, $\left|\sigma_3^k\right| \le 1\ °/\text{s}$, $k = 1, 2, \ldots, n_p$. Terminal separation angle of the module between its longitudinal axis and the plumb line is $\vartheta_{t_f} = 5°$. The scaled time interval is $s \in [0, 1]$, which is partitioned into 20 equal subintervals. Terminal time of the soft landing is free to vary. The corresponding optimal parameter selection problem is then solved by using the software MISER 3.3. Terminal conditions of the lunar module obtained are listed below.

$$x_L(t_f) = 1.0871218 \times 10^6 m,\ y_L(t_f) = 1.0849749 \times 10^6 m,\ z_L(t_f) = 8.134568 \times 10^5$$

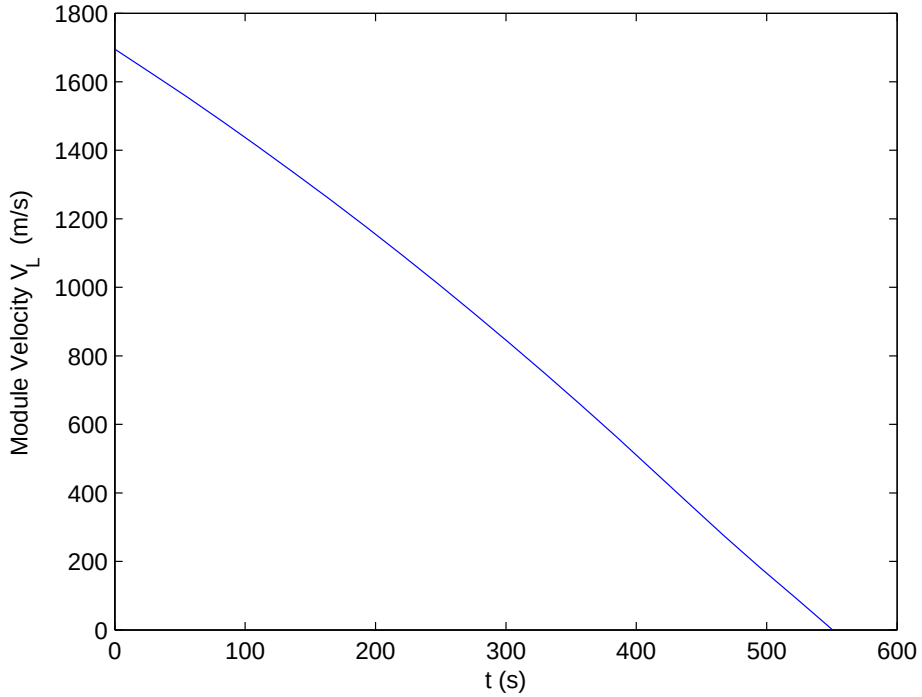

Figure 2.3: Module Velocity V_L

$$V_{xL}(t_f) = 1 \times 10^{-4}\text{m/s},\ V_{yL}(t_f) = 0\text{m/s},\ V_{zL}(t_f) = 2 \times 10^{-4}\text{m/s}$$

Figure 2.3 shows the time history of the lunar module velocity in the original time horizon $[0, t_f]$. We see that it converges smoothly to zero as the module lands on the moon. Figures 2.4 – 2.6 are optimal control outputs during the period of soft landing, also in the original time horizon $[0, t_f]$. Here, we see that the reverse force thruster works at its maximum thrust force all the time, while the two angular velocity controllers are operating within their bounds. Under the optimal control law, the lunar module is guided to the target precisely, and the optimal descent trajectory is shown in Figure 2.8. Terminal mass of the module is 319.2728kg. Figure 2.7 depicts the time scaling control. Lunar module lands on the moon surface vertically after 550.4455s, with the terminal separation angle between the module longitudinal axis and the plumb line $\vartheta(t_f) = -4.998^\circ$.

Our next task is to investigate the mission of the optimal trajectory tracking. Suppose the desired trajectory is the one obtained from the solution of Problem P. Suppose that the initial position of the lunar module is given as $x_{L0} = 8.18348 \times 10^5$m, $y_{L0} = 1.428821 \times 10^6$m, $z_{L0} = 6.01136 \times 10^5$m, which are different from those for Problem P. It is obvious that, from the perturbed initial point, the optimal control obtained by solving Problem P can not guarantee a precise soft landing of the module to the desired target. Here, we let this optimal tracking problem be referred to as Problem T. It is transformed to Problem $\tilde{\text{T}}_p$ and solved by using the approach detailed in Section 4, where the optimal control software MISER 3.3 is utilized. The optimal control obtained for Problem P is used as

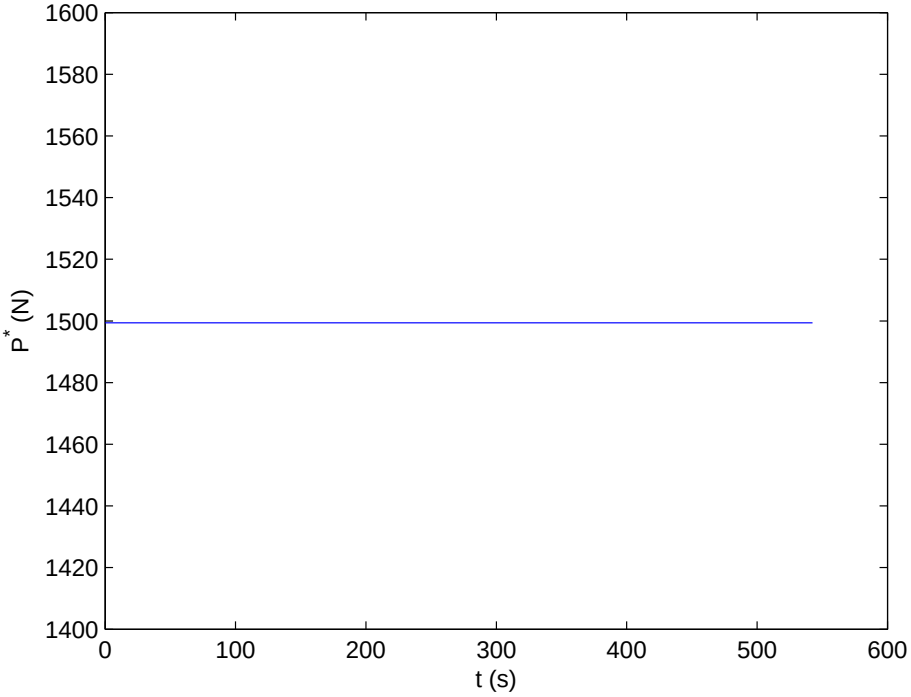

Figure 2.4: Thrust force P^*

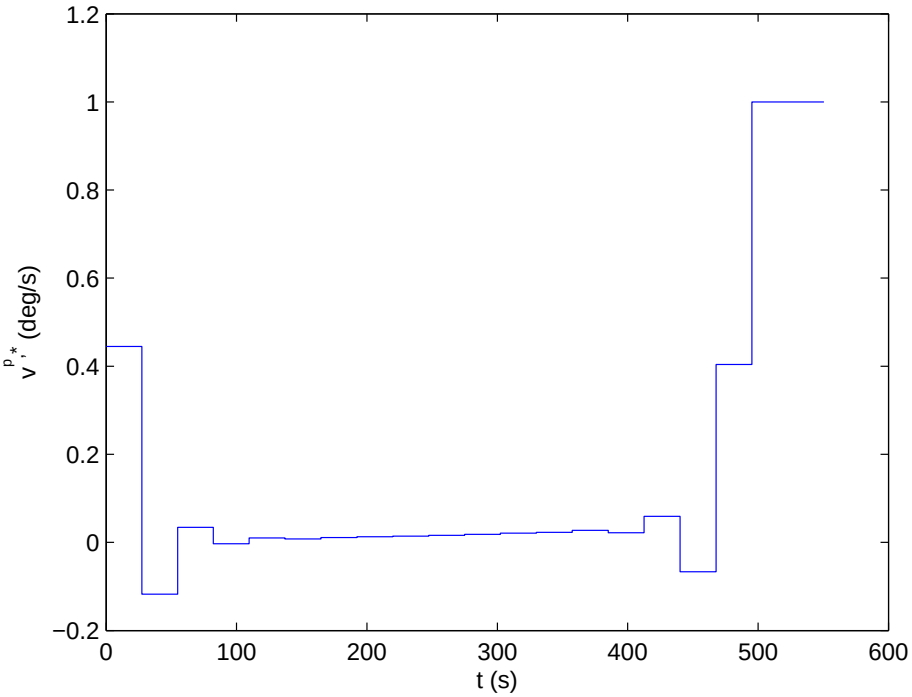

Figure 2.5: Angular velocity $v^{p,*}$

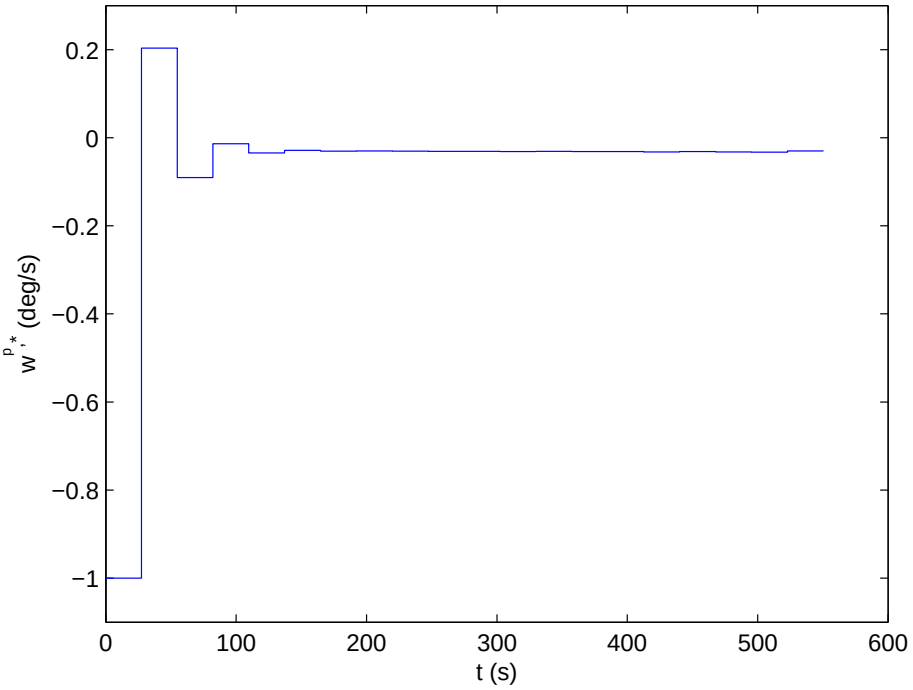

Figure 2.6: Angular velocity $w^{p,*}$

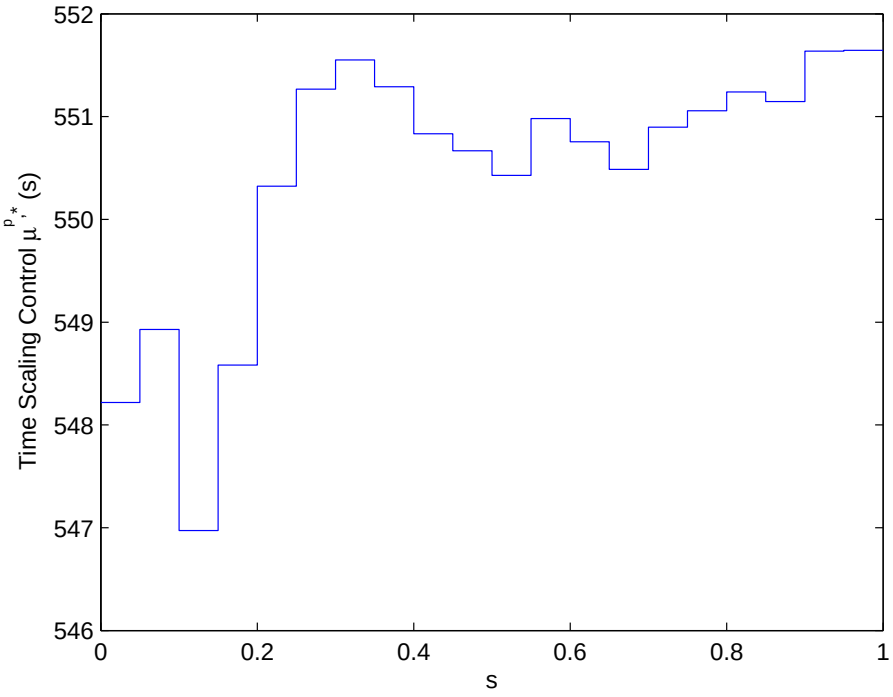

Figure 2.7: Time scaling control $\mu^{p,*}$

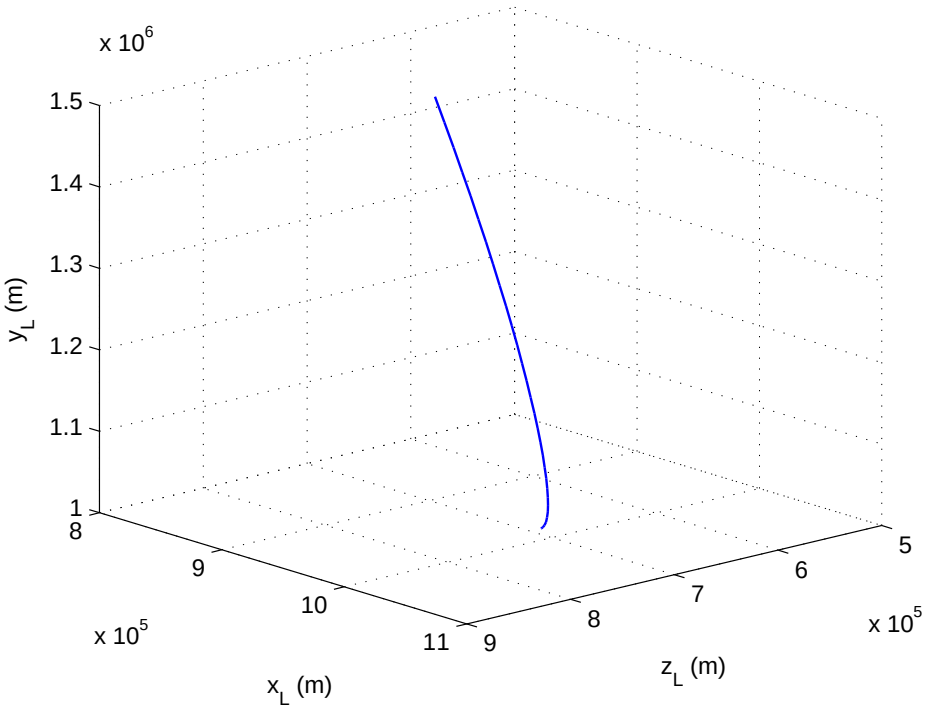

Figure 2.8: Optimal descent trajectory

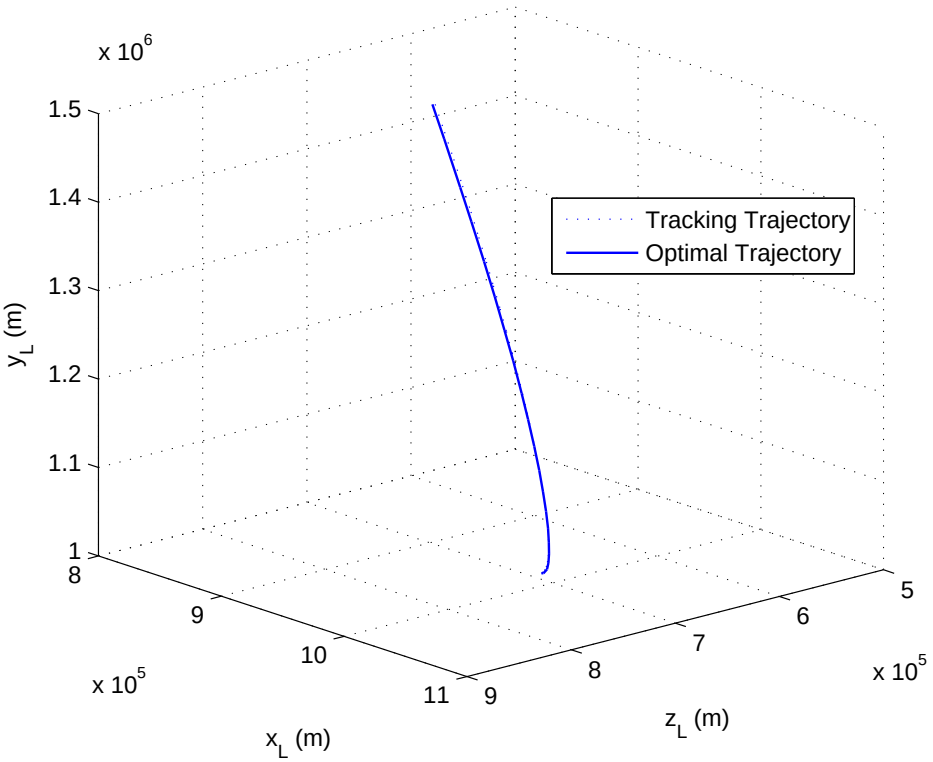

Figure 2.9: Optimal trajectory tracking

the initial guess for the search of the optimal control of Problem $\tilde{\mathrm{T}}_p$. Let the optimal control of Problem $\tilde{\mathrm{T}}_p$ obtained be denoted as $\boldsymbol{\upsilon}^*$. Then, under this control, the Lunar module is guided to the target at the terminal time $t_f = 572.8$s. The terminal velocity is 6.2e-4m/s, while the terminal mass is 315.43kg. From Figure 2.9, we see that the optimal trajectory tracks the desired trajectory satisfactorily.

2.8 Conclusion

In this chapter, we studied the optimal control problem of the lunar module soft landing with minimum fuel consumption and flight time. To describe the motion of the module precisely, we derived the three-dimensional dynamics for the lunar module in the powered descent phase, where the moon rotation is explicitly taken into consideration. The constraints on the control and the terminal state are also considered. By using the control parameterization technique and the time scaling transform, the optimal control problem is approximated as an optimal parameter selection problem which has a finite number of decision variables. Then, the optimal control software package MISER 3.3, which is a gradient-based method, is utilized to solve such a parameter selection problem, and an optimal control law is thus obtained.

This optimal control law steers the lunar module to achieve the pre-specified landing target precisely in such a way that the fuel consumption and the terminal time are minimized. The module touches down on the moon vertically with reference to the lunar surface. The same approaches are also used to deal with the task of optimal trajectory tracking where a reference trajectory of the module is to be followed. Simulation results demonstrate that the proposed approach is highly effective.

CHAPTER 3

Nonlinear optimal feedback control for lunar module soft landing

3.1 Introduction

In Chapter 2, we designed an open loop optimal guidance law for achieving the lunar module soft landing with the minimum fuel consumption and flying time. The flight of the module starts from the perilune, which is 15km above the moon, and ends on the lunar surface. In the open loop controller design, some unpredicted situations, such as initial point perturbations, are not considered. The control law may be sensitive to these situations. Thus, we propose, in this chapter, a feedback control law for the powered deceleration phase of the lunar module soft landing, which starts from the perilune and ends at a point 2km high above the moon surface. It is known that a feedback control law is more preferable to an open loop control law due to its robustness against perturbations.

As in the previous chapter, the motion of the lunar module is described in a three dimensional coordinate system. Based on the nonlinear dynamics of the module, we obtain the form of an optimal closed loop control law, where a feedback gain matrix is involved. It is then shown that this feedback gain matrix satisfies a Riccati-like matrix differential equation. Then, it is approximated in terms of the third order B-spline functions. It is known [59] that the third order B-spline functions are effective for continuous function approximation. The optimal control problem is first solved as an open loop optimal control problem by using the time scaling transform and the control parameterization method. By virtue of the relationship between the optimal open loop control and the optimal closed loop control along the optimal trajectory, we present a practical method to calculate an approximate optimal feedback gain matrix, without having to solve an optimal control problem involving the complex Riccati-like matrix differential equation coupled with the original system dynamics.

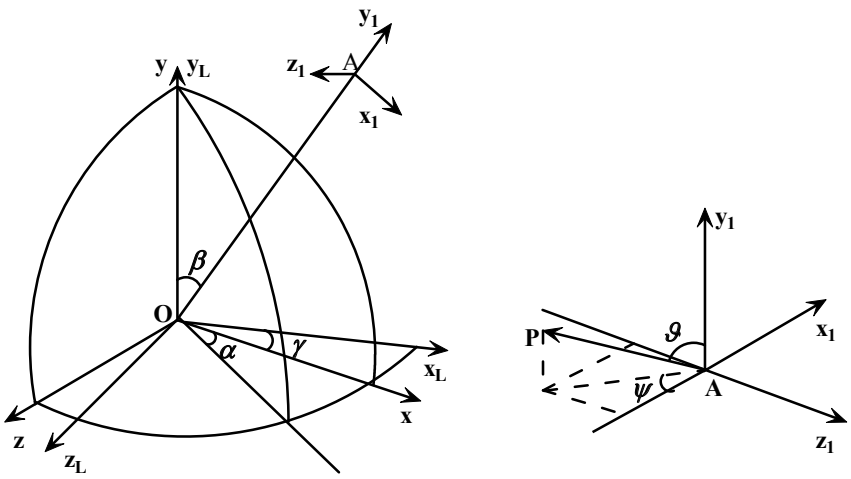

Figure 3.1: Three-dimensional coordinate systems.

3.2 Problem formulation

The motion of the lunar module soft landing is described in the three-dimensional coordinate system as depicted in Figure 2.2, Chapter 2. For convenience, we redraw the figure here, see Figure 3.1. Definitions of the elements appeared in Figure 3.1 are the same as those in Figure 2.2, Chapter 2.

The dynamic equations that describe the motion of the lunar module are rewritten as:

$$\begin{cases} \dot{x}_L = V_{xL} \\ \dot{y}_L = V_{yL} \\ \dot{z}_L = V_{zL} \\ \dot{V}_{xL} = BQV_r/m - g_{xL} - 2\omega_L V_{zL} \\ \dot{V}_{yL} = CQV_r/m - g_{yL} \\ \dot{V}_{zL} = DQV_r/m - g_{zL} + 2\omega_L V_{xL} \\ \dot{m} = -Q \end{cases} \tag{3.1}$$

where

$$\begin{aligned} B =& (\cos\alpha\cos\beta\cos\gamma - \sin\alpha\sin\gamma)\sin\vartheta\cos\psi \\ & -(\sin\alpha\cos\beta\cos\gamma + \cos\alpha\sin\gamma)\sin\vartheta\sin\psi + \sin\beta\cos\gamma\cos\vartheta, \\ C =& -\cos\alpha\sin\beta\sin\vartheta\cos\psi + \cos\beta\cos\vartheta + \sin\alpha\sin\beta\sin\vartheta\sin\psi, \\ D =& (\cos\alpha\cos\beta\sin\gamma + \sin\alpha\cos\gamma)\sin\vartheta\cos\psi \\ & -(\sin\alpha\cos\beta\sin\gamma - \cos\alpha\cos\gamma)\sin\vartheta\sin\psi + \sin\beta\sin\gamma\cos\vartheta, \end{aligned}$$

while x_L, y_L, z_L and V_{xL}, V_{yL}, V_{zL} are the positions and velocities in the Lunar Fixed

Coordinate system, m is the mass of the lunar module, Q and V_r represent, respectively, the fuel consumption rate and the specific impulse of the thruster, g_{xL}, g_{yL} and g_{zL} denote the respective components of the lunar gravity in $ox_Ly_Lz_L$, and ω_L is the angular velocity of the moon rotation.

Introduce two new state equations

$$\dot{\vartheta} = v \tag{3.2}$$

$$\dot{\psi} = w \tag{3.3}$$

and let

$$\begin{aligned} \boldsymbol{x} &= [x_L, y_L, z_L, V_{xL}, V_{yL}, V_{zL}, \vartheta, \psi, m]^T \\ &= [x_1, x_2, x_3, x_4, x_5, x_6, x_7, x_8, x_9]^T \end{aligned} \tag{3.4}$$

$$\boldsymbol{u} = [Q, v, w]^T = [u_1, u_2, u_3]^T \tag{3.5}$$

The original system dynamics (3.1) can be rewritten in the form of a nonlinear affine system given below:

$$\dot{\boldsymbol{x}}(t) = \boldsymbol{f}(\boldsymbol{x}(t)) + \boldsymbol{B}(\boldsymbol{x}(t), t)\boldsymbol{u}(t), \tag{3.6}$$

where $\boldsymbol{x} \in \mathbb{R}^9$, $\boldsymbol{u} \in \mathbb{R}^3$ and

$$\boldsymbol{f}(\boldsymbol{x}) = [x_4, x_5, x_6, -g_{xL} - 2\omega_L x_6, -g_{yL}, -g_{zL} + 2\omega_L x_4, 0, 0, 0]^T, \tag{3.7}$$

$$\boldsymbol{B}(\boldsymbol{x}, t) = \begin{bmatrix} 0 & 0 & 0 & M_1 & M_2 & M_3 & 0 & 0 & -1 \\ 0 & 0 & 0 & 0 & 0 & 0 & 1 & 0 & 0 \\ 0 & 0 & 0 & 0 & 0 & 0 & 0 & 1 & 0 \end{bmatrix}^T \tag{3.8}$$

while

$$\begin{aligned} M_1 = [&(\cos\alpha\cos\beta\cos\gamma - \sin\alpha\sin\gamma)\sin x_7\cos x_8 \\ &- (\sin\alpha\cos\beta\cos\gamma + \cos\alpha\sin\gamma)\sin x_7\sin x_8 \\ &+ \sin\beta\cos\gamma\cos x_7]V_r/x_9, \end{aligned} \tag{3.9}$$

$$\begin{aligned} M_2 = (&-\cos\alpha\sin\beta\sin x_7\cos x_8 + \sin\alpha\sin\beta\sin x_7\sin x_8 \\ &+ \cos\beta\cos x_7)V_r/x_9, \end{aligned} \tag{3.10}$$

and

$$\begin{aligned} M_3 = [&(\cos\alpha\cos\beta\sin\gamma + \sin\alpha\cos\gamma)\sin x_7\cos x_8 \\ &- (\sin\alpha\cos\beta\sin\gamma - \cos\alpha\cos\gamma)\sin x_7\sin x_8 \\ &+ \sin\beta\sin\gamma\cos x_7]V_r/x_9 \end{aligned} \tag{3.11}$$

For u_1, the first component of the control $\boldsymbol{u}$, it is required to satisfy the boundedness conditions given below.

$$\alpha_1 \le u_1(t) \le \beta_1, \quad \forall\, t \in [0, T] \tag{3.12}$$

We do not impose any bound on the other two components of the control $\boldsymbol{u}$. Let $\mathcal{U}$ be the set of all such controls $\boldsymbol{u} = [u_1, u_2, u_3]^T$. Elements from $\mathcal{U}$ are called admissible controls and $\mathcal{U}$ is referred to as the class of admissible controls.

The initial conditions of the soft landing are determined by the state of the lunar module in the perilune at the initial time $t_0 = 0$ and are given by

$$\boldsymbol{x}(t_0) = [x_{L0}, y_{L0}, z_{L0}, V_{xL_0}, V_{yL_0}, V_{zL0}, \vartheta_0, \psi_0, m_0]^T \tag{3.13}$$

Our aim is to design an optimal closed loop control law to achieve the powered deceleration phase of the lunar module soft landing such that a linear combination of the fuel consumption and the terminal time are minimized, while the terminal velocity should be approximately zero at the terminal time. This optimal control problem can be formulated as follows.

Problem Q. *Given system (3.6) with the initial condition (3.13), find a closed loop control $\boldsymbol{u} \in \mathcal{U}$ such that the cost function*

$$J = a_1 \Phi_0(\boldsymbol{x}(T)) + a_2 \int_0^T \boldsymbol{u}^T \boldsymbol{R}\, \boldsymbol{u}\, dt, \tag{3.14}$$

is minimized, where $\Phi_0(\boldsymbol{x}(T)) = (\boldsymbol{x}(T) - \boldsymbol{x}_d)^T \boldsymbol{S}(\boldsymbol{x}(T) - \boldsymbol{x}_d) + T$, T is the free terminal time of the soft landing, $\boldsymbol{x}_d$ is the desired terminal state vector, a_1 and a_2 are the weighting parameters which can be chosen according to the magnitudes of their corresponding terms in the cost function, $\boldsymbol{S} \in \mathbb{R}^{9\times 9}$ and $\boldsymbol{R} \in \mathbb{R}^{3\times 3}$ are, respectively, symmetric positive semidefinite and symmetric positive definite weighting matrices.

3.3 Optimal computation control

We first proceed to solve Problem Q as an optimal open loop control problem by using the time scaling transform and the control parameterization technique. This will provide us with an optimal open loop control and the corresponding optimal trajectory.

Let the time horizon $[0, T]$ be partitioned into p subintervals as follows:

$$0 = t_0 \le t_1 \le \cdots \le t_p = T. \tag{3.15}$$

The switching times t_k , $1 \le k \le p$, are regarded as decision variables. We shall employ the time scaling transform to map these switching times into a set of fixed time points $\eta_k = k/p$, $k = 1, \ldots, p$, on a new time horizon $[0, 1]$. This is easily achieved by the following differential equation

$$\frac{dt(s)}{ds} = \upsilon^p(s), \quad s \in [0, 1], \tag{3.16a}$$

with initial condition

$$t(0) = 0, \tag{3.16b}$$

where

$$\upsilon^p(s) = \sum_{k=1}^{p} \zeta_k \chi_{[\eta_{k-1}, \eta_k]}(s). \tag{3.17}$$

Here, $\chi_I(s)$ denotes the indicator function of I defined by

$$\chi_I(s) = \begin{cases} 1, \ s \in I \\ 0, \ \text{elsewhere} \end{cases} \tag{3.18}$$

and $\zeta_k \geq 0$, $k = 1, \ldots, p$,

$$\sum_{k=1}^{p} \zeta_k = T. \tag{3.19}$$

Let $\boldsymbol{\zeta} = [\zeta_1, \ldots, \zeta_p]^T$ and let Θ be the set containing all such $\boldsymbol{\zeta}$.

Taking integration of (3.16a) with initial condition (3.16b), it is easy to see that, for $s \in [\eta_{l-1}, \eta_l)$,

$$t(s) = \sum_{k=1}^{l-1} \zeta_k + \zeta_l (s - \eta_{l-1}) p, \tag{3.20a}$$

where $l = 1, \ldots, p$. Clearly,

$$t(1) = \sum_{k=1}^{p} \zeta_k = T. \tag{3.20b}$$

Thus, after the time scaling transform (3.16a) and (3.16b), it follows from (3.6), (3.16a) and (3.16b) that

$$\dot{\hat{\boldsymbol{x}}}(s) = \upsilon^p(s) \left\{ \boldsymbol{f}(\hat{\boldsymbol{x}}(s)) + \boldsymbol{B}(\hat{\boldsymbol{x}}(s), s) \tilde{\boldsymbol{u}}(s) \right\} \tag{3.21a}$$

with the initial condition

$$\hat{\boldsymbol{x}}(0) = \begin{bmatrix} \boldsymbol{x}^0 \\ 0 \end{bmatrix}, \tag{3.21b}$$

where $\hat{\boldsymbol{x}}(s) = [\tilde{\boldsymbol{x}}(s)^T, \, t(s)]^T$, $\tilde{\boldsymbol{x}}(s) = \boldsymbol{x}(t(s))$ and $\tilde{\boldsymbol{u}}(s) = \boldsymbol{u}(t(s))$.

We now apply the control parameterization technique to approximate the control $\tilde{\boldsymbol{u}}(s) = [\tilde{u}_1(s), \tilde{u}_2(s), \tilde{u}_3(s)]^T$ as follows.

$$\tilde{u}_i^p(s) = \sum_{k=-1}^{p+1} \sigma_k^i \Omega((\frac{1}{p})s - k), \quad i = 1, 2, 3, \tag{3.22}$$

where

$$\Omega(\tau) = \begin{cases} 0, & |\tau| > 2 \\ -\frac{1}{6}|\tau|^3 + \tau^2 - 2|\tau| + \frac{4}{3}, & 1 \leq |\tau| \leq 2 \\ \frac{1}{2}|\tau|^3 - \tau^2 + \frac{2}{3}, & |\tau| < 1 \end{cases} \tag{3.23}$$

is the cubic spline basis function, σ_k^i, $i = 1, 2, 3$; $k = -1, 0, 1, \ldots, p+1$, are decision variables.

From (3.12), we have

$$\alpha_1 \leq \sigma_k^1 \leq \beta_1, \quad k = -1, 0, 1, \ldots, p+1. \tag{3.24}$$

Define

$$\boldsymbol{\sigma}^i = [\sigma_{-1}^i, \cdots, \sigma_{p+1}^i]^T, \quad i = 1, 2, 3, \tag{3.25}$$

and

$$\boldsymbol{\sigma} = [(\boldsymbol{\sigma}^1)^T, (\boldsymbol{\sigma}^2)^T, (\boldsymbol{\sigma}^3)^T]^T \tag{3.26}$$

Let Ξ denote the set containing all such $\boldsymbol{\sigma}$. Then, $\tilde{\boldsymbol{u}}^p(s) = [\tilde{u}_1^p(s), \tilde{u}_2^p(s), \tilde{u}_3^p(s)]^T$ is determined uniquely by the switching vector $\boldsymbol{\sigma}$ in Ξ, and vice verse. Thus, it is written as $\tilde{\boldsymbol{u}}^p(\bullet|\boldsymbol{\sigma})$. We may now state the optimal parameterization selection problem, which is an approximation of Problem Q, as follows:

Problem $\tilde{\mathrm{Q}}_p$. *Given system (3.21a) with initial condition (3.21b), find a combined vector $(\boldsymbol{\sigma}, \boldsymbol{\zeta}) \in \Xi \times \Theta$, such that the cost function*

$$J(\boldsymbol{\sigma}) = a_1 \hat{\Phi}_0(\hat{\boldsymbol{x}}(1|\boldsymbol{\sigma})) + a_2 \int_0^1 \upsilon^p(s|\boldsymbol{\zeta}) \tilde{\boldsymbol{u}}^p(s|\boldsymbol{\sigma})^T \boldsymbol{R} \tilde{\boldsymbol{u}}^p(s|\boldsymbol{\sigma})\, ds \tag{3.27}$$

is minimized, where $\hat{\Phi}_0(\hat{\boldsymbol{x}}(1|\boldsymbol{\sigma})) = (\hat{\boldsymbol{x}}(1|\boldsymbol{\sigma}) - \hat{\boldsymbol{x}}_d)^T \hat{\boldsymbol{S}} (\hat{\boldsymbol{x}}(1|\boldsymbol{\sigma}) - \hat{\boldsymbol{x}}_d)$, $\hat{\boldsymbol{x}}_d$ is the desired terminal state vector, $\hat{\boldsymbol{S}} \in \mathbb{R}^{10\times 10}$, and $\tilde{\boldsymbol{u}}^p$ is given by (3.22).

As in Chapter 2, Problem Q is approximated by a sequence of optimal parameter selection problems, each of which can be viewed as a mathematical programming problem and hence can be solved by existing gradient-based optimization methods. Again, we use MISER 3.3 to solve the optimal control problem. Here, our controls are approximated in terms of cubic spline basis functions, and thus they are smooth. MISER 3.3 can be easily modified to cater for this minor modification.

Suppose that $(\tilde{\boldsymbol{u}}^{p*}, \hat{\boldsymbol{x}}^*)$ is the optimal solution of Problem $\tilde{\mathrm{Q}}_p$. Then, from (3.20a) and (3.20b), it follows that the optimal solution to Problem Q is $(\boldsymbol{u}^*, \boldsymbol{x}^*, T^*)$, where $\boldsymbol{u}^* = [u_1^*, u_2^*, u_3^*]^T$ is the optimal open loop control, $\boldsymbol{x}^*$ is the corresponding optimal state vector, and T^* is the optimal terminal time. In view of the optimal open loop control obtained, we notice that the reverse force thruster, u_1^*, works with its maximum thrust force (i.e., at its upper bound which is a constant value) throughout the entire soft landing process. This observation is confirmed by Pontryagin Maximum Principle (see [104]). Thus, for the computation of the optimal closed loop control problem, we set the first control variable of $\boldsymbol{u}$ to be equal to the constant value obtained through solving Problem Q as an open loop optimal control problem.

Correspondingly, system (3.6) can be rewritten as

$$\dot{\boldsymbol{x}}(t) = \bar{\boldsymbol{f}}(\boldsymbol{x}(t), t) + \bar{\boldsymbol{B}}\bar{\boldsymbol{u}}(t), \tag{3.28}$$

where

$$\bar{\boldsymbol{f}}(\boldsymbol{x}, t) = [x_4, x_5, x_6, -g_{xL} - 2\omega_L x_6 + cM_1, -g_{yL} + cM_2, -g_{zL} + 2\omega_L x_4 + cM_3, 0, 0, -c]^T \tag{3.29}$$

$$\bar{\boldsymbol{B}} = \begin{bmatrix} 0 & 0 & 0 & 0 & 0 & 0 & 1 & 0 & 0 \\ 0 & 0 & 0 & 0 & 0 & 0 & 0 & 1 & 0 \end{bmatrix}^T \tag{3.30}$$

while M_1, M_2 and M_3 remain the same as given by (3.9), (3.10) and (3.11), respectively. The new control vector $\bar{\boldsymbol{u}}$ is

$$\bar{\boldsymbol{u}} = [v, w]^T = [\bar{u}_1, \bar{u}_2]^T \tag{3.31}$$

Let $\bar{\mathcal{U}}$ be the set of all such controls. Elements from $\bar{\mathcal{U}}$ are called admissible controls and $\bar{\mathcal{U}}$ is referred to as the class of admissible controls.

The initial condition of the soft landing remains the same as given by (3.13). The cost function (3.14) can be rewritten as:

$$\bar{J} = a_1 \Phi_0(\boldsymbol{x}(T)) + a_2 \int_0^T \bar{\boldsymbol{u}}^T \bar{\boldsymbol{R}}\, \bar{\boldsymbol{u}} dt, \tag{3.32}$$

where $\bar{\boldsymbol{R}} \in \mathbb{R}^{2\times 2}$ is a symmetric positive definite matrix obtained from $\boldsymbol{R}$.

Now, the original optimal control Problem Q is reduced to Problem ($\bar{\text{Q}}$) given below.

Problem $\bar{\text{Q}}$. *Given system (3.28) with the initial condition (3.13), find a closed loop control such that the cost function (3.32) is minimized.*

For Problem ($\bar{\text{Q}}$), we have the following theorem.

Theorem 3.1. *The optimal closed loop control $\bar{\boldsymbol{u}}^*$ for Problem ($\bar{\text{Q}}$) is given by*

$$\bar{\boldsymbol{u}}^*(t) = \frac{1}{2a_2} \bar{\boldsymbol{R}}^{-1} \bar{\boldsymbol{B}}^T \boldsymbol{K}(t) \bar{\boldsymbol{f}}(\boldsymbol{x}^*(t), t), \tag{3.33}$$

where $\boldsymbol{x}^*$ is the optimal state, i.e. the solution of system (3.28) with initial condition (3.13) corresponding to $\bar{\boldsymbol{u}}^*$, and $\boldsymbol{K}(t)$ is the solution of the following Riccati-like differential equation

$$(\dot{\boldsymbol{K}} + \boldsymbol{K}\boldsymbol{F} + \boldsymbol{F}^T\boldsymbol{K} + \frac{1}{2}\boldsymbol{K}\boldsymbol{F}\bar{\boldsymbol{B}}\bar{\boldsymbol{R}}^{-1}\bar{\boldsymbol{B}}^T\boldsymbol{K})\bar{\boldsymbol{f}} + \boldsymbol{K}\boldsymbol{D} = 0, \tag{3.34a}$$

Here, $\boldsymbol{F} = \partial\, \bar{\boldsymbol{f}} / \partial\, \boldsymbol{x}$, $\boldsymbol{D} = \partial\, \bar{\boldsymbol{f}} / \partial\, t$, and

$$\boldsymbol{K}(T)\bar{\boldsymbol{f}}(\boldsymbol{x}(T), T) = a_1 \frac{\partial\, \Phi_0(\boldsymbol{x}(T))}{\partial\, \boldsymbol{x}(T)} = 2a_1(\boldsymbol{x}(T) - \boldsymbol{x}_d)^T \boldsymbol{S}. \tag{3.34b}$$

Proof. The proof is similar to that given for Theorem 3.1 in [36]. Let H be the Hamiltonian function defined by

$$H(\boldsymbol{x}(t), \bar{\boldsymbol{u}}(t), \boldsymbol{\lambda}(t)) = \boldsymbol{\lambda}^T(t)\bar{\boldsymbol{f}}(\boldsymbol{x}(t), t) + \boldsymbol{\lambda}^T(t)\bar{\boldsymbol{B}}\bar{\boldsymbol{u}}(t) - a_2\bar{\boldsymbol{u}}^T(t)\bar{\boldsymbol{R}}\bar{\boldsymbol{u}}(t), \tag{3.35}$$

where $\boldsymbol{\lambda}(t) \in \mathbb{R}^9$ is the costate vector.

Suppose that $(\bar{\boldsymbol{u}}^*, \boldsymbol{x}^*)$ is an optimal pair. Then, it follows from Pontryagin Maximum Principle that

$$(i) \quad \dot{\boldsymbol{x}}^*(t) = \left(\frac{\partial H^*}{\partial \boldsymbol{\lambda}(t)}\right)^T = \bar{\boldsymbol{f}}(\boldsymbol{x}^*(t), t) + \bar{\boldsymbol{B}}\bar{\boldsymbol{u}}^*(t) \tag{3.36}$$

$$(ii) \quad \boldsymbol{x}^*(0) = \boldsymbol{x}_0 \tag{3.37}$$

$$(iii) \quad \dot{\boldsymbol{\lambda}}^*(t) = -\left(\frac{\partial H^*}{\partial \boldsymbol{x}^*(t)}\right)^T \tag{3.38}$$

$$(iv) \quad \boldsymbol{\lambda}^*(T) = a_1\frac{\partial \Phi_0(\boldsymbol{x}^*(T))}{\partial \boldsymbol{x}^*(T)} = 2a_1(\boldsymbol{x}^*(T) - \boldsymbol{x}_d)^T\boldsymbol{S} \tag{3.39}$$

$$(v) \quad \frac{\partial H^*}{\partial \bar{\boldsymbol{u}}^*(t)} = 0 \tag{3.40}$$

$$(vi) \quad H^*|_{t=T} = 0 \tag{3.41}$$

where $H^* = H(\boldsymbol{x}^*(t),\ \bar{\boldsymbol{u}}^*(t),\ \boldsymbol{\lambda}^*(t))$ and the terminal time T is determined by solving Problem Q.

From (3.40), we obtain

$$\bar{\boldsymbol{u}}^*(t) = \frac{1}{2a_2}\bar{\boldsymbol{R}}^{-1}\bar{\boldsymbol{B}}^T\boldsymbol{\lambda}^*(t) \tag{3.42}$$

As in [42], we postulate that the costate vector $\boldsymbol{\lambda}^*(t)$ can be expressed as

$$\boldsymbol{\lambda}^*(t) = \boldsymbol{K}(t)\bar{\boldsymbol{f}}(\boldsymbol{x}^*(t), t) \tag{3.43}$$

Then, it follows that

$$\bar{\boldsymbol{u}}^*(t) = \frac{1}{2a_2}\bar{\boldsymbol{R}}^{-1}\bar{\boldsymbol{B}}^T\boldsymbol{K}(t)\bar{\boldsymbol{f}}(\boldsymbol{x}^*(t), t) \tag{3.44}$$

Differentiating (3.43) with respective to t, we deduce from (3.36) and (3.44) that

$$\dot{\boldsymbol{\lambda}}^*(t) = (\dot{\boldsymbol{K}} + \boldsymbol{K}\boldsymbol{F} + \frac{1}{2a_2}\boldsymbol{K}\boldsymbol{F}\bar{\boldsymbol{B}}\bar{\boldsymbol{R}}^{-1}\bar{\boldsymbol{B}}^T\boldsymbol{K})\bar{\boldsymbol{f}}(\boldsymbol{x}^*(t), t) + \boldsymbol{K}\boldsymbol{D} \tag{3.45}$$

From (3.38) and (3.43), we obtain

$$\dot{\boldsymbol{\lambda}}^*(t) = -\boldsymbol{F}^T\boldsymbol{K}(t)\bar{\boldsymbol{f}}(\boldsymbol{x}^*(t), t) \tag{3.46}$$

Combining (3.45) and (3.46), we have

$$(\dot{\boldsymbol{K}} + \boldsymbol{K}\boldsymbol{F} + \boldsymbol{F}^T\boldsymbol{K} + \frac{1}{2a_2}\boldsymbol{K}\boldsymbol{F}\bar{\boldsymbol{B}}\bar{\boldsymbol{R}}^{-1}\bar{\boldsymbol{B}}^T\boldsymbol{K})\bar{\boldsymbol{f}} + \boldsymbol{K}\boldsymbol{D} = 0 \tag{3.47}$$

From (3.39), the terminal condition for the Riccati-like differential equation (3.47) is obtained as

$$\boldsymbol{\lambda}(T) = a_1 \frac{\partial \Phi_0(\boldsymbol{x}(T))}{\partial \boldsymbol{x}(T)} = 2a_1(\boldsymbol{x}(T) - \boldsymbol{x}_d)^T \boldsymbol{S} \tag{3.48}$$

This completes the proof. □

By Theorem 3.1, we observe that the form of the optimal closed loop control law for Problem ($\bar{\text{Q}}$) is given by

$$\bar{\boldsymbol{u}}(t) = \frac{1}{2a_2} \bar{\boldsymbol{R}}^{-1} \bar{\boldsymbol{B}}^T \boldsymbol{K}(t) \bar{\boldsymbol{f}}(\boldsymbol{x}(t), t) \tag{3.49}$$

However, the matrix function $\boldsymbol{K}(t)$ is still required to be obtained. This task is, in fact, rather demanding. It involves solving a new optimal control problem, which we call Problem R.

Problem R. *subject to the dynamical systems given by (3.28), (3.13), (3.34a) and (3.34b), with* $\bar{\boldsymbol{u}} = \bar{\boldsymbol{R}}^{-1} \bar{\boldsymbol{B}}^T \boldsymbol{K}(t) \bar{\boldsymbol{f}}(\boldsymbol{x}(t), t)/2a_2$*, find a* $\boldsymbol{K}(t)$ *such that the cost function (3.32), also with* $\bar{\boldsymbol{u}} = \bar{\boldsymbol{R}}^{-1} \bar{\boldsymbol{B}}^T \boldsymbol{K}(t) \bar{\boldsymbol{f}}(\boldsymbol{x}(t), t)/2a_2$*, is minimized.*

For Problem R, the dynamical system (3.28) is required to be solved forward in time with initial condition given by (3.13). On the other hand, the dynamical system (3.34a) should be solved backward in time with partial information on the terminal state given by (3.34b). This optimal control problem is, indeed, very difficult to solve.

In this chapter, we propose an alternative approach to construct an approximate optimal matrix function $\boldsymbol{K}^*(t)$ without having to solve this complicated optimal control problem R. The basic idea is explained as follows. Suppose that $\boldsymbol{u}^* = [u_1^*, u_2^*, u_3^*]^T$ is an optimal open loop control of Problem Q and that $\boldsymbol{x}^*$ is the corresponding optimal state. As u_1^* is a constant, we fix it to the constant obtained. This gives rise to Problem ($\bar{\text{Q}}$). We now consider Problem ($\bar{\text{Q}}$) with $\boldsymbol{x} = \boldsymbol{x}^*$, i.e. along the optimal open loop path, and our task is to find a $\boldsymbol{K}^*(t)$ such that $\bar{\boldsymbol{u}}^{\#} = \bar{\boldsymbol{R}}^{-1} \bar{\boldsymbol{B}}^T \boldsymbol{K}^*(t) \bar{\boldsymbol{f}}(\boldsymbol{x}^*(t), t)/2a_2$ best approximates the control $\bar{\boldsymbol{u}}^*$ in the mean square sense, where $\bar{\boldsymbol{u}}^* = [u_2^*, u_3^*]^T$. Since the cost value for Problem ($\bar{\text{Q}}$) with $\bar{\boldsymbol{u}}$ given by $\bar{\boldsymbol{u}}^{\#} = \bar{\boldsymbol{R}}^{-1} \bar{\boldsymbol{B}}^T \boldsymbol{K}^*(t) \bar{\boldsymbol{f}}(\boldsymbol{x}^*(t), t)/2a_1$ should be close to the cost value for Problem Q with $\boldsymbol{u} = \boldsymbol{u}^*$, $\bar{\boldsymbol{u}}^{\#}$ can be regarded as a good approximate optimal feedback control for Problem ($\bar{\text{Q}}$).

In the next section, we present a practical method to find an approximate optimal gain matrix $\boldsymbol{K}(t)$ without solving the complex optimal control problem R.

3.4 A practical computational method

As the matrix function $\boldsymbol{K}(t)$ is a solution of the Riccati-like-matrix differential equation, the optimal closed loop control law (3.49) should be smooth throughout $[0, T]$, where

$T = T^*$. For this reason, $\boldsymbol{K}(t)$ is approximated in terms of cubic spline basis functions. The time horizon $[0, T^*]$ is partitioned into p equal subintervals,

$$0 = t_0 \leq t_1 \leq \cdots \leq t_p \leq t_{p+1} = T^* \tag{3.50}$$

Let

$$[\boldsymbol{K}(t)]_{i,j} \approx \sum_{k=-1}^{p+1} (c_{i,j,k})\Omega((\frac{T^*}{p})t - k) \tag{3.51}$$

where $c_{i,j,k}$, $i, j = 1, 2, \ldots, 9$; $k = -1, 0, 1, 2, \ldots, p+1$, are real constant coefficients that are to be determined, p is the number of equal subintervals on $[0, T^*]$, $p+3$ is the total number of cubic spline basis functions used in the approximation of each $[\boldsymbol{K}(t)]_{i,j}$, and $\Omega(\tau)$ is defined as in (3.23).

Let

$$\Upsilon(\boldsymbol{K}) = \int_0^{T^*} \left\{(u_2^*(t) - \bar{u}_1(t))^2 + (u_3^*(t) - \bar{u}_2(t))^2\right\} dt, \tag{3.52}$$

where

$$\bar{\boldsymbol{u}}(t) = \begin{bmatrix} \bar{u}_1(t) \\ \bar{u}_2(t) \end{bmatrix} = \frac{1}{2a_2} \bar{\boldsymbol{R}}^{-1} \bar{\boldsymbol{B}}^T \boldsymbol{K}(t) \bar{\boldsymbol{f}}(\boldsymbol{x}^*(t), t). \tag{3.53}$$

Here, we see that $\bar{\boldsymbol{u}}$ is of the same form as the optimal closed loop control given by (3.33). Our task is to choose a $\boldsymbol{K}(t)$ such that (3.52) is minimized. Let $\boldsymbol{K}^*(t)$ be the optimal matrix function obtained. It is substituted into (3.53) to give $\bar{\boldsymbol{u}}^* = [\bar{u}_1^*, \bar{u}_2^*]^T$, which is the best approximate optimal feedback control in the mean square sense of Problem ($\bar{\text{Q}}$).

Our task can be posed as the following optimization problem.

Find coefficients $c_{i,j,k}$, $i, j = 1, 2, \ldots, 9$; $k = -1, 0, 1, 2, \ldots, p+1$, such that the cost function (3.52) is minimized. These optimal coefficients can be obtained by solving the following optimality conditions

$$\boldsymbol{\Gamma} = \frac{\partial \Upsilon(\boldsymbol{K})}{\partial c_{i,j,k}} = \int_0^{T^*} \frac{\partial((u_2^* - \bar{u}_1)^2 + (u_3^* - \bar{u}_2)^2)}{\partial c_{i,j,k}} dt = 0 \tag{3.54}$$
$$i, j = 1, 2, \ldots, 9, \ k = -1, 0, 1, 2, \ldots, p+1$$

These are linear equations, and hence are easy to solve.

Let $\rho_i(\boldsymbol{\Lambda})$ and $\kappa_i(\boldsymbol{\Lambda})$ denote the $i-$th row and $i-$th column of the matrix $\boldsymbol{\Lambda}$. By a careful examination of (3.53), it is noticed that $\boldsymbol{K}(t)$ appears with $\bar{\boldsymbol{B}}^T$ multiplied from the left. If $\kappa_i(\bar{\boldsymbol{B}}^T) = 0$ for all $t \in [0, T^*]$, then $\rho_i(\boldsymbol{K}(t))$ does not affect $\bar{\boldsymbol{B}}^T \boldsymbol{K}(t)$. From (3.30), we see that $\kappa_i(\bar{\boldsymbol{B}}^T) = 0$, $i = 1, \ldots, 6, 9$, hence, there is no need to calculate those coefficients $c_{i,j,k}$ corresponding to $\rho_i(\boldsymbol{K}(t))$, $i = 1, \ldots, 6, 9$. From (3.29) and (3.53), we also notice that $\rho_i(\bar{\boldsymbol{f}}(\boldsymbol{x}^*(t), t)) = 0$, $i = 7, 8$, and $\boldsymbol{K}(t)$ is multiplied with $\bar{\boldsymbol{f}}(\boldsymbol{x}^*(t), t)$ from the right. Thus, $\kappa_i(\boldsymbol{K}(t))$, $i = 7, 8$, do not affect $\boldsymbol{K}(t)\bar{\boldsymbol{f}}(\boldsymbol{x}^*(t), t)$, and hence there is

no need to calculate the corresponding components $\kappa_i(\boldsymbol{K}(t)),\ i = 7, 8$. Therefore, we may set these components of $\boldsymbol{K}(t)$ to zero. In our problem, we only need to calculate 14 elements of $\boldsymbol{K}(t)$, i.e., $[\boldsymbol{K}(t)]_{i,j}$, $i = 7, 8$; $j = 1, 2, \ldots, 6, 9$.

3.5 Numerical simulations

In this section, two examples are involved to show the effectiveness of the proposed method. For easy illustration, we assume that the module flies from the Perilune to the moon surface directly.

3.5.1 Problem without perturbation

The initial conditions for the soft landing of a lunar module are given as: $x_{L0} = 819.371$km, $y_{L0} = 1428.867$km, $z_{L0} = 599.6306$km, $V_{xL0} = 1115$m/s, $V_{yL0} = -981.82$ m/s, $V_{zL0} = 816$m/s, $m_0 = 600$kg. At the initial time of the soft landing, the rotational angle $\gamma(t_0) = 0°$, the specific impulse $V_r = 300 \times 9.8$m/s and the angular velocity of the moon rotation $\omega_L = 2.661699 \times 10^{-6}$rad/s. The landing target is in Mare Imbrium on the moon surface with 38.3° North latitude and 35° West longitude. When the module reaches the moon surface, the terminal velocity should be less than 3m/s. The bounds on $u_1(t)$ are: $0\text{kg/s} \leq u_1(t) \leq 0.51\text{kg/s}$.

In the simulation, the time horizon $[0, T]$ is partitioned into 30 subintervals. $a_1 = 10$, $a_2 = 1$, $\boldsymbol{S} = \text{diag}(1\text{e}^{-3}, 1\text{e}^{-3}, 1\text{e}^{-3}, 1\text{e}^{-3}, 1\text{e}^{-3}, 1\text{e}^{-3}, 0, 0, 0)$ and $\boldsymbol{R} = \text{diag}(1, 1, 1)$. We first use the time scaling transform (3.16) and the control parameterization method (3.22) to construct the corresponding approximated Problem $\tilde{\text{Q}}_p$. Then, MISER 3.3 is utilized to solve it, giving rise to an optimal open loop control $\tilde{\boldsymbol{u}}^*(s)$ and the corresponding optimal trajectory $\tilde{\boldsymbol{x}}^*(s)$. Then, by (3.20a) and (3.20b), we obtain the optimal open loop solution, denoted by $(\boldsymbol{u}^*, \boldsymbol{x}^*, T^*)$ of Problem Q. Note that $u_1^* = 0.51$kg/s, i.e., the reverse force thruster works with its maximum thrust force $P = 1500$N. With $u_1^* = 0.51$kg/s, Problem Q is reduced to Problem $(\bar{\text{P}})$ with $\bar{\boldsymbol{u}} = [\bar{u}_1, \bar{u}_2]^T$, where $\bar{\boldsymbol{R}}$ is chosen from $\boldsymbol{R}$ to be $\bar{\boldsymbol{R}} = \text{diag}(1, 1)$. Set $\bar{u}_1^*(t) = u_2^*(t)$ and $\bar{u}_2^*(t) = u_3^*(t)$. The corresponding optimal state of Problem $(\bar{\text{P}})$ remains the same as that of Problem Q. Substituting $(\boldsymbol{u}^*, \boldsymbol{x}^*, T^*)$ into (3.54), the system of linear equations can be solved by a linear equations solver within the Matlab environment. The feedback gain matrix $\boldsymbol{K}^*(t)$ obtained is substituted into (3.53) to give the best approximate optimal feedback control law in the mean square sense for achieving the soft landing of the lunar module.

Under the optimal feedback control, the terminal conditions of the module are $x_L(t_f) = 1117.2919$km, $y_L(t_f) = 1077.1752$km, $z_L(t_f) = 782.3021$km, $V_{xL}(t_f) = 0.6345$m/s, $V_{yL}(t_f) = -0.9852$m/s, $V_{zL}(t_f) = 0.178$m/s.

Simulation results are depicted in Figure 3.2 to Figure 3.8. Figure 3.2 to Figure 3.4

are the time histories of the control outputs. It is seen that the thruster works with its maximum thrust force, the feedback angular velocity control laws coincide with the open loop ones precisely. Under the optimal feedback control, the lunar module lands on the moon surface after 542.268s, the velocities along the three directions in $ox_Ly_Lz_L$ are approaching to zero (see Figure 3.5 to Figure 3.7), the terminal velocity of the module is 1.185m/s. The distance between the lunar module and the preselected landing target is 27.98m. The terminal mass of the module is 323.443kg. The optimal descent trajectory is shown in Figure 3.8.

3.5.2 Problem with perturbation

Next, we let the lunar module soft landing start from a new perturbed initial point to test the robustness of the optimal feedback control law against disturbances on initial condition for the soft landing mission. The coordinates of the new starting point, which is 30m away from the original starting point, are $x_{L0N} = 819.375$km, $y_{L0N} = 1428.845$km and $z_{L0N} = 599.6507$km. Under the optimal feedback control, the lunar module lands on the moon surface after 542.26s, the terminal velocity is 1.22m/s, and the coordinates of the landing position are $x_{LC}(t_f) = 1117.3007$km, $y_{LC}(t_f) = 1077.1565$km and $z_{LC}(t_f) = 782.3153$km, which is 33.27m away from the preselected landing target.

For comparison, we let the lunar module soft landing start from the new initial point by using the open loop optimal control $\boldsymbol{u}^*$ obtained previously. Under the open loop optimal control, the lunar module lands on the moon surface after 543.05s with the terminal velocity which is 2.26m/s. The landing position is located at $x_{LO}(t_f) = 1117.1776$km, $y_{LO}(t_f) = 1077.1592$km and $z_{LO}(t_f) = 782.4896$km, which is 184.1m away from the desired landing target.

To exam how close to optimal the feedback control is for the soft landing when the initial position is perturbed to a new perturbed initial point, we calculate the open loop optimal control for the perturbed problem by using the control parameterization technique and the time scaling transform mentioned above. Under the new open loop optimal control, we calculate the optimal descent trajectory from which we observe that the lunar module lands on the desired landing target precisely after 542.541s. The finial velocity is 0m/s.

The simulation results are summarized in Table 3.1. Case 1, Case 2 and Case 3 represent the simulations from the perturbed initial point with the feedback control, the original open loop optimal control $\boldsymbol{u}^*$ and the new open loop optimal control, respectively. As we can see, the feedback control is much superior to the open loop optimal control obtained from the original initial condition under the situation when the initial position is perturbed to a new perturbed initial point. The performance of the feedback control is close to that of the optimal open loop control calculated from the perturbed initial point.

Table 3.1: Summary of simulations

simulation	distance from target	finial velocity	objective value
Case 1	33.27m	1.22m/s	5574.72
Case 2	184.1m	2.26m/s	5910.73
Case 3	0m	0m/s	5566.53

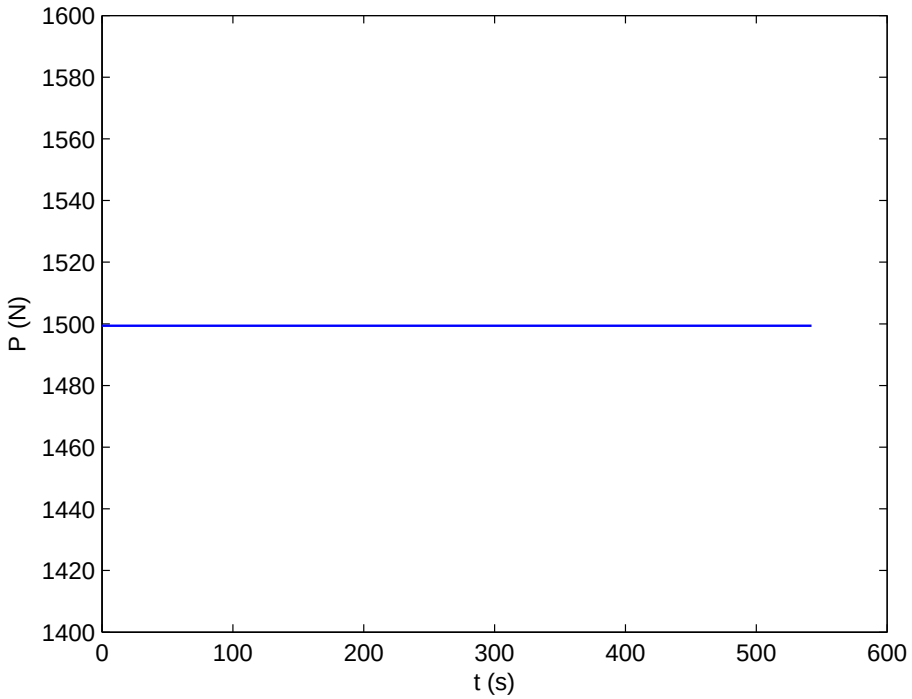

Figure 3.2: Thrust force P

The time histories of the descent trajectories are depicted in Figure 3.9.

3.6 Conclusion

The optimal control problem of lunar module soft landing was studied, where a three dimensional dynamics is employed to describe the motion of the module. We first obtained an optimal open loop control by using the control parametrization method and the time scaling transform. Then, we obtained the form of the optimal closed loop control law, where the feedback gain matrix is required to satisfy a Riccati-like matrix differential equation. On this basis, a practical method was proposed to calculate the feedback gain matrix without having to solve an optimal control problem involving a complex Riccati-like differential equation coupled with the original dynamics. Simulation results showed that the proposed method is highly efficient.

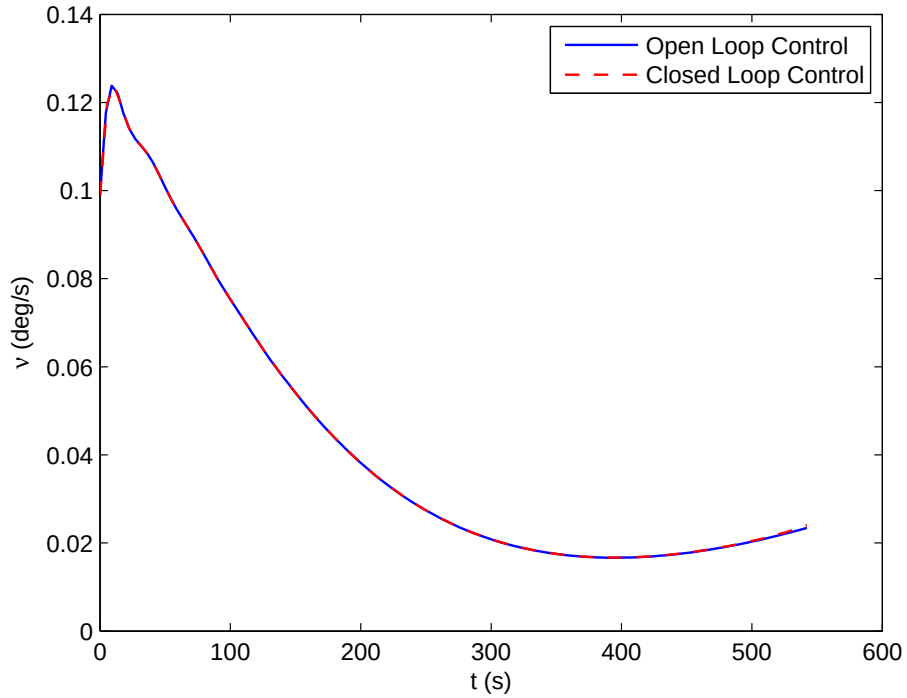

Figure 3.3: Angular velocity control v

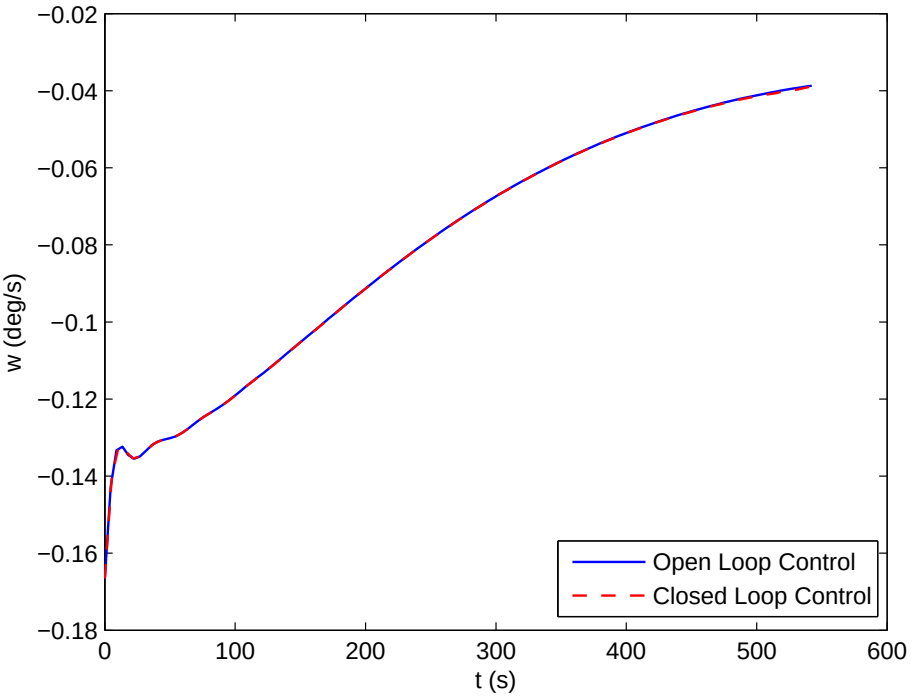

Figure 3.4: Angular velocity control w

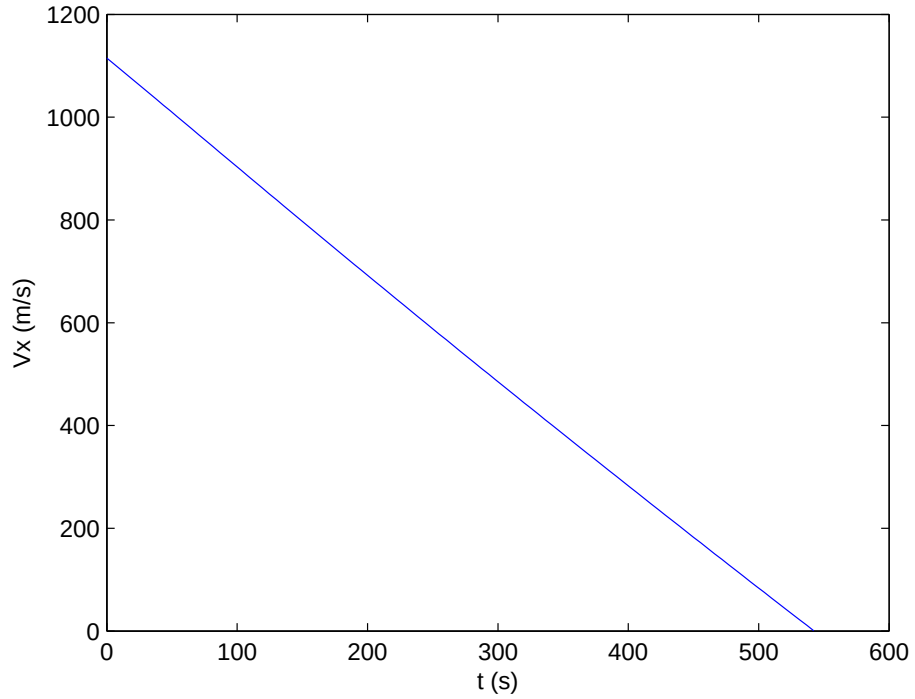

Figure 3.5: Velocity along x axis

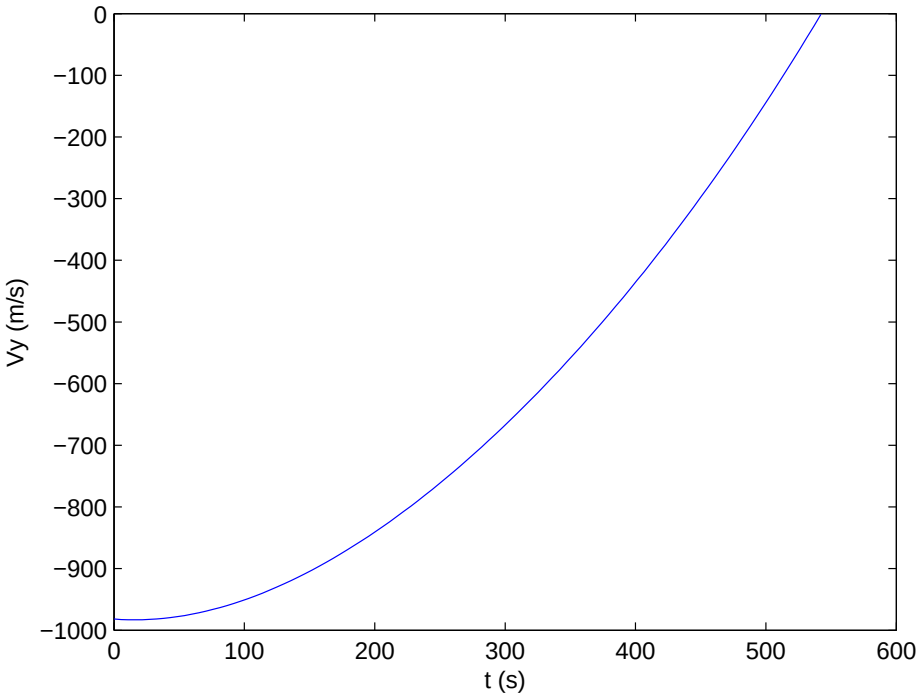

Figure 3.6: Velocity along y axis

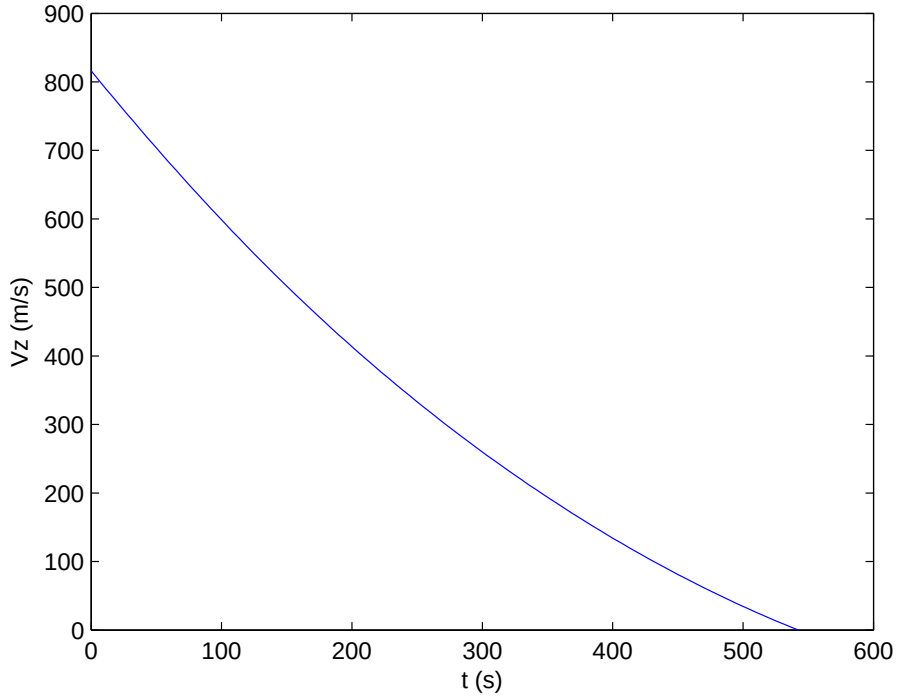

Figure 3.7: Velocity along z axis

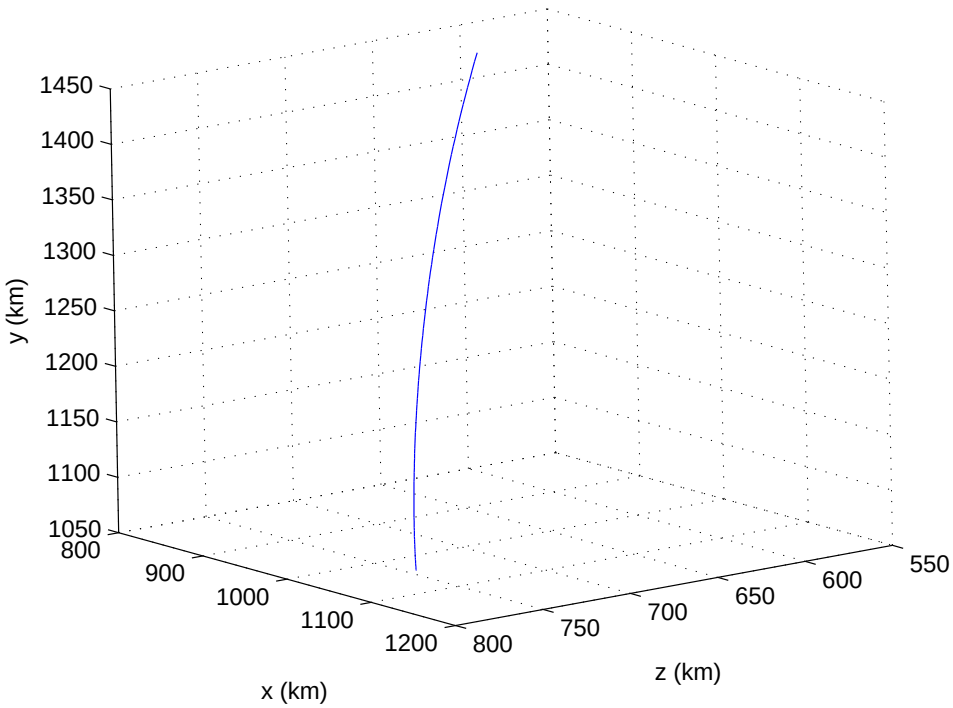

Figure 3.8: Optimal descent trajectory

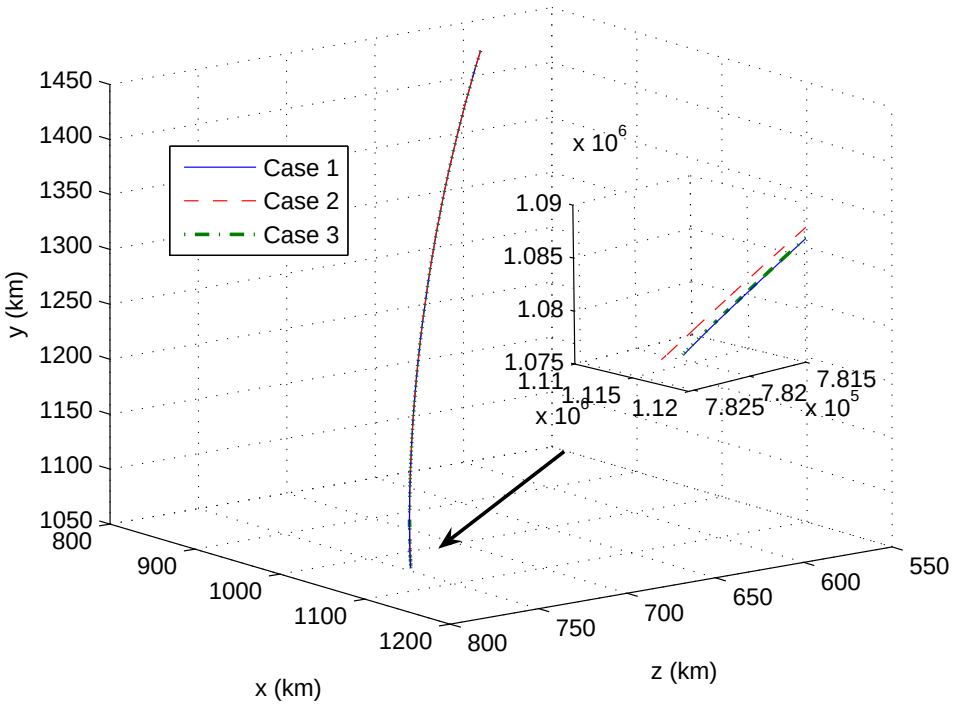

Figure 3.9: Descent trajectories

CHAPTER 4

Spacecraft attitude control with DGCMGs

4.1 Introduction

SGCMGs based spacecraft attitude control systems have been extensively studied during the past several decades. The most interesting aspects that the scientists focus on are, for example, system mathematical modeling, spacecraft attitude control strategy design, SGCMGs system configuration, steering law design and singularity analysis. As the DGCMG has one more degree of freedom (DOF) than the the SGCMG, the singularity situations of the DGCMGs system are simpler than that of the SGCMGs system. It is very promising to use the DGCMGs as the actuators for the spacecraft attitude control system. NASA has already utilized three orthogonally mounted DGCMGs to maneuver the attitude of the 'Sky Lab'. DGCMGs system can also be used as the attitude actuators for many other kinds of spacecrafts, such as the orbital module of the lunar probe, space stations and small agile satellites. However, a precise three dimensional spacecraft attitude dynamics, basing on the DGCMGs system, has not yet been found in the open literature.

In this chapter, we first derive an exact general mathematical description of spacecraft attitude motion driven by DGCMGs. With this mathematical description, a nonlinear control law is designed based on the second method of Lyapunov for spacecraft large angle attitude maneuvers. Stability of the attitude control system is proved during the design process. The singularity robustness plus null motion (SRNM) steering law is designed to realize the control law. Principle of DGCMGs' singularity is proved, and singularity analysis of the orthogonally mounted three DGCMGs system and that of the parallel mounted four DGCMGs system are presented. Finally, numerical simulations are utilized to verify the system performances.

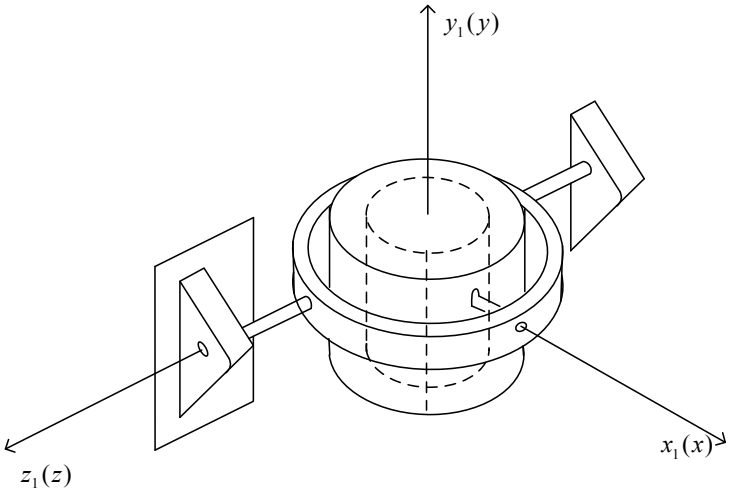

Figure 4.1: Structure of a DGCMG.

4.2 Spacecraft attitude system modeling with DGCMGs

4.2.1 Coordinates definition

First, we shall introduce some frames that will be used in this section.

a. Inertial frame $o_N x_N y_N z_N$, $\{N\}$.

b. Spacecraft vehicle frame $o_V x_V y_V z_V$, $\{V\}$. o_V is the spacecraft centroid. $o_V x_V$, $o_V y_V$ and $o_V z_V$ are, respectively, the three principal inertia axes of the spacecraft.

c. DGCMG reference frame $o x_R y_R z_R$, $\{R\}$. o is the centroid of a certain DGCMG.

d. DGCMG outer gimbal frame $o x_1 y_1 z_1$, $\{G_o\}$. $o x_1$ and $o z_1$ align, respectively, the inner gimbal axis and the outer gimbal axis.

e. DGCMG inner gimbal frame $oxyz$, $\{G_i\}$. ox and oy coincide with, respectively, the inner gimbal axis and the rotor axis.

The structure of a DGCMG is shown in Figure 4.1. When the inner gimbal angle and the outer gimbal angle are all zero, the three frames ($\{R\}$, $\{G_o\}$ and $\{G_i\}$) are coincide with each other.

4.2.2 Coordinates transformation

The relationships between these frames can be expressed by the coordinate transformation matrices listed below.

a. Coordinate transformation matrix $\boldsymbol{C}_V(\boldsymbol{q})$ from the inertial frame $\{N\}$ to the vehicle frame $\{V\}$, $\{V\} = \boldsymbol{C}_V(\boldsymbol{q})\{N\}$.

$\boldsymbol{C}_V(\boldsymbol{q})$ is determined by the spacecraft attitude, $\boldsymbol{q} = [q_0, q_1, q_2, q_3]^T$ represents the quaternion vector, and

$$\boldsymbol{C}_V(\boldsymbol{q}) = \begin{bmatrix} q_0^2+q_1^2-q_2^2-q_3^2 & 2(q_1q_2+q_0q_3) & 2(q_1q_3-q_0q_2) \\ 2(q_1q_2-q_0q_3) & q_0^2-q_1^2+q_2^2-q_3^2 & 2(q_2q_3+q_0q_1) \\ 2(q_1q_3+q_0q_2) & 2(q_2q_3-q_0q_1) & q_0^2-q_1^2-q_2^2+q_3^2 \end{bmatrix} \tag{4.1}$$

b. Coordinate transformation matrix $\boldsymbol{C}_R(\boldsymbol{\beta})$ from the vehicle frame $\{V\}$ to the DGCMG reference frame $\{R\}$, $\{R\} = \boldsymbol{C}_R(\boldsymbol{\beta})\{V\}$.

$\boldsymbol{C}_R(\boldsymbol{\beta})$ is determined by the configuration of the DGCMGs system. $\boldsymbol{\beta} = [\beta_1, \beta_2, \beta_3]^T$ represents the mounting angle vector of the DGCMGs system with reference to the vehicle frame.

c. Coordinate transformation matrix $\boldsymbol{C}_{oR}(\gamma)$ from the DGCMG reference frame $\{R\}$ to the DGCMG outer gimbal frame $\{G_o\}$, $\{G_o\} = \boldsymbol{C}_{oR}(\gamma)\{R\}$.

γ denotes the precession angle of the DGCMG about the outer gimbal axis,

$$\boldsymbol{C}_{oR}(\gamma) = \begin{bmatrix} \cos\gamma & \sin\gamma & 0 \\ -\sin\gamma & \cos\gamma & 0 \\ 0 & 0 & 1 \end{bmatrix} \tag{4.2}$$

d. Coordinate transformation matrix $\boldsymbol{C}(\delta)$ from the DGCMG outer gimbal frame $\{G_o\}$ to the DGCMG inner gimbal frame $\{G_i\}$, $\{G_i\} = \boldsymbol{C}(\delta)\{G_o\}$.

δ denotes the precession angle of the DGCMG about the inner gimbal axis,

$$\boldsymbol{C}(\delta) = \begin{bmatrix} 1 & 0 & 0 \\ 0 & \cos\delta & \sin\delta \\ 0 & -\sin\delta & \cos\delta \end{bmatrix} \tag{4.3}$$

e. Coordinate transformation matrix $\boldsymbol{C}_o$ from the vehicle frame $\{V\}$ to the DGCMG outer gimbal frame $\{G_o\}$, $\{G_o\} = \boldsymbol{C}_o\{V\}$.

Based on the previous definitions, $\boldsymbol{C}_o$ can be expressed as:

$$\boldsymbol{C}_o = \boldsymbol{C}_{oR}(\gamma)\boldsymbol{C}_R(\boldsymbol{\beta}) \tag{4.4}$$

f. Coordinate transformation matrix $\boldsymbol{C}_i$ from the vehicle frame $\{V\}$ to the DGCMG inner gimbal frame $\{G_i\}$, $\{G_i\} = \boldsymbol{C}_i\{V\}$.

$\boldsymbol{C}_i$ can be written as:

$$\boldsymbol{C}_i = \boldsymbol{C}(\delta)\boldsymbol{C}_{oR}(\gamma)\boldsymbol{C}_R(\boldsymbol{\beta}) = \boldsymbol{C}(\delta)\boldsymbol{C}_o \tag{4.5}$$

In the rest of the chapter, for any vector $\boldsymbol{x} = [x_1, x_2, x_3]^T$, $\tilde{\boldsymbol{x}}$ represents the skew

symmetric cross product matrix

$$\tilde{\boldsymbol{x}} = \begin{bmatrix} 0 & -x_3 & x_2 \\ x_3 & 0 & -x_1 \\ -x_2 & x_1 & 0 \end{bmatrix} \tag{4.6}$$

4.2.3 Spacecraft attitude kinematics

The spacecraft attitude kinematic equation can be expressed as:

$$\dot{\boldsymbol{q}} = \frac{1}{2}\boldsymbol{G}(\boldsymbol{q})\boldsymbol{\omega} \tag{4.7}$$

where

$$\boldsymbol{G}(\boldsymbol{q}) = \begin{bmatrix} -q_1 & -q_2 & -q_3 \\ q_0 & -q_3 & q_2 \\ q_3 & q_0 & -q_1 \\ -q_2 & q_1 & q_0 \end{bmatrix}, \tag{4.8}$$

while $\boldsymbol{\omega}$ is the angular velocity of the spacecraft with respect to the the inertial frame, and $\boldsymbol{\omega} = [\omega_x, \omega_y, \omega_z]^T$. Here, ω_x, ω_y and ω_z are the projections of $\boldsymbol{\omega}$ onto the vehicle frame.

4.2.4 Spacecraft attitude dynamics

Assume that n identical DGCMGs are equipped in a rigid spacecraft. Let $\boldsymbol{I}_{\mathrm{S}}$ represent the system inertia matrix with DGCMGs locked. Let $\boldsymbol{J}_o$ represent the outer gimbal inertia matrix in $\{G_o\}$, and let $\boldsymbol{J}_i$ and $\boldsymbol{J}_w$ be, respectively, the inertia matrix of inner gimbal and rotor in $\{G_i\}$. The rotor angular momentum can be expressed as $\boldsymbol{h} = \boldsymbol{J}_w\boldsymbol{\Omega}$, where $\boldsymbol{\Omega}$ is the angular velocity of the rotor. For the lth DGCMG, the outer gimbal rate in $\{G_{lo}\}$ can be written as $\dot{\boldsymbol{\gamma}}_l = [0, 0, \dot{\gamma}_l]^T$, and the inner gimbal rate in $\{G_{li}\}$ can be written as $\dot{\boldsymbol{\delta}}_l = [\dot{\delta}_l, 0, 0]^T$.

The total angular momentum of the lth DGCMG in $\{V\}$ can be expressed as:

$$\begin{aligned} \boldsymbol{H}_l^{G/CG} = {} & \boldsymbol{C}_{lo}^T(\boldsymbol{J}_o\boldsymbol{C}_{lo}\boldsymbol{\omega} + \boldsymbol{J}_o\dot{\boldsymbol{\gamma}}_l) + \boldsymbol{C}_{li}^T(\boldsymbol{J}_i\boldsymbol{C}_{li}\boldsymbol{\omega} + \boldsymbol{J}_i\boldsymbol{C}_l\dot{\boldsymbol{\gamma}}_l + \boldsymbol{J}_i\dot{\boldsymbol{\delta}}_l) \\ & + \boldsymbol{C}_{li}^T(\boldsymbol{J}_w\boldsymbol{C}_{li}\boldsymbol{\omega} + \boldsymbol{J}_w\boldsymbol{C}_l\dot{\boldsymbol{\gamma}}_l + \boldsymbol{J}_w\dot{\boldsymbol{\delta}}_l + \boldsymbol{J}_w\boldsymbol{\Omega}) \end{aligned} \tag{4.9}$$

Equation (4.9) can be rewritten as:

$$\boldsymbol{H}_l^{G/CG} = \boldsymbol{C}_{lo}^T(\boldsymbol{J}_o\boldsymbol{C}_{lo}\boldsymbol{\omega} + \boldsymbol{J}_o\dot{\boldsymbol{\gamma}}_l) + \boldsymbol{C}_{li}^T(\boldsymbol{I}_i\boldsymbol{C}_{li}\boldsymbol{\omega} + \boldsymbol{I}_i\boldsymbol{C}_l\dot{\boldsymbol{\gamma}}_l + \boldsymbol{I}_i\dot{\boldsymbol{\delta}}_l) + \boldsymbol{C}_{li}^T\boldsymbol{h}, \tag{4.10}$$

where $\boldsymbol{I}_i = \boldsymbol{J}_i + \boldsymbol{J}_w$.

The total angular momentum of the system about the spacecraft centroid can be

written as:

$$\begin{aligned}\boldsymbol{H}^{S/C} &= \boldsymbol{I}^S\boldsymbol{\omega} + \sum_{l=1}^{n}\boldsymbol{H}_l^{G/CG} \\ &= \boldsymbol{I}^S\boldsymbol{\omega} + \sum_{l}^{n}\left[\boldsymbol{C}_{lo}^T(\boldsymbol{J}_o\boldsymbol{C}_{lo}\boldsymbol{\omega} + \boldsymbol{J}_o\dot{\boldsymbol{\gamma}}_l) + \boldsymbol{C}_{li}^T(\boldsymbol{I}_i\boldsymbol{C}_{li}\boldsymbol{\omega} + \boldsymbol{I}_i\boldsymbol{C}_l\dot{\boldsymbol{\gamma}}_l + \boldsymbol{I}_i\dot{\boldsymbol{\delta}}_l) + \boldsymbol{C}_{li}^T\boldsymbol{h}\right]\end{aligned} \tag{4.11}$$

According to the momentum moment theorem [57], time derivative of the total angular momentum in the inertia frame is the external torque $\boldsymbol{L}_e$ exerted on the system about the mass center. Hence,

$$\boldsymbol{L}_e = \frac{d\boldsymbol{H}^{S/C}}{dt}_N = \boldsymbol{I}^S\dot{\boldsymbol{\omega}} + \tilde{\boldsymbol{\omega}}\boldsymbol{I}^S\boldsymbol{\omega} + \sum_{l=1}^{n}\frac{d\boldsymbol{H}_l^{G/CG}}{dt}_N \tag{4.12}$$

where $d\boldsymbol{H}_l^{G/CG}/dt_N$ represents the torque exerted on the lth DGCMG and can be derived as:

$$\frac{d\boldsymbol{H}_l^{G/CG}}{dt}_N = \frac{d(\boldsymbol{J}_o\boldsymbol{C}_{lo}\boldsymbol{\omega} + \boldsymbol{J}_o\dot{\boldsymbol{\gamma}}_l)}{dt}_N + \frac{d(\boldsymbol{I}_i\boldsymbol{C}_{li}\boldsymbol{\omega} + \boldsymbol{I}_i\boldsymbol{C}_l\dot{\boldsymbol{\gamma}}_l + \boldsymbol{I}_i\dot{\boldsymbol{\delta}}_l)}{dt}_N + \frac{d\boldsymbol{h}}{dt}_N \tag{4.13}$$

Let ${}^{N-G_{lo}}\boldsymbol{\omega}_l$ represent the angular velocity vector of the lth outer gimbal frame $\{G_{lo}\}$ with reference to the inertial frame $\{N\}$ given by

$${}^{N-G_{lo}}\boldsymbol{\omega}_l = \boldsymbol{\omega} + \dot{\boldsymbol{\gamma}}_l \tag{4.14}$$

and let ${}^{V-G_{lo}}\boldsymbol{\omega}_l$ be the angular velocity vector of the lth outer gimbal frame $\{G_{lo}\}$ with reference to the vehicle frame $\{V\}$ given by

$${}^{V-G_{lo}}\boldsymbol{\omega}_l = \dot{\boldsymbol{\gamma}}_l \tag{4.15}$$

The first fraction on the right hand side of (4.13) can be derived in the outer gimbal frame $\{G_{lo}\}$ as:

$$\begin{aligned}&\frac{d(\boldsymbol{J}_o\boldsymbol{C}_{lo}\boldsymbol{\omega} + \boldsymbol{J}_o\dot{\boldsymbol{\gamma}}_l)}{dt}_N = \frac{d(\boldsymbol{J}_o\boldsymbol{C}_{lo}\boldsymbol{\omega})}{dt}_N + \frac{d(\boldsymbol{J}_o\dot{\boldsymbol{\gamma}}_l)}{dt}_N \\ &= \frac{d(\boldsymbol{J}_o\boldsymbol{C}_{lo}\boldsymbol{\omega})}{dt}_{G_{lo}} + {}^{N-G_{lo}}\boldsymbol{\omega}_l \times (\boldsymbol{J}_o\boldsymbol{C}_{lo}\boldsymbol{\omega}) + \frac{d(\boldsymbol{J}_o\dot{\boldsymbol{\gamma}}_l)}{dt}_{G_{lo}} + {}^{N-G_{lo}}\boldsymbol{\omega}_l \times \boldsymbol{J}_o\dot{\boldsymbol{\gamma}}_l \\ &= \boldsymbol{J}_o\left[\boldsymbol{C}_{lo}\frac{d(\boldsymbol{\omega})}{dt}_V - {}^{V-G_{lo}}\boldsymbol{\omega}_l \times (\boldsymbol{C}_{lo}\boldsymbol{\omega})\right] + (\boldsymbol{\omega} + \dot{\boldsymbol{\gamma}}_l) \times (\boldsymbol{J}_o\boldsymbol{C}_{lo}\boldsymbol{\omega}) + \boldsymbol{J}_o\ddot{\boldsymbol{\gamma}}_l + (\boldsymbol{\omega} + \dot{\boldsymbol{\gamma}}_l) \times (\boldsymbol{J}_o\dot{\boldsymbol{\gamma}}_l) \\ &= \boldsymbol{J}_o\boldsymbol{C}_{lo}\dot{\boldsymbol{\omega}} - \boldsymbol{J}_o\tilde{\dot{\boldsymbol{\gamma}}}_l\boldsymbol{C}_{lo}\boldsymbol{\omega} + \boldsymbol{C}_{lo}\tilde{\boldsymbol{\omega}}\boldsymbol{C}_{lo}^T\boldsymbol{J}_o\boldsymbol{C}_{lo}\boldsymbol{\omega} + \tilde{\dot{\boldsymbol{\gamma}}}_l\boldsymbol{J}_o\boldsymbol{C}_{lo}\boldsymbol{\omega} + \boldsymbol{J}_o\ddot{\boldsymbol{\gamma}}_l + \boldsymbol{C}_{lo}\tilde{\boldsymbol{\omega}}\boldsymbol{C}_{lo}^T\boldsymbol{J}_o\dot{\boldsymbol{\gamma}}_l\end{aligned} \tag{4.16}$$

Let ${}^{N-G_{li}}\boldsymbol{\omega}_l$ denote the angular velocity vector of the lth inner gimbal frame $\{G_{li}\}$ with

reference to the inertial frame $\{N\}$ given by

$$^{N-G_{li}}\boldsymbol{\omega}_l = \boldsymbol{\omega} + \dot{\boldsymbol{\gamma}}_l + \dot{\boldsymbol{\delta}}_l \tag{4.17}$$

and let $^{V-G_{li}}\boldsymbol{\omega}_l$ be the angular velocity vector of the lth inner gimbal frame $\{G_{li}\}$ with reference to the vehicle frame $\{V\}$ given by

$$^{V-G_{li}}\boldsymbol{\omega}_l = \dot{\boldsymbol{\gamma}}_l + \dot{\boldsymbol{\delta}}_l \tag{4.18}$$

$^{G_{lo}-G_{li}}\boldsymbol{\omega}_l$ represents the angular velocity vector of the lth inner gimbal frame $\{G_{li}\}$ with reference to the outer frame $\{G_{lo}\}$ given by

$$^{G_{lo}-G_{li}}\boldsymbol{\omega}_l = \dot{\boldsymbol{\delta}}_l \tag{4.19}$$

The second fraction on the right hand side of (4.13) can be derived in the inner gimbal frame $\{G_{li}\}$ as:

$$\begin{aligned}
&\frac{d(\boldsymbol{I}_i\boldsymbol{C}_{li}\boldsymbol{\omega} + \boldsymbol{I}_i\boldsymbol{C}_l\dot{\boldsymbol{\gamma}}_l + \boldsymbol{I}_i\dot{\boldsymbol{\delta}}_l)}{dt}_N = \frac{d(\boldsymbol{I}_i\boldsymbol{C}_{li}\boldsymbol{\omega})}{dt}_N + \frac{d(\boldsymbol{I}_i\boldsymbol{C}_l\dot{\boldsymbol{\gamma}}_l)}{dt}_N + \frac{d(\boldsymbol{I}_i\dot{\boldsymbol{\delta}}_l)}{dt}_N \\
=&\boldsymbol{I}_i\frac{d(\boldsymbol{C}_{li}\boldsymbol{\omega})}{dt}_{G_{li}} + {}^{N-G_{li}}\boldsymbol{\omega}\times(\boldsymbol{I}_i\boldsymbol{C}_{li}\boldsymbol{\omega}) + \boldsymbol{I}_i\frac{d(\boldsymbol{C}_l\dot{\boldsymbol{\gamma}}_l)}{dt}_{G_{li}} \\
&+ {}^{N-G_{li}}\boldsymbol{\omega}\times(\boldsymbol{I}_i\boldsymbol{C}_l\dot{\boldsymbol{\gamma}}_l) + \boldsymbol{I}_i\ddot{\boldsymbol{\delta}}_l + {}^{N-G_{li}}\boldsymbol{\omega}\times(\boldsymbol{I}_i\dot{\boldsymbol{\delta}}_l) \\
=&\boldsymbol{I}_i\boldsymbol{C}_{li}\dot{\boldsymbol{\omega}} - \boldsymbol{I}_i\boldsymbol{C}_l\tilde{\dot{\boldsymbol{\gamma}}}_l\boldsymbol{C}_{lo}\boldsymbol{\omega} - \boldsymbol{I}_i\tilde{\dot{\boldsymbol{\delta}}}_l\boldsymbol{C}_{li}\boldsymbol{\omega} + \boldsymbol{C}_{li}\tilde{\boldsymbol{\omega}}\boldsymbol{C}_{li}^T\boldsymbol{I}_i\boldsymbol{C}_{li}\boldsymbol{\omega} + \boldsymbol{C}_l\tilde{\dot{\boldsymbol{\gamma}}}_l\boldsymbol{C}_l^T\boldsymbol{I}_i\boldsymbol{C}_{li}\boldsymbol{\omega} \\
&+ \tilde{\dot{\boldsymbol{\delta}}}_l\boldsymbol{I}_i\boldsymbol{C}_{li}\boldsymbol{\omega} + \boldsymbol{I}_i\boldsymbol{C}_l\ddot{\boldsymbol{\gamma}}_l - \boldsymbol{I}_i\tilde{\dot{\boldsymbol{\delta}}}_l\boldsymbol{C}_l\dot{\boldsymbol{\gamma}}_l + \boldsymbol{C}_{li}\tilde{\boldsymbol{\omega}}\boldsymbol{C}_{li}^T\boldsymbol{I}_i\boldsymbol{C}_l\dot{\boldsymbol{\gamma}}_l + \boldsymbol{C}_l\tilde{\dot{\boldsymbol{\gamma}}}_l\boldsymbol{C}_l^T\boldsymbol{I}_i\boldsymbol{C}_l\dot{\boldsymbol{\gamma}}_l \\
&+ \tilde{\dot{\boldsymbol{\delta}}}_l\boldsymbol{I}_i\boldsymbol{C}_l\dot{\boldsymbol{\gamma}}_l\boldsymbol{I}_i\ddot{\boldsymbol{\delta}}_l + \boldsymbol{C}_{li}\tilde{\boldsymbol{\omega}}\boldsymbol{C}_{li}^T\boldsymbol{I}_i\dot{\boldsymbol{\delta}}_l + \boldsymbol{C}_l\tilde{\dot{\boldsymbol{\gamma}}}_l\boldsymbol{C}_l^T\boldsymbol{I}_i\dot{\boldsymbol{\delta}}_l
\end{aligned} \tag{4.20}$$

The third fraction on the right hand side of (4.13) can be derived in the inner gimbal frame $\{G_{li}\}$ as:

$$\frac{d\boldsymbol{h}}{dt}_N = \frac{d\boldsymbol{h}}{dt}_{G_i} + {}^{N-G_i}\boldsymbol{\omega}\times\boldsymbol{h} = (\boldsymbol{\omega} + \dot{\boldsymbol{\gamma}}_l + \dot{\boldsymbol{\delta}}_l)\times\boldsymbol{h} = \boldsymbol{C}_{li}\tilde{\boldsymbol{\omega}}\boldsymbol{C}_{li}^T\boldsymbol{h} + \boldsymbol{C}_l\tilde{\dot{\boldsymbol{\gamma}}}_l\boldsymbol{C}_l^T\boldsymbol{h} + \tilde{\dot{\boldsymbol{\delta}}}_l\boldsymbol{h} \tag{4.21}$$

Hence, the torque generated by the lth DGCMG can be expressed in the vehicle frame

as:

$$\begin{aligned}\boldsymbol{L}_{Gl} =&\frac{d\boldsymbol{H}_l^{G/CG}}{dt}_N\\ =&\boldsymbol{C}_{lo}^T\boldsymbol{J}_o\boldsymbol{C}_{lo}\dot{\boldsymbol{\omega}} - \boldsymbol{C}_{lo}^T\boldsymbol{J}_o\tilde{\dot{\boldsymbol{\gamma}}}_l\boldsymbol{C}_{lo}\boldsymbol{\omega} + \tilde{\boldsymbol{\omega}}\boldsymbol{C}_{lo}^T\boldsymbol{J}_o\boldsymbol{C}_{lo}\boldsymbol{\omega} + \boldsymbol{C}_{lo}^T\tilde{\dot{\boldsymbol{\gamma}}}_l\boldsymbol{J}_o\boldsymbol{C}_{lo}\boldsymbol{\omega}\\ &+\boldsymbol{C}_{lo}^T\boldsymbol{J}_o\ddot{\boldsymbol{\gamma}}_l + \tilde{\boldsymbol{\omega}}\boldsymbol{C}_{lo}^T\boldsymbol{J}_o\dot{\boldsymbol{\gamma}}_l + \boldsymbol{C}_{li}^T\boldsymbol{I}_i\boldsymbol{C}_{li}\dot{\boldsymbol{\omega}} - \boldsymbol{C}_{li}^T\boldsymbol{I}_i\boldsymbol{C}_l\tilde{\dot{\boldsymbol{\gamma}}}_l\boldsymbol{C}_{lo}\boldsymbol{\omega} - \boldsymbol{C}_{li}^T\boldsymbol{I}_i\tilde{\dot{\boldsymbol{\delta}}}_l\boldsymbol{C}_{li}\boldsymbol{\omega}\\ &+\tilde{\boldsymbol{\omega}}\boldsymbol{C}_{li}^T\boldsymbol{I}_i\boldsymbol{C}_{li}\boldsymbol{\omega} + \boldsymbol{C}_{lo}^T\tilde{\boldsymbol{\gamma}}_l\boldsymbol{C}_l^T\boldsymbol{I}_i\boldsymbol{C}_{li}\boldsymbol{\omega} + \boldsymbol{C}_{li}^T\tilde{\dot{\boldsymbol{\delta}}}_l\boldsymbol{I}_i\boldsymbol{C}_{li}\boldsymbol{\omega} + \boldsymbol{C}_{li}^T\boldsymbol{I}_i\boldsymbol{C}_l\ddot{\boldsymbol{\gamma}}_l - \boldsymbol{C}_{li}^T\boldsymbol{I}_i\tilde{\dot{\boldsymbol{\delta}}}_l\boldsymbol{C}_l\dot{\boldsymbol{\gamma}}_l\\ &+\tilde{\boldsymbol{\omega}}\boldsymbol{C}_{li}^T\boldsymbol{I}_i\boldsymbol{C}_l\dot{\boldsymbol{\gamma}}_l + \boldsymbol{C}_{lo}^T\tilde{\boldsymbol{\gamma}}_l\boldsymbol{C}_l^T\boldsymbol{I}_i\boldsymbol{C}_l\dot{\boldsymbol{\gamma}}_l + \boldsymbol{C}_{li}^T\tilde{\boldsymbol{\delta}}_l\boldsymbol{I}_i\boldsymbol{C}_l\dot{\boldsymbol{\gamma}}_l + \boldsymbol{C}_{li}^T\boldsymbol{I}_i\ddot{\boldsymbol{\delta}}_l + \tilde{\boldsymbol{\omega}}\boldsymbol{C}_{li}^T\boldsymbol{I}_i\dot{\boldsymbol{\delta}}_l\\ &+\boldsymbol{C}_{lo}^T\tilde{\boldsymbol{\gamma}}_l\boldsymbol{C}_l^T\boldsymbol{I}_i\dot{\boldsymbol{\delta}}_l + \tilde{\boldsymbol{\omega}}\boldsymbol{C}_{li}^T\boldsymbol{h} + \boldsymbol{C}_{lo}^T\tilde{\boldsymbol{\gamma}}_l\boldsymbol{C}_l^T\boldsymbol{h} + \boldsymbol{C}_{li}^T\tilde{\boldsymbol{\delta}}_l\boldsymbol{h}\end{aligned} \tag{4.22}$$

Substitute (4.22) into (4.12), we obtain

$$\begin{aligned}\boldsymbol{L}_e =&\boldsymbol{I}\dot{\boldsymbol{\omega}} + \tilde{\boldsymbol{\omega}}\boldsymbol{I}^S\boldsymbol{\omega} + \sum_{l=1}^{n}\tilde{\boldsymbol{\omega}}(\boldsymbol{C}_{lo}^T\boldsymbol{J}_o\boldsymbol{C}_{lo}\boldsymbol{\omega} + \boldsymbol{C}_{li}^T\boldsymbol{I}_i\boldsymbol{C}_{li}\boldsymbol{\omega} + \boldsymbol{C}_{li}^T\boldsymbol{h})\\ &+\sum_{l=1}^{n}[(\boldsymbol{C}_{lo}^T\boldsymbol{J}_o + \boldsymbol{C}_{li}^T\boldsymbol{I}_i\boldsymbol{C}_l)\ddot{\boldsymbol{\gamma}}_l + \boldsymbol{C}_{li}^T\boldsymbol{I}_i\ddot{\boldsymbol{\delta}}_l]\\ &+\sum_{l=1}^{n}(\boldsymbol{C}_{lo}^T\tilde{\boldsymbol{\gamma}}_l\boldsymbol{J}_o\boldsymbol{C}_{lo} - \boldsymbol{C}_{lo}^T\boldsymbol{J}_o\tilde{\boldsymbol{\gamma}}_l\boldsymbol{C}_{lo} + \boldsymbol{C}_{lo}^T\dot{\boldsymbol{\gamma}}_l\boldsymbol{C}_l^T\boldsymbol{I}_i\boldsymbol{C}_{li} - \boldsymbol{C}_{li}^T\boldsymbol{I}_i\boldsymbol{C}_l\tilde{\boldsymbol{\gamma}}_l\boldsymbol{C}_{lo})\boldsymbol{\omega}\\ &+\sum_{l=1}^{n}\tilde{\boldsymbol{\omega}}(\boldsymbol{C}_{lo}^T\boldsymbol{J}_o + \boldsymbol{C}_{li}^T\boldsymbol{I}_i\boldsymbol{C}_l)\dot{\boldsymbol{\gamma}}_l + \sum_{l=1}^{n}\boldsymbol{C}_{lo}^T\tilde{\dot{\boldsymbol{\gamma}}}_l\boldsymbol{C}_l^T\boldsymbol{h}\\ &+\sum_{l=1}^{n}(\boldsymbol{C}_{li}^T\tilde{\dot{\boldsymbol{\delta}}}_l\boldsymbol{I}_i\boldsymbol{C}_{li} - \boldsymbol{C}_{li}^T\boldsymbol{I}_i\tilde{\dot{\boldsymbol{\delta}}}_l\boldsymbol{C}_{li})\boldsymbol{\omega} + \sum_{l=1}^{n}\tilde{\boldsymbol{\omega}}\boldsymbol{C}_{li}^T\boldsymbol{I}_i\dot{\boldsymbol{\delta}}_l + \sum_{l=1}^{n}\boldsymbol{C}_{li}^T\tilde{\dot{\boldsymbol{\delta}}}_l\boldsymbol{h}\\ &+\sum_{l=1}^{n}(\boldsymbol{C}_{li}^T\tilde{\dot{\boldsymbol{\delta}}}_l\boldsymbol{I}_i\boldsymbol{C}_l - \boldsymbol{C}_{li}^T\boldsymbol{I}_i\tilde{\dot{\boldsymbol{\delta}}}_l\boldsymbol{C}_l)\dot{\boldsymbol{\gamma}}_l + \sum_{l=1}^{n}\boldsymbol{C}_{lo}^T\tilde{\dot{\boldsymbol{\gamma}}}_l\boldsymbol{C}_l^T\boldsymbol{I}_i(\boldsymbol{C}_l\dot{\boldsymbol{\gamma}}_l + \dot{\boldsymbol{\delta}}_l)\end{aligned} \tag{4.23}$$

where

$$\boldsymbol{I} = \boldsymbol{I}^S + \sum_{l=1}^{n}(\boldsymbol{C}_{lo}^T\boldsymbol{J}_o\boldsymbol{C}_{lo} + \boldsymbol{C}_{li}^T\boldsymbol{I}_i\boldsymbol{C}_{li}) \tag{4.24}$$

Equation (4.23) can be rewritten as:

$$\begin{aligned}\dot{\boldsymbol{\omega}} =&-\boldsymbol{I}^{-1}[\tilde{\boldsymbol{\omega}}\boldsymbol{I}^S\boldsymbol{\omega} - \boldsymbol{L}_e + \sum_{l=1}^{n}\tilde{\boldsymbol{\omega}}(\boldsymbol{C}_{lo}^T\boldsymbol{J}_o\boldsymbol{C}_{lo}\boldsymbol{\omega} + \boldsymbol{C}_{li}^T\boldsymbol{I}_i\boldsymbol{C}_{li}\boldsymbol{\omega} + \boldsymbol{C}_{li}^T\boldsymbol{h})\\ &+\boldsymbol{B}\ddot{\boldsymbol{\sigma}} + \boldsymbol{D}_{o3}\dot{\boldsymbol{\gamma}} + \boldsymbol{D}_{o2}\dot{\boldsymbol{\gamma}} + \boldsymbol{D}_{o1}\dot{\boldsymbol{\gamma}} + \boldsymbol{D}_{i3}\dot{\boldsymbol{\delta}} + \boldsymbol{D}_{i2}\dot{\boldsymbol{\delta}} + \boldsymbol{D}_{i1}\dot{\boldsymbol{\delta}}\\ &+\sum_{l=1}^{n}(\boldsymbol{C}_{li}^T\tilde{\dot{\boldsymbol{\delta}}}_l\boldsymbol{I}_i\boldsymbol{C}_l - \boldsymbol{C}_{li}^T\boldsymbol{I}_i\tilde{\dot{\boldsymbol{\delta}}}_l\boldsymbol{C}_l)\dot{\boldsymbol{\gamma}}_l + \sum_{l=1}^{n}\boldsymbol{C}_{lo}^T\tilde{\dot{\boldsymbol{\gamma}}}_l\boldsymbol{C}_l^T\boldsymbol{I}_i(\boldsymbol{C}_l\dot{\boldsymbol{\gamma}}_l + \dot{\boldsymbol{\delta}}_l)]\end{aligned} \tag{4.25}$$

where

$$\dot{\boldsymbol{\gamma}} = [\dot{\gamma}_1, \dot{\gamma}_2, \cdots, \dot{\gamma}_n]^T \tag{4.26}$$

$$\dot{\boldsymbol{\delta}} = \left[\dot{\delta}_1, \dot{\delta}_2, \cdots, \dot{\delta}_n\right]^T \tag{4.27}$$

and

$$\ddot{\boldsymbol{\sigma}} = \left[\ddot{\boldsymbol{\gamma}}^T, \ddot{\boldsymbol{\delta}}^T\right]^T, \tag{4.28}$$

while

$$\boldsymbol{B}\ddot{\boldsymbol{\sigma}} = \sum_{l=1}^{n} [(\boldsymbol{C}_{lo}^T \boldsymbol{J}_o + \boldsymbol{C}_{li}^T \boldsymbol{I}_i \boldsymbol{C}_l)\ddot{\boldsymbol{\gamma}}_l + \boldsymbol{C}_{li}^T \boldsymbol{I}_i \ddot{\boldsymbol{\delta}}_l] \tag{4.29}$$

$$\boldsymbol{D}_{o3}\dot{\boldsymbol{\gamma}} = \sum_{l=1}^{n} (\boldsymbol{C}_{lo}^T \tilde{\dot{\boldsymbol{\gamma}}}_l \boldsymbol{J}_o \boldsymbol{C}_{lo} - \boldsymbol{C}_{lo}^T \boldsymbol{J}_o \tilde{\dot{\boldsymbol{\gamma}}}_l \boldsymbol{C}_{lo} + \boldsymbol{C}_{lo}^T \dot{\boldsymbol{\gamma}}_l \boldsymbol{C}_l^T \boldsymbol{I}_i \boldsymbol{C}_{li} - \boldsymbol{C}_{li}^T \boldsymbol{I}_i \boldsymbol{C}_l \tilde{\dot{\boldsymbol{\gamma}}}_l \boldsymbol{C}_{lo})\boldsymbol{\omega} \tag{4.30}$$

$$\boldsymbol{D}_{o2}\dot{\boldsymbol{\gamma}} = \sum_{l=1}^{n} \tilde{\boldsymbol{\omega}}(\boldsymbol{C}_{lo}^T \boldsymbol{J}_o + \boldsymbol{C}_{li}^T \boldsymbol{I}_i \boldsymbol{C}_l)\dot{\boldsymbol{\gamma}}_l \tag{4.31}$$

$$\boldsymbol{D}_{o1}\dot{\boldsymbol{\gamma}} = \sum_{l=1}^{n} \boldsymbol{C}_{lo}^T \tilde{\dot{\boldsymbol{\gamma}}}_l \boldsymbol{C}_l^T \boldsymbol{h} \tag{4.32}$$

$$\boldsymbol{D}_{i3}\dot{\boldsymbol{\delta}} = \sum_{l=1}^{n} (\boldsymbol{C}_{li}^T \tilde{\dot{\boldsymbol{\delta}}}_l \boldsymbol{I}_i \boldsymbol{C}_{li} - \boldsymbol{C}_{li}^T \boldsymbol{I}_i \tilde{\dot{\boldsymbol{\delta}}}_l \boldsymbol{C}_{li})\boldsymbol{\omega} \tag{4.33}$$

$$\boldsymbol{D}_{i2}\dot{\boldsymbol{\delta}} = \sum_{l=1}^{n} \tilde{\boldsymbol{\omega}} \boldsymbol{C}_{li}^T \boldsymbol{I}_i \dot{\boldsymbol{\delta}}_l \tag{4.34}$$

and

$$\boldsymbol{D}_{i1}\dot{\boldsymbol{\delta}} = \sum_{l=1}^{n} \boldsymbol{C}_{li}^T \tilde{\dot{\boldsymbol{\delta}}}_l \boldsymbol{h} \tag{4.35}$$

4.3 Spacecraft attitude control law design

Suppose the spacecraft attitude angular and angular velocity commands are given by $\boldsymbol{q}_c$ and $\boldsymbol{\omega}_c$, respectively, as below.

$$\dot{\boldsymbol{q}}_c = \frac{1}{2}\boldsymbol{G}(\boldsymbol{q}_c)\boldsymbol{\omega}_c \tag{4.36}$$

Define the tracking errors as:

$$\begin{cases} \boldsymbol{e}_1 = \boldsymbol{q} - \boldsymbol{q}_c \\ \boldsymbol{e}_2 = \boldsymbol{\omega} - \boldsymbol{\omega}_c \end{cases} \tag{4.37}$$

Then, we have

$$\begin{cases} \dot{\boldsymbol{e}}_1 = \dot{\boldsymbol{q}} - \dot{\boldsymbol{q}}_c \\ \dot{\boldsymbol{e}}_2 = \dot{\boldsymbol{\omega}} - \dot{\boldsymbol{\omega}}_c \end{cases} \tag{4.38}$$

Assume that $\boldsymbol{q}$ and $\boldsymbol{\omega}$ are measurable. We then utilize the second method of Lyapunov to design the attitude control law. The control Lyapunov function (CLF) is constructed as:

$$V(\boldsymbol{e}_1, \boldsymbol{e}_2) = k\boldsymbol{e}_1^T \boldsymbol{e}_1 + \frac{1}{2}\boldsymbol{e}_2^T \boldsymbol{I} \boldsymbol{e}_2 \tag{4.39}$$

where k is a constant weighting coefficient. The time derivative of the CLF gives

$$\begin{aligned}\dot{V} =&2k\boldsymbol{e}_1^T\dot{\boldsymbol{e}}_1+\boldsymbol{e}_2^T\boldsymbol{I}\dot{\boldsymbol{e}}_2\\ =&k(\boldsymbol{q}^T-\boldsymbol{q}_c^T)[\boldsymbol{G}(\boldsymbol{q})\boldsymbol{\omega}-\boldsymbol{G}(\boldsymbol{q}_c)\boldsymbol{\omega}_c]+(\boldsymbol{\omega}^T-\boldsymbol{\omega}_c^T)\boldsymbol{I}(\dot{\boldsymbol{\omega}}-\dot{\boldsymbol{\omega}}_c)\\ =&k[-\boldsymbol{q}^T\boldsymbol{G}(\boldsymbol{q}_c)\boldsymbol{\omega}_c-\boldsymbol{q}_c^T\boldsymbol{G}(\boldsymbol{q})\boldsymbol{\omega}]+(\boldsymbol{\omega}^T-\boldsymbol{\omega}_c^T)\boldsymbol{I}(\dot{\boldsymbol{\omega}}-\dot{\boldsymbol{\omega}}_c)\\ =&-(\boldsymbol{\omega}^T-\boldsymbol{\omega}_c^T)[k\boldsymbol{G}^T(\boldsymbol{q})\boldsymbol{q}_c+\boldsymbol{I}\dot{\boldsymbol{\omega}}_c+\tilde{\boldsymbol{\omega}}\boldsymbol{I}^S\boldsymbol{\omega}-\boldsymbol{L}_e\\ &+\sum_{l=1}^{n}\tilde{\boldsymbol{\omega}}(\boldsymbol{C}_{lo}^T\boldsymbol{J}_o\boldsymbol{C}_{lo}\boldsymbol{\omega}+\boldsymbol{C}_{li}^T\boldsymbol{I}_i\boldsymbol{C}_{li}\boldsymbol{\omega}+\boldsymbol{C}_{li}^T\boldsymbol{h})+\boldsymbol{B}\ddot{\boldsymbol{\sigma}}+\boldsymbol{D}_o\dot{\boldsymbol{\gamma}}+\boldsymbol{D}_i\dot{\boldsymbol{\delta}}\\ &+\sum_{l=1}^{n}(\boldsymbol{C}_{li}^T\tilde{\dot{\boldsymbol{\delta}}}_l\boldsymbol{I}_i\boldsymbol{C}_l-\boldsymbol{C}_{li}^T\boldsymbol{I}_i\tilde{\dot{\boldsymbol{\delta}}}_l\boldsymbol{C}_l)\dot{\boldsymbol{\gamma}}_l+\sum_{l=1}^{n}\boldsymbol{C}_{lo}^T\tilde{\dot{\boldsymbol{\gamma}}}_l\boldsymbol{C}_l^T\boldsymbol{I}_i(\boldsymbol{C}_l\dot{\boldsymbol{\gamma}}_l+\dot{\boldsymbol{\delta}}_l)]\end{aligned}\tag{4.40}$$

where $\boldsymbol{D}_o=\boldsymbol{D}_{o1}+\boldsymbol{D}_{o2}+\boldsymbol{D}_{o3}$ and $\boldsymbol{D}_i=\boldsymbol{D}_{i1}+\boldsymbol{D}_{i2}+\boldsymbol{D}_{i3}$.

From (4.40), it follows that a feedback attitude control law can be designed as follows.

$$\begin{aligned}\boldsymbol{L}_r=&\boldsymbol{K}(\boldsymbol{\omega}-\boldsymbol{\omega}_c)-k\boldsymbol{G}^T(\boldsymbol{q})\boldsymbol{q}_c-\boldsymbol{I}\dot{\boldsymbol{\omega}}_c-\tilde{\boldsymbol{\omega}}\boldsymbol{I}^S\boldsymbol{\omega}+\boldsymbol{L}_e\\ &-\sum_{l=1}^{n}\tilde{\boldsymbol{\omega}}(\boldsymbol{C}_{lo}^T\boldsymbol{J}_o\boldsymbol{C}_{lo}\boldsymbol{\omega}+\boldsymbol{C}_{li}^T\boldsymbol{I}_i\boldsymbol{C}_{li}\boldsymbol{\omega}+\boldsymbol{C}_{li}^T\boldsymbol{h})\end{aligned}\tag{4.41}$$

where $\boldsymbol{K}$ is a positive definite matrix with an appropriate dimension. To realize the control law (4.41), the gimbal rates and accelerations must satisfy the following equation

$$\begin{aligned}\boldsymbol{L}_r=&\boldsymbol{K}(\boldsymbol{\omega}-\boldsymbol{\omega}_c)-k\boldsymbol{G}^T(\boldsymbol{q})\boldsymbol{q}_c-\boldsymbol{I}\dot{\boldsymbol{\omega}}_c-\tilde{\boldsymbol{\omega}}\boldsymbol{I}^S\boldsymbol{\omega}+\boldsymbol{L}_e\\ &-\sum_{l=1}^{n}\tilde{\boldsymbol{\omega}}(\boldsymbol{C}_{lo}^T\boldsymbol{J}_o\boldsymbol{C}_{lo}\boldsymbol{\omega}+\boldsymbol{C}_{li}^T\boldsymbol{I}_i\boldsymbol{C}_{li}\boldsymbol{\omega}+\boldsymbol{C}_{li}^T\boldsymbol{h})\\ =&\boldsymbol{B}\ddot{\boldsymbol{\sigma}}+\boldsymbol{D}_o\dot{\boldsymbol{\gamma}}+\boldsymbol{D}_i\dot{\boldsymbol{\delta}}+\sum_{l=1}^{n}(\boldsymbol{C}_{li}^T\tilde{\dot{\boldsymbol{\delta}}}_l\boldsymbol{I}_i\boldsymbol{C}_l-\boldsymbol{C}_{li}^T\boldsymbol{I}_i\tilde{\dot{\boldsymbol{\delta}}}_l\boldsymbol{C}_l)\dot{\boldsymbol{\gamma}}_l\\ &+\sum_{l=1}^{n}\boldsymbol{C}_{lo}^T\tilde{\dot{\boldsymbol{\gamma}}}_l\boldsymbol{C}_l^T\boldsymbol{I}_i(\boldsymbol{C}_l\dot{\boldsymbol{\gamma}}_l+\dot{\boldsymbol{\delta}}_l)\end{aligned}\tag{4.42}$$

Substituting (4.42) into (4.40) yields

$$\dot{V}=-(\boldsymbol{\omega}^T-\boldsymbol{\omega}_c^T)\boldsymbol{K}(\boldsymbol{\omega}-\boldsymbol{\omega}_c)<0,\quad \boldsymbol{\omega}\neq\boldsymbol{\omega}_c\tag{4.43}$$

Thus, the tracking errors convergence to zero under the feedback control law (4.41).

However, the steering law of the system described by (4.25) is too complicated to be realized. In practice, $\boldsymbol{J}_o$, $\boldsymbol{J}_i$ and $\boldsymbol{J}_w$ are far less than $\boldsymbol{I}^S$, and hence they can be neglected during the design process. Thus, (4.25) can be simplified as:

$$\dot{\boldsymbol{\omega}}=-(\boldsymbol{I}^S)^{-1}[\tilde{\boldsymbol{\omega}}\boldsymbol{I}^S\boldsymbol{\omega}-\boldsymbol{L}_e+\sum_{l=1}^{n}\tilde{\boldsymbol{\omega}}\boldsymbol{C}_{li}^T\boldsymbol{h}+\boldsymbol{D}_{o1}\dot{\boldsymbol{\gamma}}+\boldsymbol{D}_{i1}\dot{\boldsymbol{\delta}}]\tag{4.44}$$

Consequently, the feedback attitude control law (4.41) can be simplified as:

$$\boldsymbol{L}_r = \boldsymbol{K}(\boldsymbol{\omega} - \boldsymbol{\omega}_c) - k\boldsymbol{G}^T(\boldsymbol{q})\boldsymbol{q}_c - \boldsymbol{I}^S\dot{\boldsymbol{\omega}}_c - \tilde{\boldsymbol{\omega}}\boldsymbol{I}^S\boldsymbol{\omega} + \boldsymbol{L}_e - \sum_{l=1}^{n}\tilde{\boldsymbol{\omega}}\boldsymbol{C}_{li}^T\boldsymbol{h} \tag{4.45}$$

To realize this control law, the gimbal rates should satisfy the following equation

$$\boldsymbol{D}_{o1}\dot{\boldsymbol{\gamma}} + \boldsymbol{D}_{i1}\dot{\boldsymbol{\delta}} = \boldsymbol{L}_r \tag{4.46}$$

Equation (4.46) can be written as:

$$\boldsymbol{D}\dot{\boldsymbol{\sigma}} = \boldsymbol{L}_r \tag{4.47}$$

where $\boldsymbol{D} = [\boldsymbol{D}_{o1}, \boldsymbol{D}_{i1}]$, $\dot{\boldsymbol{\sigma}} = \left[\dot{\boldsymbol{\gamma}}^T, \dot{\boldsymbol{\delta}}^T\right]^T$.

4.4 DGCMGs system singularity analysis and steering law design

Singular directions of a DGCMGs system are the directions along which the output torque can not be produced. A single DGCMG has two gimbals – the outer gimbal and the inner gimbal. Each gimbal can precess around its gimbal axis. Rotations of the two gimbals provide two degree of freedom for the rotor, which can be pointed to any direction of the inertial space. Hence the momentum envelop of the DGCMGs system is a sphere which is much efficient in configuration. In practice, to avoid exorbitant outer gimbal rates, inner gimbal angles are always restricted to be less than $\pm 90°$, whereas restrictions on the outer gimbal angles are not necessary.

4.4.1 Singularity theorem

Theorem 4.1. *Consider the situations except the one in which the inner gimbal angles are equal to $\pm 90°$, i.e., the rotor axes align with the outer gimbal axes. Then, the necessary and sufficient condition for singularity is that all the angular momentums of the rotors are parallel or antiparallel.*

Proof. Necessity. When all the angular momentums of the rotors are parallel or antiparallel along one direction, it follows from the theorem on moment of momentum [57] that all the torques produced by the rotors lie in a plane which is perpendicular to the given direction, i.e., no torque can be produced along this direction, so the singularity occurs.

Sufficiency. Suppose that the angular momentums (h_1 and h_2) of two identical rotors are not parallel or antiparallel to each other (see Figure 4.2), and that the inner gimbal angles are not equal to $\pm 90°$. The control torques, which are perpendicular to their rotor

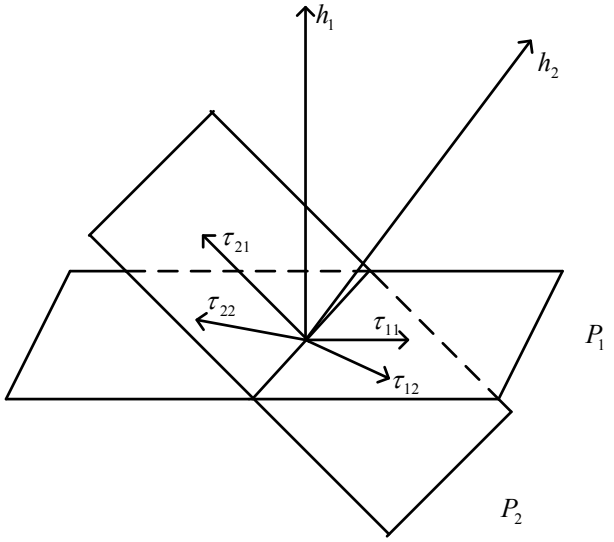

Figure 4.2: Sketch of DGCMGs singularity principle.

axis, can be produced by the rotations of either the inner gimbals or the outer gimbals, and they are not in the same direction.

From Figure 4.2, we observe that the torques $\boldsymbol{\tau}_{11}$ and $\boldsymbol{\tau}_{12}$ produced by the first DGCMG are in the plane P_1 which is perpendicular to h_1, while the torques $\boldsymbol{\tau}_{21}$ and $\boldsymbol{\tau}_{22}$ produced by the second DGCMG are in the plane P_2 which is perpendicular to h_2. If h_1 and h_2 are not parallel, then the planes P_1 and P_2 will not be parallel. Thus, there must exist an intersection line between them. Because $\boldsymbol{\tau}_{21}$ and $\boldsymbol{\tau}_{22}$ are not in the same line, at least one of them is not coincide with the intersection line, and must lie out of the plane P_1. This means that the control torques can be produced in any direction of the three dimensional space, showing that no singularity can occur. This completes the proof. □

Suppose that the magnitude of each DGCMG angular momentum is 1. Then, it follows from Theorem 4.1 that in the configuration where three DGCMGs are orthogonally mounted (see Figure 4.3), it is clear that the internal singular surface and the external singular surface are two spheres with the radii of 1 and 3, respectively (Figure 4.4). In the configuration where four DGCMGs are parallel mounted (see Figure 4.5), the internal singular surfaces are the original point and a sphere with radius 2. The external singular surface is a sphere with radius 4 (Figure 4.6). As we can see, DGCMGs system has very simple singular surfaces and is much efficient in configuration.

4.4.2 Steering law design

From (4.47), we can see that, for any given demanded control torque $\boldsymbol{L}_r$, it can be expressed as a function of the gimbal angle $\boldsymbol{\sigma}$ and the gimbal angle velocity $\dot{\boldsymbol{\sigma}}$. To realize the feedback control law (4.45), we must find a suitable combination of the inner gimbal

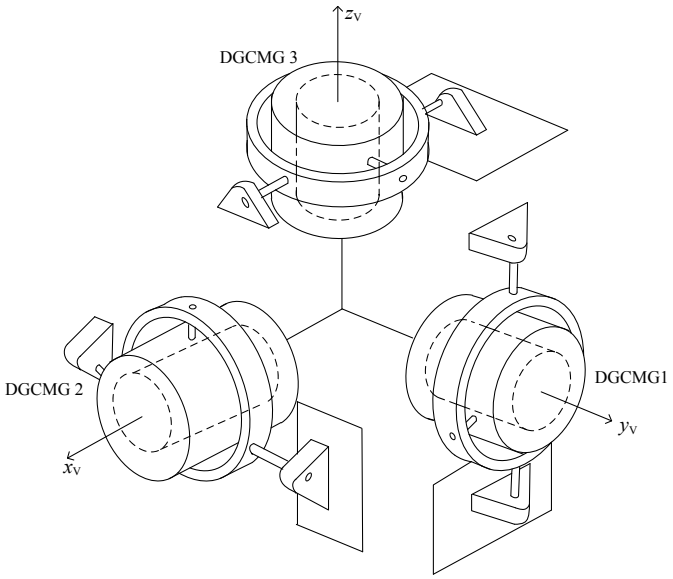

Figure 4.3: Three DGCMGs in orthogonal configuration.

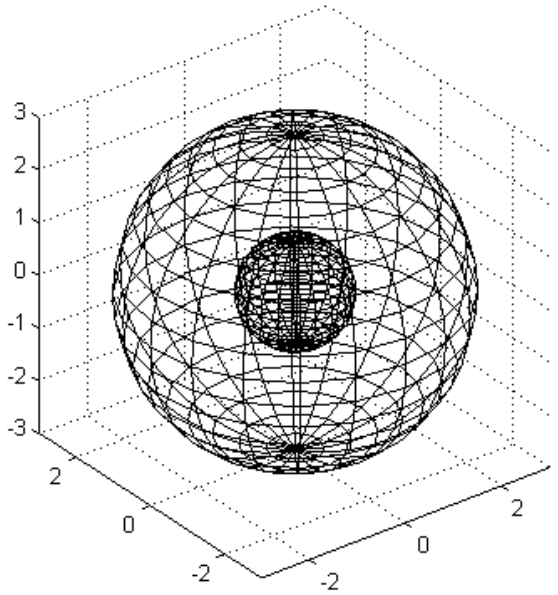

Figure 4.4: Singular surface of 3 DGCMGs orthogonally mounted.

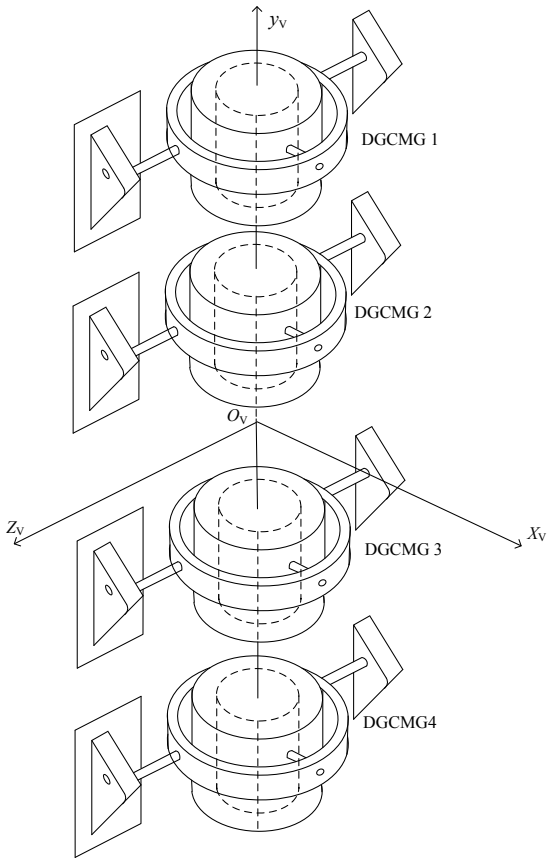

Figure 4.5: Four DGCMGs in parallel configuration.

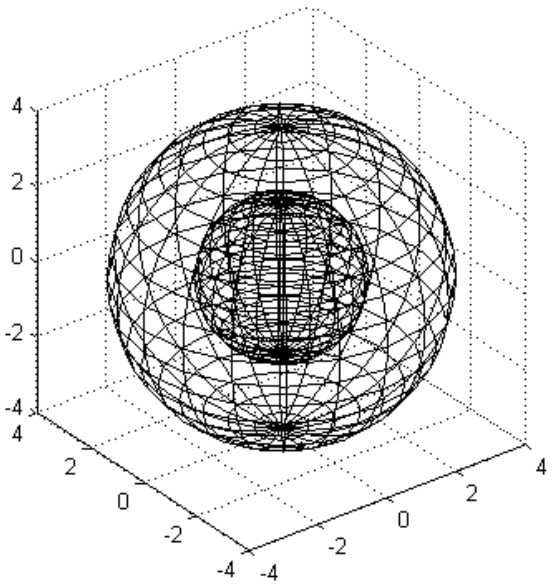

Figure 4.6: Singular surface of 4 DGCMGs parallel mounted.

angle velocities and the outer gimbal angle velocities such that (4.47) is satisfied.

In the following, we will derive a Singularity-Robustness plus null motion steering law which could avoid the internal singularity states of the DGCMGs system.

First we shall introduce the well-known Moore-Penrose (MP) steering law [5]. From the minimization of the cost function

$$f_{MP} = \frac{1}{2}\dot{\boldsymbol{\sigma}}^T\dot{\boldsymbol{\sigma}} \tag{4.48}$$

subject to (4.47), it follows that the MP steering law is given by

$$\dot{\boldsymbol{\sigma}} = \boldsymbol{D}^T(\boldsymbol{D}\boldsymbol{D}^T)^{-1}\boldsymbol{L}_r \tag{4.49}$$

Clearly, the MP steering law aims to compute the desired gimbal velocities which could generate the commanded torque with minimum gimbal velocity efforts. The idea of the MP steering law is straightforward, and its form is concise. However, if $\text{rank}(\boldsymbol{D}) < 3$, then $\boldsymbol{D}\boldsymbol{D}^T$ is noninvertible, i.e., singularity occurs. The magnitude of $\dot{\boldsymbol{\sigma}}$ will also be increased tremendously as the system approaching singularity. With these defects, the applicability of the MP steering law is somewhat restricted.

To overcome this problem, a Singularity-Robustness (SR) steering law is proposed as follows:

$$\dot{\boldsymbol{\sigma}} = \boldsymbol{D}^T(\boldsymbol{D}\boldsymbol{D}^T + \alpha\boldsymbol{I}_n)^{-1}\boldsymbol{L}_r \tag{4.50}$$

It is obtained through minimizing the following cost function

$$f_{SR} = \frac{1}{2}\alpha\dot{\boldsymbol{\sigma}}^T\dot{\boldsymbol{\sigma}} + \frac{1}{2}(\boldsymbol{D}\dot{\boldsymbol{\sigma}} - \boldsymbol{L}_r)^T(\boldsymbol{D}\dot{\boldsymbol{\sigma}} - \boldsymbol{L}_r) \tag{4.51}$$

subject to (4.47). $\boldsymbol{I}_n$ is an identity matrix with an appropriate dimension, α is a weighting coefficient and can be chosen as:

$$\alpha = \alpha_0 \exp[-\det(\boldsymbol{D}\boldsymbol{D}^T)] \tag{4.52}$$

where α_0 is the maximum value of α. As $\boldsymbol{D}\boldsymbol{D}^T$ approaches to singularity, α will increase to α_0, and the inverse computation in (4.50) can be carried out. When $\boldsymbol{D}\boldsymbol{D}^T$ is moving far away from the singularity status, α will decrease to zero exponentially. In this situation, the SR steering law is equivalent to the MP steering law. The output torque, by using the SR steering law, will have a small deviation from the desired torque when the system is close to singularity. There is a tradeoff between the singularity status and the control torque deviation.

By examining (4.47), we see that the MP steering law is the particular solution, while

the homogeneous solution of (4.47) is obtained by solving the following equation

$$\boldsymbol{D}\boldsymbol{n} = 0 \tag{4.53}$$

where $\boldsymbol{n}$ is a vector in the null space of $\boldsymbol{D}$ and is expressed as:

$$\boldsymbol{n} = (\boldsymbol{I}_n - \boldsymbol{D}^+\boldsymbol{D})\boldsymbol{d} \tag{4.54}$$

$\boldsymbol{D}^+ = \boldsymbol{D}^T(\boldsymbol{D}\boldsymbol{D}^T)^{-1}$, and $\boldsymbol{d}$ is an arbitrary nonzero vector.

Thus, the general solution of (4.47) can be written as:

$$\dot{\boldsymbol{\sigma}} = \boldsymbol{D}^T(\boldsymbol{D}\boldsymbol{D}^T)^{-1}\boldsymbol{L}_r + \rho\boldsymbol{n} \tag{4.55}$$

where $\rho > 0$ is a constant scalar.

From the SR steering law (4.50), we can design a Singularity-Robustness plus Null Motion steering law given by

$$\dot{\boldsymbol{\sigma}} = \boldsymbol{D}^T(\boldsymbol{D}\boldsymbol{D}^T + \alpha\boldsymbol{I})^{-1}\boldsymbol{L}_r + \rho(\boldsymbol{I}_n - \boldsymbol{D}^+\boldsymbol{D})\boldsymbol{d} \tag{4.56}$$

Using different methods to choose $\boldsymbol{d}$ will yield different null motion steering laws. Here, the preferred gimbal angle method [81] is used and hence we choose $\boldsymbol{d}$ as:

$$\boldsymbol{d} = (\boldsymbol{\sigma}^* - \boldsymbol{\sigma}) \tag{4.57}$$

where $\boldsymbol{\sigma}^*$ denotes the preferred gimbal angle vector. The steering law (4.56) can be rewritten as:

$$\dot{\boldsymbol{\sigma}} = \boldsymbol{D}^T(\boldsymbol{D}\boldsymbol{D}^T + \alpha\boldsymbol{I})^{-1}\boldsymbol{L}_r + \rho(\boldsymbol{I}_n - \boldsymbol{D}^+\boldsymbol{D})(\boldsymbol{\sigma}^* - \boldsymbol{\sigma}) \tag{4.58}$$

4.5 Numerical simulations

In this section, we make use of a simulation program designed in the Matlab-Simulink environment to verify the performance of the proposed feedback control law and the SRNM steering law.

The spacecraft inertia matrix can be parameterized as:

$$\boldsymbol{I}^S = \begin{bmatrix} 300 & 0 & 0 \\ 0 & 305 & 0 \\ 0 & 0 & 330 \end{bmatrix} \text{Kg} \cdot \text{m}^2 \tag{4.59}$$

The inertia matrices of the outer gimbal, inner gimbal and rotor of each DGCMG are:

$$\boldsymbol{J}_o = \begin{bmatrix} 0.05 & 0 & 0 \\ 0 & 0.055 & 0 \\ 0 & 0 & 0.05 \end{bmatrix} \text{Kg} \cdot \text{m}^2 \tag{4.60}$$

$$\boldsymbol{J}_i = \begin{bmatrix} 0.01 & 0 & 0 \\ 0 & 0.02 & 0 \\ 0 & 0 & 0.01 \end{bmatrix} \text{Kg} \cdot \text{m}^2 \tag{4.61}$$

and

$$\boldsymbol{J}_w = \begin{bmatrix} 0.04 & 0 & 0 \\ 0 & 0.05 & 0 \\ 0 & 0 & 0.04 \end{bmatrix} \text{Kg} \cdot \text{m}^2 \tag{4.62}$$

The rotor spin velocity is:

$$\boldsymbol{\Omega} = [0, 1500, 0]^T \text{rad/s} \tag{4.63}$$

Substituting (4.62) and (4.63) into the equation $\boldsymbol{h} = \boldsymbol{J}_w\boldsymbol{\Omega}$, we obtain the magnitude of the rotor angular momentum, which is $h = 75\text{Kgm}^2/s$. Assume that the constraints on the gimbal velocities are

$$-7.64^\circ/\text{s} \leq \dot{\sigma}_i \leq 7.64^\circ/\text{s}, \quad i = 1, \ldots, r, \tag{4.64}$$

where $r/2$ is the number of the DGCMGs used and $\dot{\boldsymbol{\sigma}} = [\dot{\sigma}_1, \ldots, \dot{\sigma}_r]^T$. Then, the maximum control torque generated by the precession motion of each outer gimbal (or inner gimbal) is 10Nm.

4.5.1 Simulation analysis on DGCMG steering law

A Three DGCMGs orthogonally mounted

The orthogonally mounted three DGCMGs system is shown in Figure 4.3. The initial inner gimbal angles and outer gimbal angles are chosen as:

$$\delta_1(0) = 0^\circ,\ \delta_2(0) = 0^\circ,\ \delta_3(0) = 0^\circ \tag{4.65}$$

and

$$\gamma_1(0) = 45^\circ,\ \gamma_2(0) = 45^\circ,\ \gamma_3(0) = 45^\circ \tag{4.66}$$

respectively. The total angular momentum of the three DGCMGs system is zero, i.e.,

$$\sum_{i=1}^{3} \boldsymbol{h}_i = [0, 0, 0]^T \tag{4.67}$$

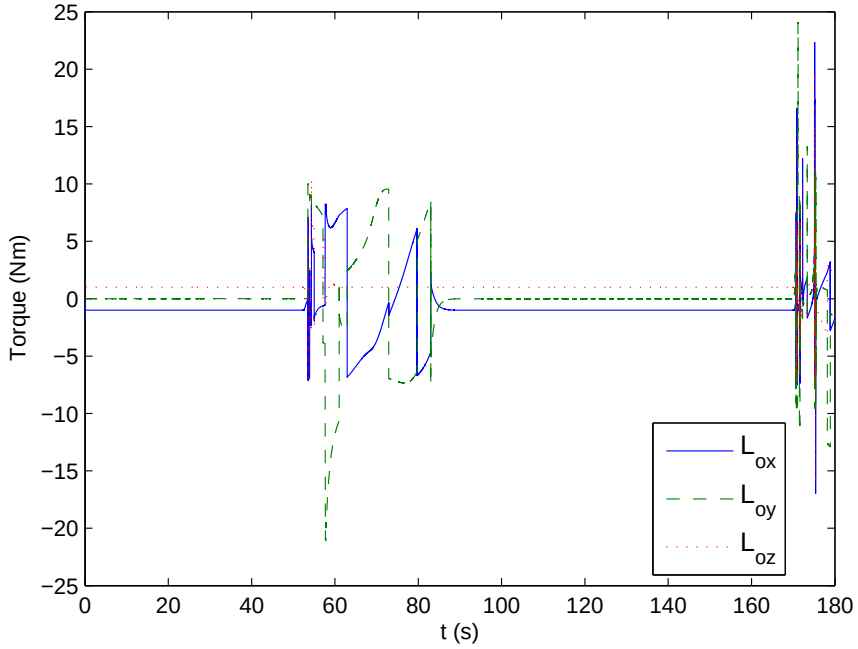

Figure 4.7: Constant torque tracking (MP 3DGCMG).

The separation angles between $\boldsymbol{h}_1$, $\boldsymbol{h}_2$ and $\boldsymbol{h}_3$ are all 120°. According to the principle of isogonal distribution [28], such an initial condition avails to avoiding the singular states.

When the system is influenced by constant external disturbance torques, the DGCMGs are required to output the corresponding control torques to stabilize the spacecraft. In practice, the disturbances are usually small.

Suppose that the demanded control torque is:

$$\boldsymbol{L}_r = [-1, 0, 1]^T \text{Nm} \tag{4.68}$$

First, we use the MP steering law to generate the control torque. The simulation results are shown in Figure 4.7 to Figure 4.9. It can be seen that the internal singularity status occurs at 53s, where $\boldsymbol{h}_1$, $\boldsymbol{h}_2$ and $\boldsymbol{h}_3$ are in the position of antiparallel (Figure 4.8). Because in the numerical simulations, there are always calculation errors. Thus, the system transits the internal singularity (Figure 4.9). However, when the system approaches to singularity status, gimbal velocities are saturated. During this period, the output control torque can not track the command precisely (Figure 4.7). Finally, the system achieves external singularity for which the system can not transit without the help of other torques.

In the second experiment, the SR steering law is used to produce the same control torque given by (4.68). We see that the SR steering law can not avoid the system to approach the internal singularity. However, it can transit such a singularity. (see Figure 4.11). The torque command is not well followed during the transition period (Figure 4.10)

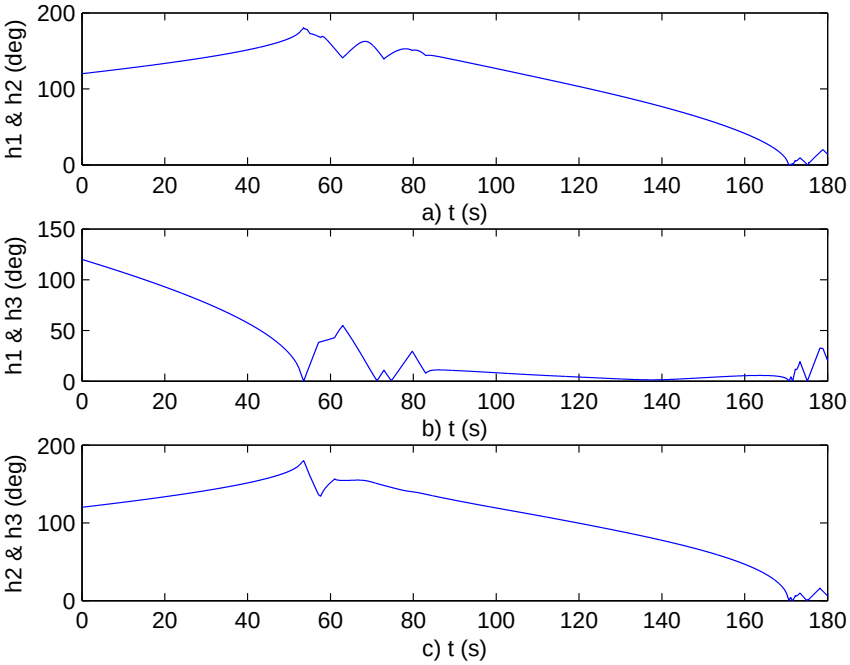

Figure 4.8: Separation angles (MP 3DGCMG).

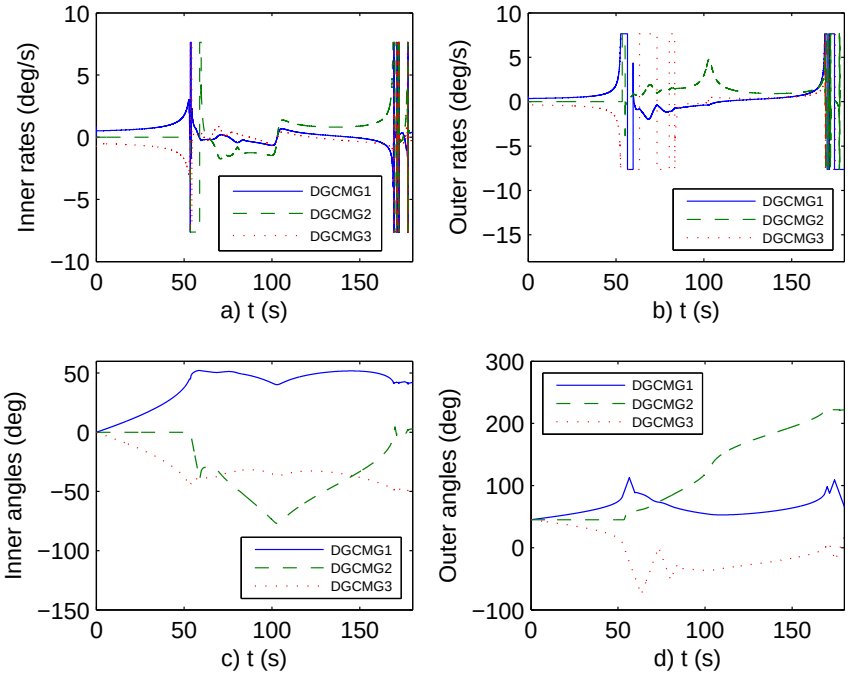

Figure 4.9: Gimbal angles and velocities (MP 3DGCMG).

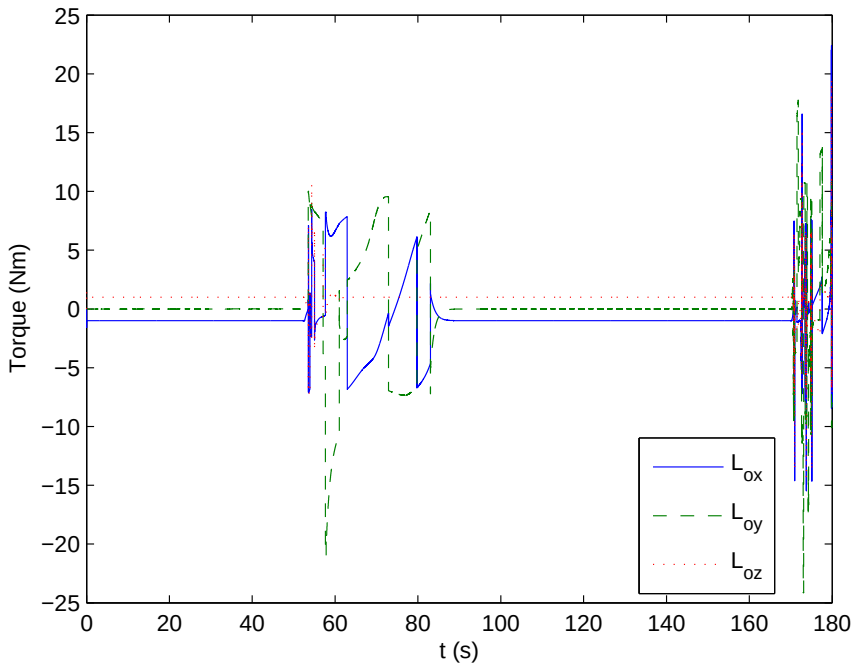

Figure 4.10: Constant torque tracking (SR 3DGCMG).

and the gimbal velocities are also saturated (Figure 4.12). The system achieves external singularity eventually.

One way to avoid the internal singularity is to introduce zero motions into the steering law. So, we use the SRNM steering law to perform the constant torque tracking task. In order to avoid the singularities, the initial gimbal angles $\sigma_i(0), i = 1, \ldots, r$, may not be taken as the preferred gimbal angles. Here, we choose $\sigma_i^* = 0, i = 1, \ldots, r$, as the preferred gimbal angles, and the coefficient of the zero motion is $\rho = 0.1$. Simulation results are shown in Figure 4.13 to Figure 4.15. From Figure 4.14, we notice that the internal singularity status has been avoided. The torque command is followed precisely (Figure 4.13). The DGCMGs system falls into the external singularity after about 159s as a consequence of the constant torque tracking task (Figure 4.15).

B Four DGCMGs parallel mounted

The configuration of the parallel mounted four DGCMGs is shown in Figure 4.5. Based on the principle of isogonal distribution, the initial inner and outer gimbal angles are chosen as:

$$\delta_1(0) = 0^\circ,\ \delta_2(0) = 0^\circ,\ \delta_3(0) = 0^\circ,\ \delta_4(0) = 0^\circ \tag{4.69}$$

and

$$\gamma_1(0) = 0^\circ,\ \gamma_2(0) = 90^\circ,\ \gamma_3(0) = 180^\circ,\ \gamma_3(0) = 270^\circ \tag{4.70}$$

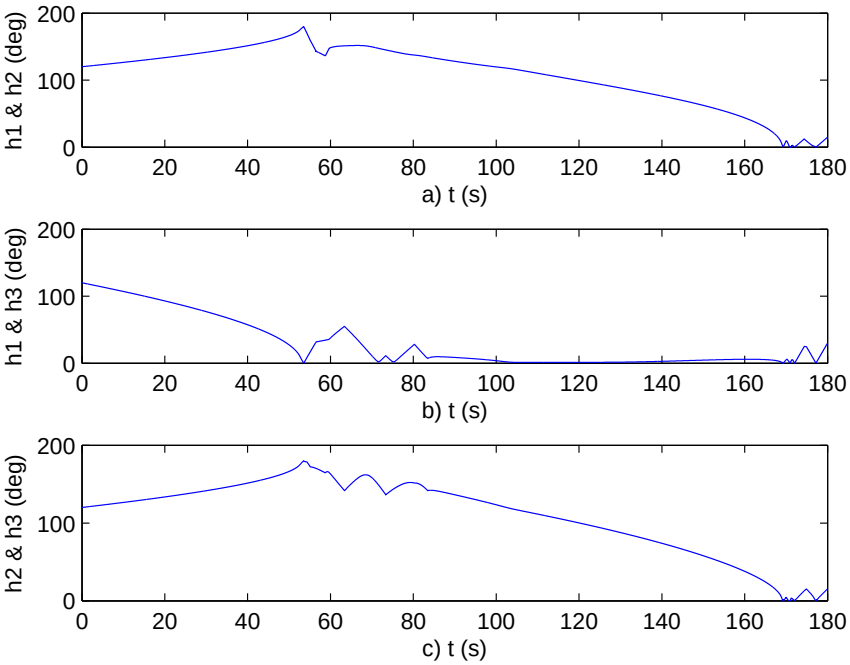

Figure 4.11: Separation angles (SR 3DGCMG).

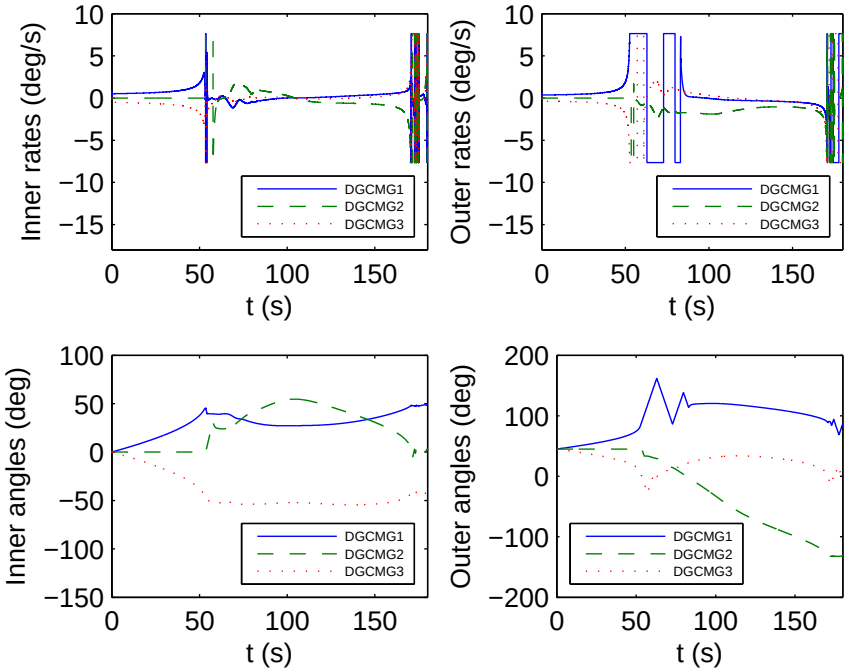

Figure 4.12: Gimbal angles and velocities (SR 3DGCMG).

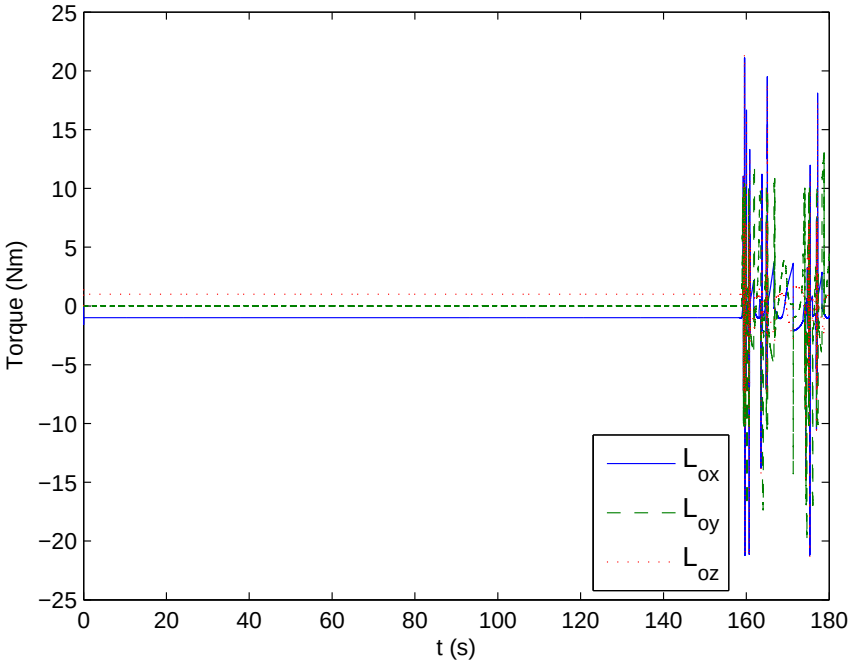

Figure 4.13: Constant torque tracking (SRNM 3DGCMG).

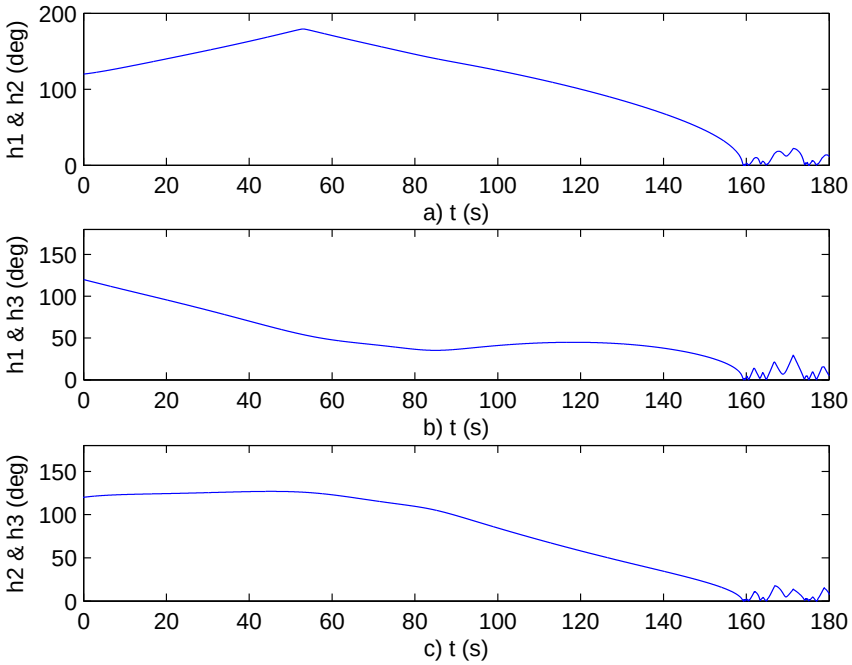

Figure 4.14: Separation angles (SRNM 3DGCMG).

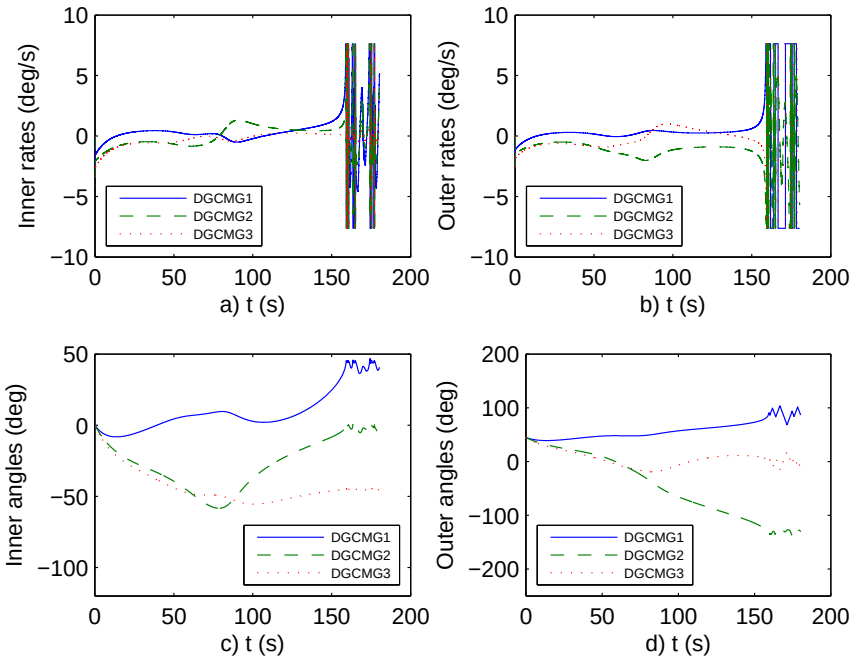

Figure 4.15: Gimbal angles and velocities (SRNM 3DGCMG).

The total angular momentum of the DGCMGs system is:

$$\sum_{i=1}^{4} \boldsymbol{h}_i = [0, 0, 0]^T \tag{4.71}$$

where $\boldsymbol{h}_1$ is antiparallel to $\boldsymbol{h}_3$, $\boldsymbol{h}_2$ is antiparallel to $\boldsymbol{h}_4$, and $\boldsymbol{h}_1$, $\boldsymbol{h}_3$ are orthogonal to $\boldsymbol{h}_2$ and $\boldsymbol{h}_4$.

The torque command is:

$$\boldsymbol{L}_r = [0, 1, 0]^T \text{Nm} \tag{4.72}$$

For the four DGCMGs system, the simulation results of the MP and SR steering laws are similar to those obtained from the three DGCMGs system. Both of these two steering laws encounter internal singularities during the process of constant torque tracking. Hence, to avoid the internal singularity status, we need to introduce null motion into the steering law. Again, the SRNM steering law is used in this simulation, and the preferred gimbal angles are chosen as $\gamma_1^* = 45°$, $\gamma_2^* = 135°$, $\gamma_3^* = 225°$, $\gamma_4^* = 315°$ and $\delta_1^* = \delta_2^* = \delta_3^* = \delta_4^* = 0°$.

Simulation results are depicted in Figures 4.16 to 4.18. From Figure 4.17 showing the relationships of the separation angles amongst $\boldsymbol{h}_1$ to $\boldsymbol{h}_4$, we can see that the internal singularity does not occur during the system operation. After 300s, the system achieves external singularity and the gimbal angle velocities are saturated (Figure 4.18). The output torque can not track the command. Due to the action of the SRNM steering law, the DGCMGs system retreats from the singularity after 410s and the torque command

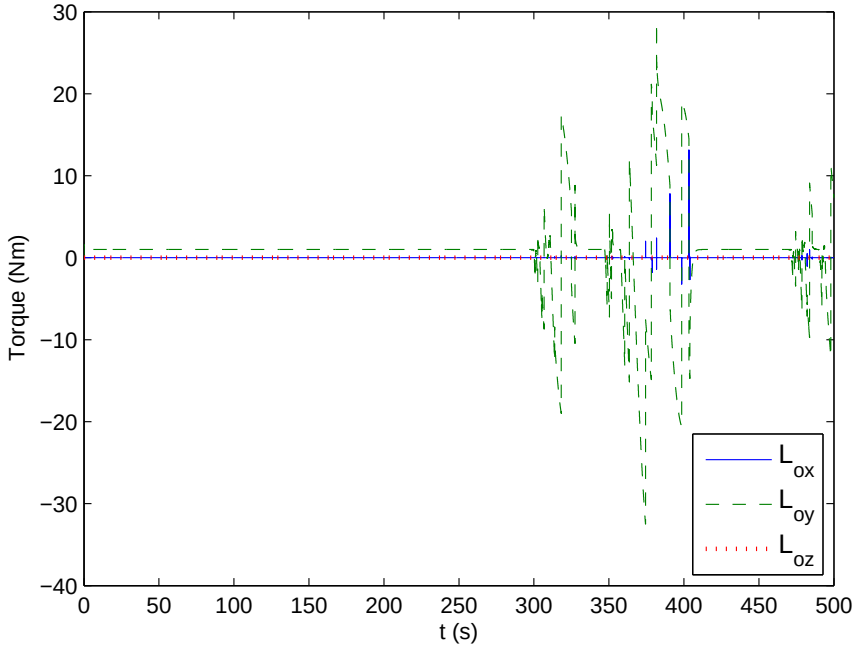

Figure 4.16: Constant torque tracking (SRNM 4DGCMG).

is followed once more (Figure 4.16). However, at 470s, the system falls into singularity again and keep chattering about the singular direction from that moment onward.

By examining the simulation results mentioned above, we know that the internal singularity can be avoided by introducing null motion into the steering law. But if the system achieves external singularity, the singular situation can not be eliminated by only using the null motion steering law. To entirely retreat the system from the external singular status, some other torque generation devices must be utilized, such as the reverse force thruster.

4.5.2 Spacecraft attitude maneuver

In this section, we verify the performance of the spacecraft attitude control system under a large angle maneuver command. The spacecraft attitude motion is describe by the kinematics (4.7) and dynamics (4.25). The simplified feedback attitude control law (4.45) and the corresponding SRNM steering law (4.58) are used in the simulation.

Suppose that the initial attitude angles of the spacecraft are:

$$\psi(0) = 0^\circ,\ \theta(0) = 0^\circ,\ \phi(0) = 0^\circ \tag{4.73}$$

and the initial attitude velocities are

$$\omega_x(0) = 0^\circ/s,\ \omega_y(0) = 0^\circ/s,\ \omega_z(0) = 0^\circ/s \tag{4.74}$$

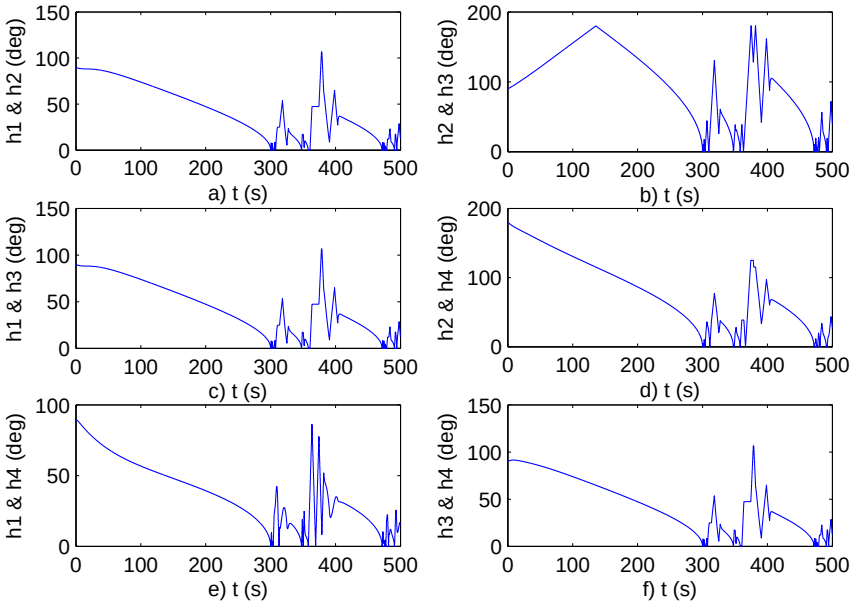

Figure 4.17: Separation angles (SRNM 4DGCMG).

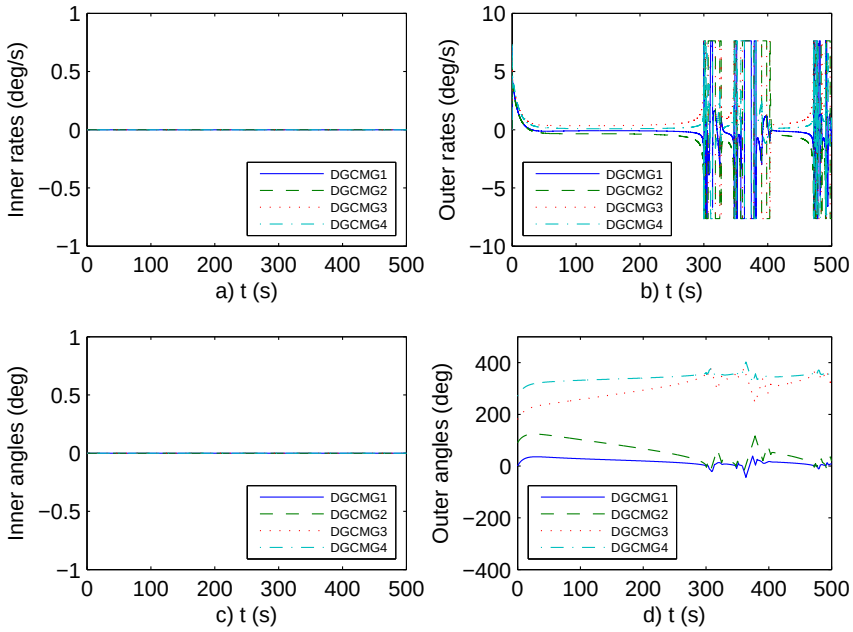

Figure 4.18: Gimbal angles and velocities (SRNM 4DGCMG).

The parameters in the attitude feedback control law are selected as:

$$k = 40, \quad \boldsymbol{K} = \begin{bmatrix} 300 & 0 & 0 \\ 0 & 300 & 0 \\ 0 & 0 & 300 \end{bmatrix} \tag{4.75}$$

The external disturbance torque is set to be $\boldsymbol{L}_e = [0, 0, 0]^T$Nm, and the maximum output torque of a single DGCMG is 10Nm.

The spacecraft attitude maneuver commands are given by

$$\phi_c = -90^\circ,\ \theta_c = 80^\circ,\ \psi_c = 180^\circ \tag{4.76}$$

and

$$\omega_{xc} = 0^\circ/s,\ \omega_{yc} = 0^\circ/s,\ \omega_{zc} = 0^\circ/s \tag{4.77}$$

The parallel mounted four DGCMGs system is adopted in this simulation. The initial outer gimbal angles and inner gimbal angles are chosen, respectively, as:

$$\gamma_1 = 0^\circ,\ \gamma_2 = 90^\circ,\ \gamma_3 = 180^\circ,\ \gamma_4 = 270^\circ \tag{4.78}$$

and

$$\delta_1 = 0^\circ,\ \delta_2 = 0^\circ,\ \delta_3 = 0^\circ,\ \delta_4 = 0^\circ \tag{4.79}$$

The preferred gimbal angle vector $\boldsymbol{\sigma}^*$ is:

$$\boldsymbol{\sigma}^* = [30^\circ, 120^\circ, 210^\circ, 300^\circ, 0^\circ, 0^\circ, 0^\circ, 0^\circ]^T \tag{4.80}$$

Figure 4.19 illustrates the time histories of the attitude angles and velocities. It is clear to observe that the attitude maneuver mission is well accomplished. The output torque $\boldsymbol{L}_o$ follows the command $\boldsymbol{L}_r$ precisely (Figure 4.20). From the separation angles between $\boldsymbol{h}_1$ to $\boldsymbol{h}_4$, we can see that the system does not encounter singularities (Figure 4.21). The precession angles and velocities of the outer gimbals and inner gimbals are shown in Figure 4.22. All the inner gimbal angles are within 6°, and the gimbal velocities are smooth.

4.5.3 Spacecraft attitude maneuver with DGCMG failure

In the attitude control missions, some of the DGCMGs may fail during the precessions. For this situation, in order to successfully achieve the attitude control target, the influence of the failed DGCMGs must be cut off such that the attitude maneuver can still be accomplished by the operations of the remaining DGCMGs. In practice, we can achieve these by cutting off the power of the rotor motor of the failed DGCMGs whose inner and

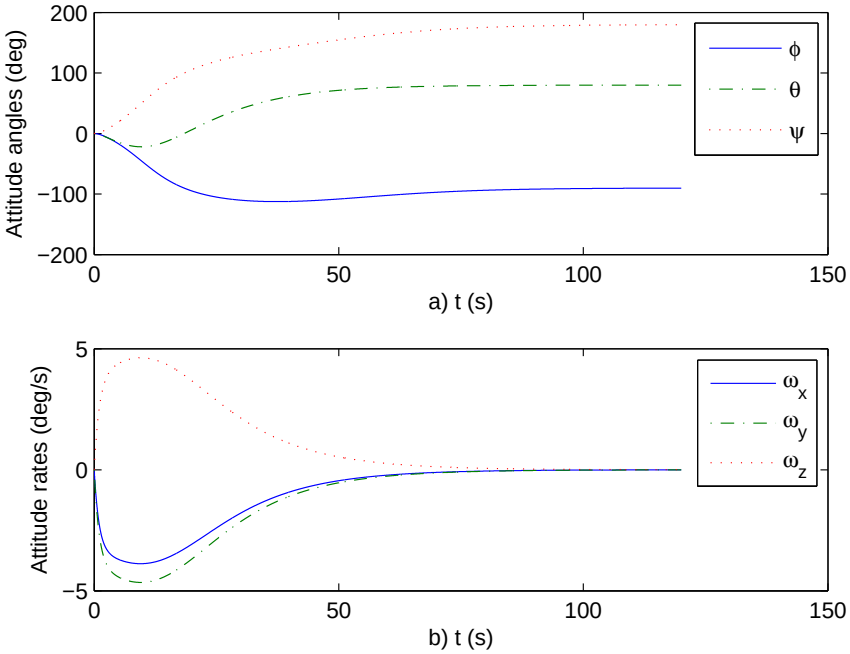

Figure 4.19: Attitude angles and velocities.

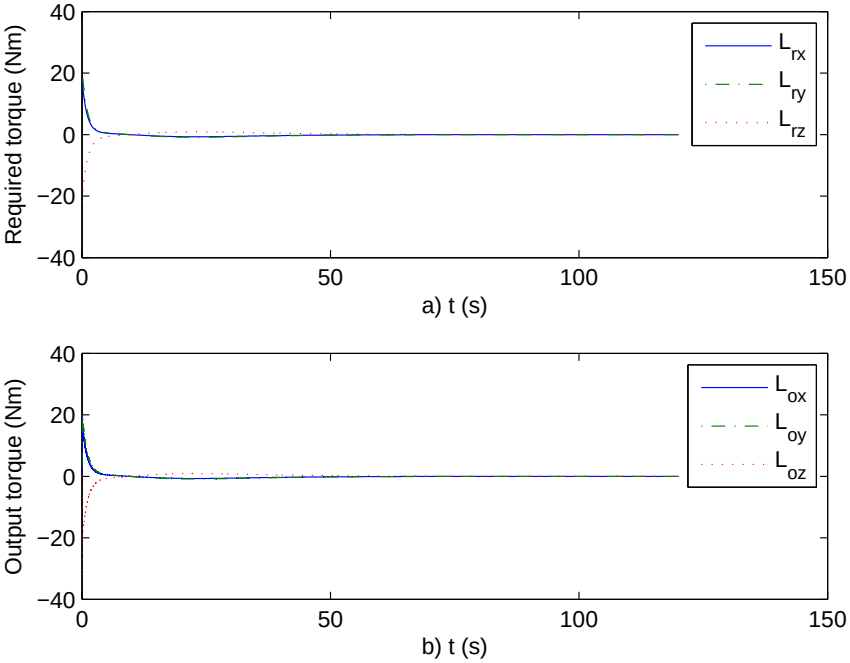

Figure 4.20: Required torque and output torque.

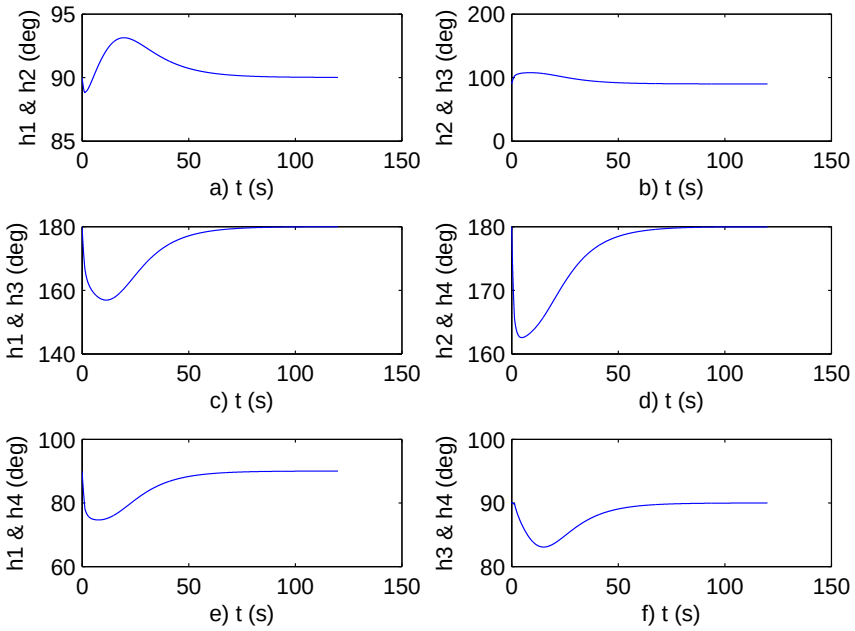

Figure 4.21: Separation angles.

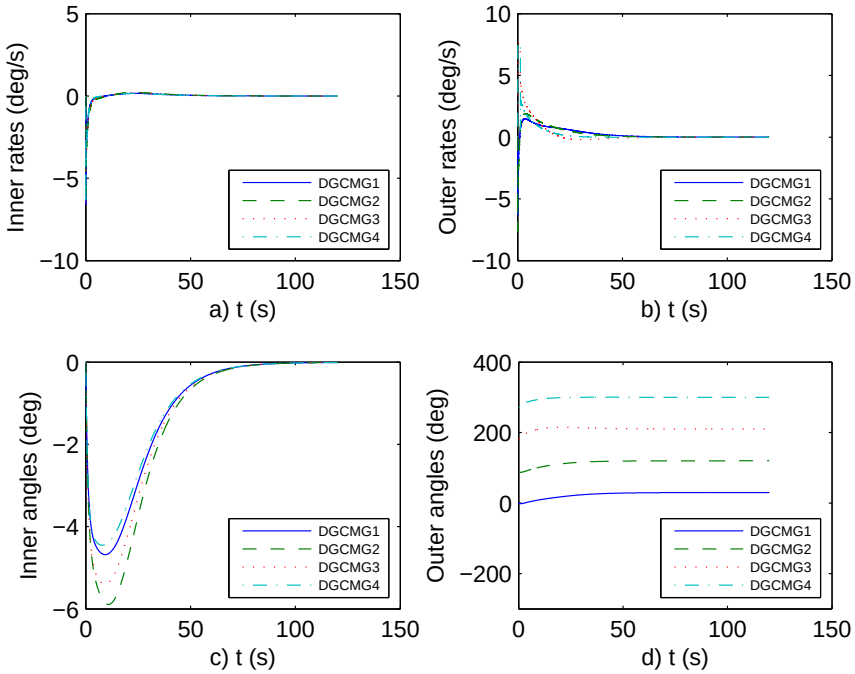

Figure 4.22: Precession angles and velocities.

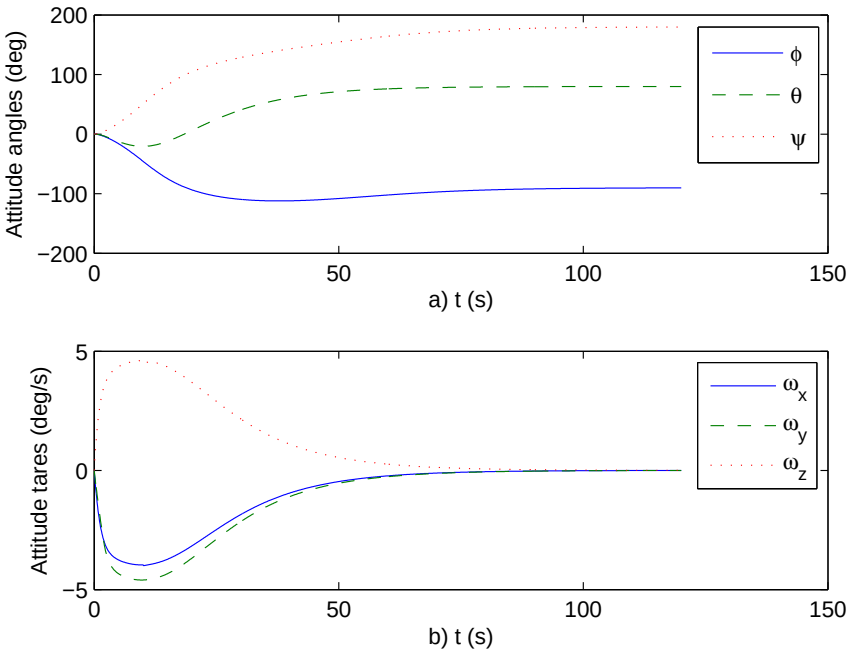

Figure 4.23: Attitude angles and velocities (1st fail).

outer gimbals should also be locked. In this section, we will use a numerical simulation to verify the effectiveness of the proposed attitude control law and steering law in the case of DGCMG failure.

The simulation environment is the same as that in Section 4.5.2. Suppose that the first DGCMG fails at the time $t = 10$s. The simulation results are shown in Figures 4.23 to 4.26. It can be seen that, even with the failure of the first DGCMG, the attitude maneuver command can still be well accomplished (Figure 4.23) and the output torque can also follow the torque command precisely (Figure 4.24). From the relationship of the separation angles shown in Figure 4.25, we can see that the system did not encounter any singularity status during the simulation. The gimbal angle velocity of the failed DGCMG becomes zero from the moment $t = 10$s onward and the gimbal angle is locked at the position where the failure happens (Figure 4.26). Hence, it is clear that the proposed feedback attitude control law and the steering law can ensure a good performance of the DGCMGs system even in the presence of the DGCMG failure.

4.6 Conclusion

In this chapter, we derived an exact mathematical description of the spacecraft attitude motion driven by DGCMGs system. Based on the second method of Lyapunov stability theory, a feedback control law is designed so as to ensure that the tracking errors converge to zero. The system stability is guaranteed during the design process. A singularity theorem for the DGCMGs system is proposed, and the singularity analysis of the orthog-

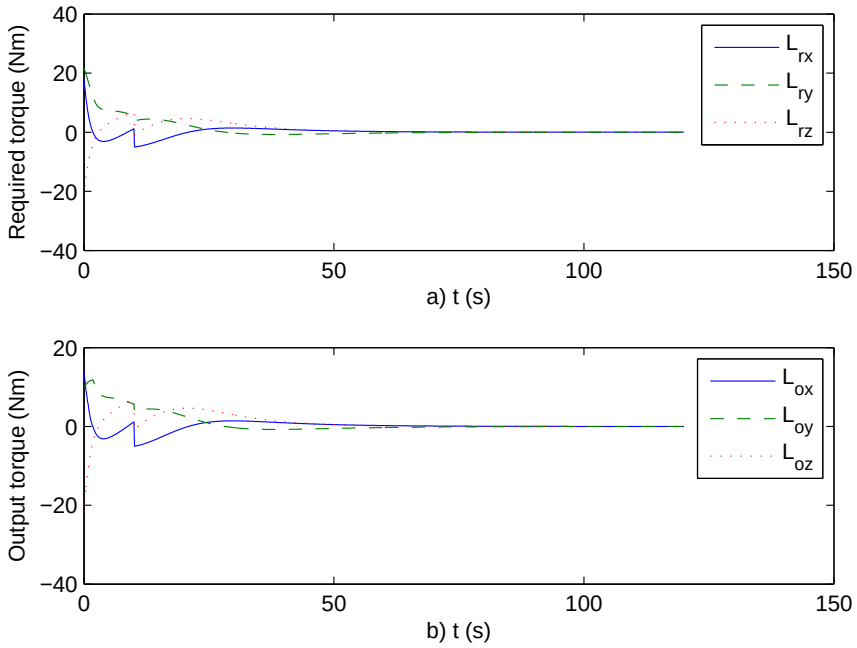

Figure 4.24: Required torque and output torque (1st fail).

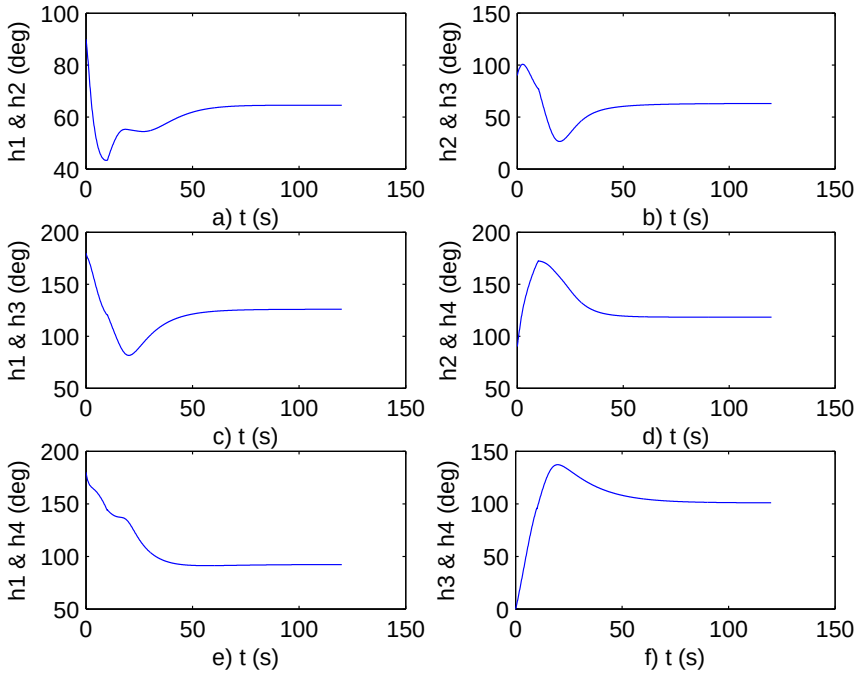

Figure 4.25: Separation angles (1st fail).

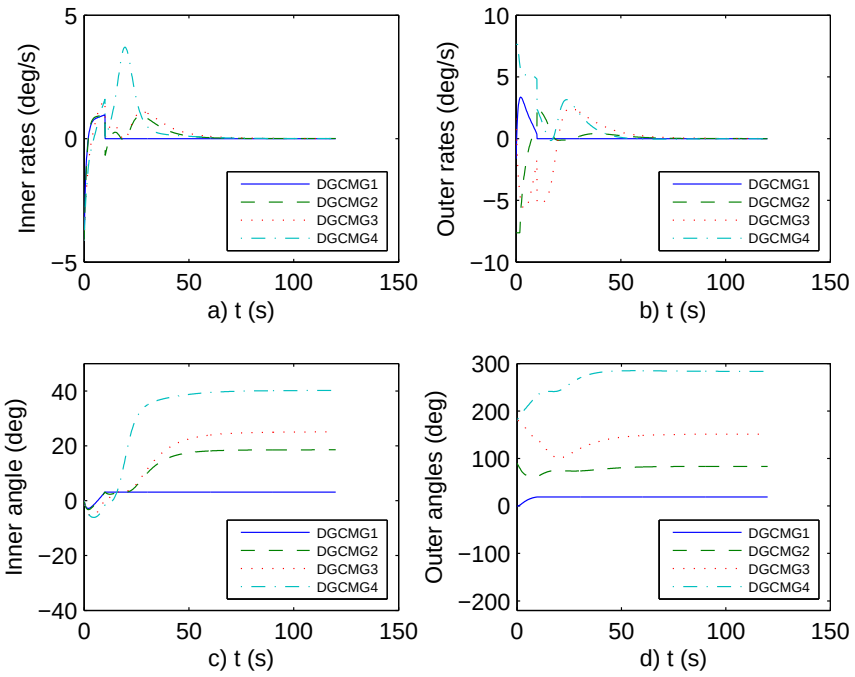

Figure 4.26: Precession angles and velocities (1st fail).

onally mounted three DGCMGs system and that of the parallel mounted four DGCMGs system are presented, singularity surfaces are described. Simulation results showed that the proposed control law and the steering law could accomplish the large angle attitude maneuver missions of the spacecraft even in the presence of the DGCMG failure.

CHAPTER 5

On a Class of Nonlinear Optimal Synchronization and Tracking Control Problems

5.1 Introduction

Synchronization control of different objects aiming at achieving the synchronized motions of the objects with reference to desired target motions has been well studied in recent years. In this chapter, we consider a new class of nonlinear optimal tracking and synchronizing control problems subject to control constraints, where the motions of two distinct objects are required to achieve synchronization at the minimum time while achieving the optimal tracking of a reference target. This class of optimal control problems arises naturally from the study of angular velocity tracking and synchronization of two spacecrafts during their formation flight, where their system dynamics are in equal status mode. In this chapter, we first provide a rigorous mathematical formulation for this class of optimal control problems. A new result ensuring the synchronization of the two distinct objects is obtained. On this basis, a computational method is developed for constructing an optimal switching control law under which the motions of the two distinct objects will achieve synchronization at the minimum time while achieving the optimal tracking of a reference target. This computational method is developed based on novel applications of the control parameterization method and a time scaling transform. A practical problem arising from the study of the angular velocity tracking and synchronization of two spacecrafts during their formation flight is formulated and solved by the method proposed.

5.2 Problem Formulation

Consider a process described by the following system of nonlinear differential equations on $[0, T]$.

$$\dot{\boldsymbol{x}}_1(t) = \boldsymbol{f}(t, \boldsymbol{x}(t), \boldsymbol{u}_1(t)) \tag{5.1a}$$

$$\dot{\boldsymbol{x}}_2(t) = \boldsymbol{g}_1(t, \boldsymbol{x}(t)) + \boldsymbol{C}_1(t, \boldsymbol{x}(t))\boldsymbol{u}_2(t) \tag{5.1b}$$

$$\dot{\boldsymbol{x}}_3(t) = \boldsymbol{g}_2(t, \boldsymbol{x}(t)) + \boldsymbol{C}_2(t, \boldsymbol{x}(t))\boldsymbol{u}_3(t) \tag{5.1c}$$

where $\boldsymbol{x}_1 = [x_{1,1}, \ldots, x_{1,m}]^T \in \mathbb{R}^m$, $\boldsymbol{x}_2 = [x_{2,1}, \ldots, x_{2,n}]^T \in \mathbb{R}^n$ and $\boldsymbol{x}_3 = [x_{3,1}, \ldots, x_{3,n}]^T \in \mathbb{R}^n$ are the state vectors, $\dot{\boldsymbol{x}}_i(t) = d\boldsymbol{x}_i(t)/dt$, $i = 1, 2, 3$, and $\boldsymbol{x} = [\boldsymbol{x}_1^T, \boldsymbol{x}_2^T, \boldsymbol{x}_3^T]^T \in \mathbb{R}^{m+2n}$. $\boldsymbol{u}_1 = [u_{1,1}, \ldots, u_{1,r_1}]^T \in \mathbb{R}^{r_1}$, $\boldsymbol{u}_2 = [u_{2,1}, \ldots, u_{2,r_2}]^T \in \mathbb{R}^{r_2}$ and $\boldsymbol{u}_3 = [u_{3,1}, \ldots, u_{3,r_3}]^T \in \mathbb{R}^{r_3}$ are the control vectors, and $\boldsymbol{u} = [\boldsymbol{u}_1^T, \boldsymbol{u}_2^T, \boldsymbol{u}_3^T]^T \in \mathbb{R}^{r_1+r_2+r_3}$. The vector-valued functions $\boldsymbol{f} : \mathbb{R} \times \mathbb{R}^{m+2n} \times \mathbb{R}^{r_1} \to \mathbb{R}^m$, $\boldsymbol{g}_1 : \mathbb{R} \times \mathbb{R}^{m+2n} \to \mathbb{R}^n$, $\boldsymbol{g}_2 : \mathbb{R} \times \mathbb{R}^{m+2n} \to \mathbb{R}^n$ and the matrix-valued functions $\boldsymbol{C}_1 : \mathbb{R} \times \mathbb{R}^{m+2n} \to \mathbb{R}^{n \times r_2}$, $\boldsymbol{C}_2 : \mathbb{R} \times \mathbb{R}^{m+2n} \to \mathbb{R}^{n \times r_3}$ are continuously differentiable with respect to all their respective arguments.

The initial condition for (5.1a)-(5.1c) is:

$$\boldsymbol{x}(0) = [\boldsymbol{x}_{1,0}^T \;\; \boldsymbol{x}_{2,0}^T \;\; \boldsymbol{x}_{3,0}^T]^T \tag{5.1d}$$

The boundedness constraints on the control $\boldsymbol{u}(t)$ are specified below:

$$\boldsymbol{\alpha} \leq \boldsymbol{u}(t) \leq \boldsymbol{\beta}, \quad \forall\, t \in [0, T] \tag{5.2}$$

where $\boldsymbol{\alpha} = [\boldsymbol{\alpha}_1^T, \boldsymbol{\alpha}_2^T, \boldsymbol{\alpha}_3^T]^T$ and $\boldsymbol{\beta} = [\boldsymbol{\beta}_1^T, \boldsymbol{\beta}_2^T, \boldsymbol{\beta}_3^T]^T$, while $\boldsymbol{\alpha}_1 \in \mathbb{R}^{r_1}$, $\boldsymbol{\alpha}_2 \in \mathbb{R}^{r_2}$, $\boldsymbol{\alpha}_3 \in \mathbb{R}^{r_3}$ and $\boldsymbol{\beta}_1 \in \mathbb{R}^{r_1}$, $\boldsymbol{\beta}_2 \in \mathbb{R}^{r_2}$, $\boldsymbol{\beta}_3 \in \mathbb{R}^{r_3}$ are given constant vectors. A control $\boldsymbol{u}$ satisfying the boundedness constraints (5.2) is called an admissible control. Let $\mathcal{U}$ be the set of all such admissible controls.

Let $\tau \in (0, T)$ be the time from which it holds that

$$\|\boldsymbol{x}_2(t) - \boldsymbol{x}_3(t)\|^2 = 0, \quad \forall\, t \in [\tau, T] \tag{5.3}$$

where $\| \bullet \|$ denotes the usual Euclidian norm. Such a τ is referred to as a synchronization time.

We assume that the following condition is satisfied.

Assumption (A): $\operatorname{rank}(\boldsymbol{C}_1) = r_2$ or $\operatorname{rank}(\boldsymbol{C}_2) = r_3$. Without loss of generality, we assume that $\operatorname{rank}(\boldsymbol{C}_2) = r_3$.

We wish to note that Assumption (A) is not restrictive, as it can be quite easily satisfied in practice. For example, it is satisfied for the practical problem, which arises from the study of the angular velocity tracking and synchronization of two spacecrafts during their formation flight to be considered in Section 5.

Our aim is to find an admissible control $\boldsymbol{u}(t) \in \mathcal{U}$ such that the synchronization time of $\boldsymbol{x}_2$ and $\boldsymbol{x}_3$ and the deviation of the state vector $\boldsymbol{x}(t)$ from a desired trajectory are minimized. This tracking and synchronization optimal control problem may be stated formally as follows.

Problem S. *Subject to system (5.1a)-(5.1d), find an admissible control* $\boldsymbol{u} \in \mathcal{U}$ *such that the following cost function*

$$J(\boldsymbol{u}) = a_0\tau + \int_0^T \left\{a_1\|\boldsymbol{x}_1(t) - \boldsymbol{x}_{1r}(t)\|^2 + a_2\|\boldsymbol{x}_2(t) - \boldsymbol{x}_{2r}(t)\|^2 + a_3\|\boldsymbol{x}_3(t) - \boldsymbol{x}_{2r}(t)\|^2\right\}dt \tag{5.4}$$

is minimized subject to (5.3), where $\boldsymbol{x}_{1r}(t)$ *and* $\boldsymbol{x}_{2r}(t)$ *are the relevant components of the desired trajectory, and* a_i, $i = 0, 1, 2, 3$, *are weighting coefficients.*

5.3 Switching Synchronization Control

In the following theorem, the form of the switching synchronization control is obtained.

Theorem 5.1. *Consider system (5.1a)-(5.1d). Let* $\tau \in (0, T)$ *be a synchronization time of* $\boldsymbol{x}_2$ *and* $\boldsymbol{x}_3$. *Then,*

$$\hat{\boldsymbol{u}}_3(t) = \begin{cases} \boldsymbol{u}_3(t), & t \in [0, \tau] \\ (\boldsymbol{C}_2^T\boldsymbol{C}_2)^{-1}\boldsymbol{C}_2^T(\boldsymbol{g}_1 - \boldsymbol{g}_2 + \boldsymbol{C}_1\boldsymbol{u}_2(t)), & t \in (\tau, T], \end{cases} \tag{5.5}$$

where

$$\boldsymbol{\alpha}_2 \le \boldsymbol{u}_2(t) \le \boldsymbol{\beta}_2, \quad \forall\, t \in [0, T], \tag{5.6}$$

$$\boldsymbol{\alpha}_3 \le \boldsymbol{u}_3(t) \le \boldsymbol{\beta}_3, \quad \forall\, t \in [0, \tau], \tag{5.7}$$

and

$$\boldsymbol{\alpha}_3 \le (\boldsymbol{C}_2^T\boldsymbol{C}_2)^{-1}\boldsymbol{C}_2^T(\boldsymbol{g}_1 - \boldsymbol{g}_2 + \boldsymbol{C}_1\boldsymbol{u}_2(t)) \le \boldsymbol{\beta}_3, \quad \forall\, t \in (\tau, T] \tag{5.8}$$

Proof. For the first part of the theorem, it suffices to show that, at $t = \tau \in (0, T)$,

$$\boldsymbol{x}_2(\tau) = \boldsymbol{x}_3(\tau), \tag{5.9}$$

and

$$\dot{\boldsymbol{x}}_2(t) = \dot{\boldsymbol{x}}_3(t), \quad \forall\, t \in (\tau, T]. \tag{5.10}$$

For (5.10) to hold, it follows from (5.1b), (5.1c) and (A) that $\boldsymbol{u}_3$ is expressed explicitly in terms of $\boldsymbol{u}_2$ as follows.

$$\boldsymbol{u}_3(t) = (\boldsymbol{C}_2^T\boldsymbol{C}_2)^{-1}\boldsymbol{C}_2^T(\boldsymbol{g}_1 - \boldsymbol{g}_2 + \boldsymbol{C}_1\boldsymbol{u}_2(t)), \quad \forall\, t \in (\tau, T] \tag{5.11}$$

So, if (5.3) is to be satisfied, i.e., to achieve synchronization of $\boldsymbol{x}_2$ and $\boldsymbol{x}_3$ at the synchronization time τ, we need only to replace $\boldsymbol{u}_3$ with that given by (5.11) from $t = \tau$. Thus, the required switching control vector $\hat{\boldsymbol{u}}_3$ is given by (5.5). For (5.6) and (5.7), they follow from (5.2), while (5.8) is obtained from (5.5) and (5.2). This completes the proof. □

Let $\hat{\boldsymbol{u}} = (\boldsymbol{u}_1^T, \boldsymbol{u}_2^T, \hat{\boldsymbol{u}}_3^T)^T$ and let $\hat{\mathcal{U}} \times (0, T)$ be the set which consists of all those $(\hat{\boldsymbol{u}}, \tau) = (\boldsymbol{u}_1^T, \boldsymbol{u}_2^T, \hat{\boldsymbol{u}}_3^T, \tau)^T$ such that constraints (5.6), (5.7) and (5.8) are satisfied. The optimal tracking and synchronization control problem may now be stated equivalently below.

Problem $\hat{\mathrm{S}}$. *Given the dynamical system*

$$\dot{\boldsymbol{x}}_1(t) = \boldsymbol{f}(t, \boldsymbol{x}(t), \boldsymbol{u}_1(t)) \tag{5.12a}$$

$$\dot{\boldsymbol{x}}_2(t) = \boldsymbol{g}_1(t, \boldsymbol{x}(t)) + \boldsymbol{C}_1(t, \boldsymbol{x}(t))\boldsymbol{u}_2(t) \tag{5.12b}$$

$$\dot{\boldsymbol{x}}_3(t) = \boldsymbol{g}_2(t, \boldsymbol{x}(t)) + \boldsymbol{C}_2(t, \boldsymbol{x}(t))\hat{\boldsymbol{u}}_3(t) \tag{5.12c}$$

with initial condition (5.1d), where $\hat{\boldsymbol{u}}_3$ is given by (5.5), find a $(\hat{\boldsymbol{u}}, \tau) = (\boldsymbol{u}_1^T, \boldsymbol{u}_2^T, \hat{\boldsymbol{u}}_3^T, \tau)^T \in \hat{\mathcal{U}} \times (0, T)$ such that the cost function (5.4) is minimized subject to constraints (5.6), (5.7) and (5.8).

5.4 Parameterization of the Control

To solve Problem $\hat{\mathrm{S}}$, we shall utilize the control parameterization technique to approximate the control vector $\hat{\boldsymbol{u}}$ with piecewise constant functions over the time interval $[0, T]$ as:

$$\boldsymbol{u}_1^p(t) = \sum_{k=1}^{p} \boldsymbol{\sigma}_1^k \chi_{[\tau_{k-1}, \tau_k)}(t), \quad t \in [0, T] \tag{5.13}$$

$$\boldsymbol{u}_2^p(t) = \sum_{k=1}^{p} \boldsymbol{\sigma}_2^k \chi_{[\tau_{k-1}, \tau_k)}(t), \quad t \in [0, T] \tag{5.14}$$

$$\hat{\boldsymbol{u}}_3^p(t) = \begin{cases} \sum\limits_{k=1}^{\bar{p}} \boldsymbol{\sigma}_3^k \chi_{[\tau_{k-1}, \tau_k)}(t), & t \in [0, \tau] \\ (\boldsymbol{C}_2^T \boldsymbol{C}_2)^{-1} \boldsymbol{C}_2^T (\boldsymbol{g}_1 - \boldsymbol{g}_2 + \boldsymbol{C}_1 \sum\limits_{k=\bar{p}+1}^{p} \boldsymbol{\sigma}_2^k \chi_{[\tau_{k-1}, \tau_k)}(t)), & t \in (\tau, T], \end{cases} \tag{5.15}$$

where $\bar{p} < p$,

$$\tau_0, \tau_1, \ldots, \tau_{\bar{p}}, \tau_{\bar{p}+1}, \ldots, \tau_p, \ \tau_{k-1} < \tau_k, \ k = 1, 2, \ldots, p \tag{5.16}$$

(with $\tau_0 = 0$, $\tau_{\bar{p}} = \tau$ and $\tau_p = T$) are partition points of the time interval $[0, T]$, and $\chi_I(t)$ denotes the indicator function of I defined by

$$\chi_I(t) = \begin{cases} 1, \ t \in I \\ 0, \ \text{elsewhere.} \end{cases} \tag{5.17}$$

For each $j = 1, 2, 3$, and $k = 1, 2, \ldots, p$, $\boldsymbol{\sigma}_j^k$ is a constant control vector, while τ_k, $k = 1, \ldots, p-1$, are switching times. Let $\boldsymbol{\gamma} = [\tau_1, \ldots, \tau_p]^T$, which is referred to as a switching time vector. Let Υ^p be the set which consists of all such $\boldsymbol{\gamma}$.

Define

$$\boldsymbol{\sigma} = [(\boldsymbol{\sigma}_1)^T, (\boldsymbol{\sigma}_2)^T, (\boldsymbol{\sigma}_3)^T]^T \tag{5.18}$$

where $\boldsymbol{\sigma}_j = [(\boldsymbol{\sigma}_j^1)^T, \cdots, (\boldsymbol{\sigma}_j^p)^T]^T,\ j = 1, 2, 3$. Let Ξ^p denote the set containing all such $\boldsymbol{\sigma}$.

To solve Problem $\hat{\text{S}}$ by using a gradient-based optimization method, we need the gradient formulas of the cost function and the constraint functions with respect to the control vector $\boldsymbol{\sigma}$ and the switching time vector $\boldsymbol{\gamma}$. However, the gradient formulas of these functions with respect to the switching time vector $\boldsymbol{\gamma}$ are known to be discontinuous (See Chapter 5 of [74] for details). For this reason, these gradient formulas were never implemented for a practical problem.

To overcome this deficiency, we shall use the time scaling transform [75] to map all these variable time points τ_k, $k = 1, \ldots, p-1$, into fixed time points ς_k, $k = 1, \ldots, p-1$, in a new time horizon $[0, 1]$, such that

$$0 = \varsigma_0 < \varsigma_1 < \cdots < \varsigma_{\bar{p}} < \varsigma_{\bar{p}+1} < \ldots < \varsigma_{p-1} < \varsigma_p = 1 \tag{5.19}$$

where $\tau_{\bar{p}}$ is mapped to the fixed point $\varsigma_{\bar{p}}$.

To achieve this, we introduce a new state equation defined on $[0, 1]$:

$$\frac{dt(s)}{ds} = \nu^p(s) \tag{5.20}$$

where $t(0) = 0$, $t(1) = T$, and

$$\nu^p(s) = \sum_{k=1}^{p} \delta_k \chi_{[\varsigma_{k-1}, \varsigma_k)}(s) \tag{5.21}$$

Here, $\delta_k \geq 0$, $k = 1, \ldots, p$, are decision variables, and

$$\sum_{k=1}^{p} \delta_k = T. \tag{5.22}$$

$\nu^p(s)$ is called the time scaling control. It is a nonnegative piecewise constant function with possible discontinuities at the pre-fixed knots ς_k, $k = 1, \ldots, p-1$. Let $\boldsymbol{\delta} = [\delta_1, \cdots, \delta_p]^T$.

By applying the time scaling transform (5.20), the original system dynamics can be rewritten as:

$$\dot{\tilde{\boldsymbol{x}}}_1(s) = \nu^p(s) \boldsymbol{f}(t(s), \tilde{\boldsymbol{x}}(s), \tilde{\boldsymbol{u}}_1(s)) \tag{5.23a}$$

$$\dot{\tilde{\boldsymbol{x}}}_2(s) = \nu^p(s)[\boldsymbol{g}_1(t(s), \tilde{\boldsymbol{x}}(s)) + \boldsymbol{C}_1(t(s), \tilde{\boldsymbol{x}}(s))\tilde{\boldsymbol{u}}_2(s)] \tag{5.23b}$$

$$\dot{\tilde{\boldsymbol{x}}}_3(s) = \nu^p(s)[\boldsymbol{g}_2(t(s), \tilde{\boldsymbol{x}}(s)) + \boldsymbol{C}_2(t(s), \tilde{\boldsymbol{x}}(s))\tilde{\boldsymbol{u}}_3(s)] \tag{5.23c}$$

$$\dot{\tilde{x}}_4(s) = \nu^p(s) \tag{5.23d}$$

with initial condition

$$\tilde{\boldsymbol{x}}(0) = [\tilde{\boldsymbol{x}}_{1,0}^T, \tilde{\boldsymbol{x}}_{2,0}^T, \tilde{\boldsymbol{x}}_{3,0}^T, \tilde{x}_{4,0}]^T \tag{5.23e}$$

where $\tilde{\boldsymbol{x}} = [\tilde{\boldsymbol{x}}_1^T, \tilde{\boldsymbol{x}}_2^T, \tilde{\boldsymbol{x}}_3^T, \tilde{x}_4]^T = [\boldsymbol{x}^T(t(s)), t(s)]^T$. $\tilde{\boldsymbol{u}}^p = [\tilde{\boldsymbol{u}}_1^T, \tilde{\boldsymbol{u}}_2^T, \tilde{\hat{\boldsymbol{u}}}_3^T, \nu^p]^T$ is given by

$$\tilde{\boldsymbol{u}}^p(s) = \begin{cases} \sum\limits_{k=1}^{p} \boldsymbol{\sigma}_1^k \chi_{[\varsigma_{k-1},\varsigma_k)}(s) \\ \sum\limits_{k=1}^{p} \boldsymbol{\sigma}_2^k \chi_{[\varsigma_{k-1},\varsigma_k)}(s) \\ \tilde{\hat{\boldsymbol{u}}}_3(s) \\ \sum\limits_{k=1}^{p} \delta_k \chi_{[\varsigma_{k-1},\varsigma_k)}(s) \end{cases}, \quad s \in [0,1] \tag{5.24}$$

while

$$\tilde{\hat{\boldsymbol{u}}}_3(s) = \begin{cases} \sum\limits_{k=1}^{\bar{p}} \boldsymbol{\sigma}_3^k \chi_{[\varsigma_{k-1},\varsigma_k)}(s), & s \in [0, \varsigma_{\bar{p}}] \\ (\boldsymbol{C}_2^T \boldsymbol{C}_2)^{-1} \boldsymbol{C}_2^T (\boldsymbol{g}_1 - \boldsymbol{g}_2 + \boldsymbol{C}_1 \sum\limits_{k=\bar{p}+1}^{p} \boldsymbol{\sigma}_2^k \chi_{[\varsigma_{k-1},\varsigma_k)}(s)), & s \in (\varsigma_{\bar{p}}, 1] \end{cases} \tag{5.25}$$

Clearly, by integrating (5.20) with initial condition $t(0) = 0$, we obtain, for $s \in [\varsigma_{l-1}, \varsigma_l]$

$$t(s) = \sum_{k=1}^{l-1} \delta_k + \delta_l (s - \varsigma_{l-1}) p, \tag{5.26}$$

where $l = 1, \ldots, p$.

In particular, the switching times τ_i, $i = 1, 2, \ldots, \bar{p}, \bar{p}+1, \ldots, p-1$, in the original time horizon $[0, T]$, are given by

$$\tau_i = \sum_{k=1}^{i} \delta_k, \ \ i = 1, 2, \ldots, \bar{p}, \bar{p}+1, \ldots, p-1 \tag{5.27}$$

$$\tau_{\bar{p}} = \sum_{k=1}^{\bar{p}} \delta_k = \tau \tag{5.28}$$

Thus, (5.23a)-(5.23e) can be written in the form below.

$$\dot{\tilde{\boldsymbol{x}}}(s) = \tilde{\boldsymbol{q}}(t(s), \tilde{\boldsymbol{x}}(s), \tilde{\boldsymbol{u}}^p(s)) \tag{5.29a}$$

with the initial condition

$$\tilde{\boldsymbol{x}}(0) = [\tilde{\boldsymbol{x}}_{1,0}^T, \tilde{\boldsymbol{x}}_{2,0}^T, \tilde{\boldsymbol{x}}_{3,0}^T, \tilde{x}_{4,0}]^T \tag{5.29b}$$

where

$$\tilde{\boldsymbol{q}} = \nu^p [\boldsymbol{f}^T, (\boldsymbol{g}_1 + \boldsymbol{C}_1 \tilde{\boldsymbol{u}}_2)^T, (\boldsymbol{g}_2 + \boldsymbol{C}_2 \tilde{\hat{\boldsymbol{u}}}_3)^T, 1]^T$$

The cost function (5.3) is transformed into the following form in the new time horizon

$[0,1]$:

$$\tilde{J}(\tilde{\boldsymbol{u}}^p) = \int_0^1 \tilde{\mathcal{L}}_0(s, \tilde{\boldsymbol{x}}(s), \boldsymbol{\sigma}, \boldsymbol{\delta}) ds \tag{5.30}$$

where

$$\begin{aligned}&\tilde{\mathcal{L}}_0(s, \tilde{\boldsymbol{x}}(s), \boldsymbol{\sigma}, \boldsymbol{\delta}) = \\ &\chi_{[0,\varsigma_{\bar{p}}]}(s) \left[a_0 \nu^p(s) + a_1 \|\tilde{\boldsymbol{x}}_1(s) - \tilde{\boldsymbol{x}}_{1r}(s)\|^2 + a_2 \|\tilde{\boldsymbol{x}}_2(s) - \tilde{\boldsymbol{x}}_{2r}(s)\|^2 + a_3 \|\tilde{\boldsymbol{x}}_3(s) - \tilde{\boldsymbol{x}}_{2r}(s)\|^2\right] \\ &+\chi_{(\varsigma_{\bar{p}},1]}(s) \left[a_1 \|\tilde{\boldsymbol{x}}_1(s) - \tilde{\boldsymbol{x}}_{1r}(s)\|^2 + a_2 \|\tilde{\boldsymbol{x}}_2(s) - \tilde{\boldsymbol{x}}_{2r}(s)\|^2\right]\end{aligned} \tag{5.31}$$

From (5.25), it is clear that

$$t(\varsigma_{\bar{p}}) = \tau \tag{5.32}$$

$$t(1) = T \tag{5.33}$$

i.e.,

$$\sum_{k=1}^{\bar{p}} \delta_k = \tau \tag{5.34}$$

$$\sum_{k=1}^{p} \delta_k - T = 0 \tag{5.35}$$

Let $\boldsymbol{\delta} = [\delta_1, \ldots, \delta_p]^T$ and let $\mathcal{D}^p$ be the set containing all such $\boldsymbol{\delta}$. Furthermore, under the time scaling transform, the interior point state equality constraint (5.4) is transformed into

$$\|\tilde{\boldsymbol{x}}_2(\varsigma_{\bar{p}}) - \tilde{\boldsymbol{x}}_3(\varsigma_{\bar{p}})\|^2 = 0 \tag{5.36}$$

where $\varsigma_{\bar{p}} \in (0,1)$. The cost function and the state constraint can be written in canonical form as:

$$\tilde{g}_0(\boldsymbol{\sigma}, \boldsymbol{\delta}) = \tilde{\Phi}_0(\tilde{\boldsymbol{x}}(1|\boldsymbol{\sigma}, \boldsymbol{\delta})) + \int_0^1 \tilde{\mathcal{L}}_0(s,\ \tilde{\boldsymbol{x}}(s|\boldsymbol{\sigma}, \boldsymbol{\delta}),\ \boldsymbol{\sigma}, \boldsymbol{\delta}) ds \tag{5.37}$$

and

$$\tilde{g}_1(\boldsymbol{\sigma}, \boldsymbol{\delta}) = \tilde{\Phi}_1(\tilde{\boldsymbol{x}}(1|\boldsymbol{\sigma}, \boldsymbol{\delta})) + \int_0^1 \tilde{\mathcal{L}}_1(s,\ \tilde{\boldsymbol{x}}(s|\boldsymbol{\sigma}, \boldsymbol{\delta}),\ \boldsymbol{\sigma}, \boldsymbol{\delta}) ds = 0 \tag{5.38}$$

where $\tilde{\mathcal{L}}_1 = 0$ and $\tilde{\Phi}_0 = 0$, while $\tilde{\Phi}_1(\tilde{\boldsymbol{x}}(1|\boldsymbol{\sigma}, \boldsymbol{\delta})) = \|\tilde{\boldsymbol{x}}_2(\varsigma_{\bar{p}}) - \tilde{\boldsymbol{x}}_3(\varsigma_{\bar{p}})\|^2$, which is obtained from (5.36).

The original optimal control problem is now approximated by a sequence of optimal parameter selection problems depending on p, the number of the partition points of the time horizon $[0, T]$, given below.

Problem $\tilde{\mathrm{S}}_p$. *Given system (5.29a) with initial condition (5.29b) on the time interval $s \in [0,1]$, find a control parameter vector $\boldsymbol{\sigma} \in \Xi^p$ and a switching time vector $\boldsymbol{\delta} \in \mathcal{D}^p$, such that the cost function (5.30) is minimized subject to the constraints (5.35) and (5.38).*

For each p, Problem $\tilde{\mathrm{S}}_p$ can be solved as a nonlinear optimization problem, where the cost function (5.37) is minimized subject to constraints (5.35) and (5.38). Existing

gradient-based optimization methods (see, for example, [46]) can be used to solve Problem $\tilde{\mathrm{S}}_p$. For this, we need the gradient formulas of the cost function and the constraint functions given bellow.

Remark 5.1. The gradient formula of the constraint function $\tilde{\Phi}_2(\boldsymbol{\delta}) = \sum_{k=1}^{p} \delta_k - T$ (obtained from (5.35)) is:

$$\frac{\partial \tilde{\Phi}_2(\boldsymbol{\delta})}{\partial \boldsymbol{\delta}} = \underbrace{[1, \ldots, 1]}_{p}^T \tag{5.39}$$

For the gradient formulas of the cost function (5.37) and the constraint function (5.38), they are given in the following theorem.

Theorem 5.2. *For each $i = 0, 1$, the gradient of the function $\tilde{g}_i$ with respect to $\boldsymbol{\sigma}$ and $\boldsymbol{\delta}$ are given by*

$$\frac{\partial \tilde{g}_i(\boldsymbol{\sigma}, \boldsymbol{\delta})}{\partial \boldsymbol{\sigma}} = \int_0^1 \frac{\partial \tilde{H}_i(s, \tilde{\boldsymbol{x}}(s), \boldsymbol{\sigma}, \boldsymbol{\delta}, \tilde{\boldsymbol{\lambda}}^i(s|\boldsymbol{\sigma}, \boldsymbol{\delta}))}{\partial \boldsymbol{\sigma}} ds \tag{5.40}$$

and

$$\frac{\partial \tilde{g}_i(\boldsymbol{\sigma}, \boldsymbol{\delta})}{\partial \boldsymbol{\delta}} = \int_0^1 \frac{\partial \tilde{H}_i(s, \tilde{\boldsymbol{x}}(s), \boldsymbol{\sigma}, \boldsymbol{\delta}, \tilde{\boldsymbol{\lambda}}^i(s|\boldsymbol{\sigma}, \boldsymbol{\delta}))}{\partial \boldsymbol{\delta}} ds \tag{5.41}$$

where

$$\tilde{H}_i(s, \tilde{\boldsymbol{x}}, \boldsymbol{\sigma}, \boldsymbol{\delta}, \tilde{\boldsymbol{\lambda}}^i) = \tilde{\mathcal{L}}_i(s, \tilde{\boldsymbol{x}}, \boldsymbol{\sigma}, \boldsymbol{\delta}) + (\tilde{\boldsymbol{\lambda}}^i)^T \tilde{\boldsymbol{q}}(s, \tilde{\boldsymbol{x}}, \boldsymbol{\sigma}, \boldsymbol{\delta}) \tag{5.42}$$

and, for each $i = 0, 1$, $\tilde{\boldsymbol{\lambda}}^i(s|\boldsymbol{\sigma}, \boldsymbol{\delta})$ is the solution of the following costate system corresponding to $(\boldsymbol{\sigma}, \boldsymbol{\delta})$:

$$\frac{d\tilde{\boldsymbol{\lambda}}(s)}{ds} = -\left[\frac{\partial \tilde{H}_i(s, \tilde{\boldsymbol{x}}(s|\boldsymbol{\sigma}, \boldsymbol{\delta}), \boldsymbol{\sigma}, \boldsymbol{\delta}, \tilde{\boldsymbol{\lambda}}(s))}{\partial \tilde{\boldsymbol{x}}}\right]^T, \ s \in [0, 1) \tag{5.43}$$

with

$$\tilde{\boldsymbol{\lambda}}(1) = \left[\frac{\partial \tilde{\Phi}_i(\tilde{\boldsymbol{x}}(1|\boldsymbol{\sigma}, \boldsymbol{\delta}))}{\partial \tilde{\boldsymbol{x}}}\right]^T \tag{5.44}$$

Proof. The proof follows from arguments similar to that given for Theorem 2.1 of Chapter 2. Thus, it is omitted. □

For each p, Problem $\tilde{\mathrm{S}}_p$ is an optimal parameter selection problem, which can be viewed as a nonlinear optimization problem. Thus, any existing gradient-based optimization method, such as the sequential quadratic programming approximation algorithm, can be used to solve Problem $\tilde{\mathrm{S}}_p$. Here the optimal control software MISER 3.3, which was developed based on these ideas, is implemented to solve Problem $\tilde{\mathrm{S}}_p$.

Remark 5.2. Let $\tilde{\boldsymbol{u}}^{p,*}$ be the optimal piecewise constant control of Problem $\tilde{\mathrm{S}}_p$ given by

$$\tilde{\boldsymbol{u}}^{p,*}(s) = [(\tilde{\hat{\boldsymbol{u}}}^{p,*}(s))^T, \nu^{p,*}(s)]^T \tag{5.45}$$

with $\tilde{\hat{\boldsymbol{u}}}^{p,*}(s) = [(\tilde{\boldsymbol{u}}_1^{p,*}(s))^T, (\tilde{\boldsymbol{u}}_2^{p,*}(s))^T, (\tilde{\hat{\boldsymbol{u}}}_3^{p,*}(s))^T]^T$. In the original time horizon , we have

$$\hat{\boldsymbol{u}}^{p,*} = [(\boldsymbol{u}_1^{p,*})^T, (\boldsymbol{u}_2^{p,*})^T, (\hat{\boldsymbol{u}}_3^{p,*})^T]^T \tag{5.46}$$

Let $\hat{\boldsymbol{u}}^*$ be the optimal control of Problem $\hat{\mathrm{S}}$. As discussed in Section 2.5 of Chapter 2, $J(\hat{\boldsymbol{u}}^{p,*})$ will converge to $J(\hat{\boldsymbol{u}}^*)$ as $p \to \infty$. Furthermore, due to the time scaling control, the optimal switching points in Problem $\tilde{\mathrm{S}}_p$ will capture those in the original time horizon, such that $J(\tilde{\boldsymbol{u}}^{p,*}) \leq J(\hat{\boldsymbol{u}}^{p,*})$ which means that $J(\tilde{\boldsymbol{u}}^{p,*})$ converges to $J(\hat{\boldsymbol{u}}^*)$.

From our extensive simulation study, we observe that p does not need to be chosen to be too large. In fact, the difference in the cost values between $p = 20$ and those with larger p is, in general, insignificant. Thus, $p = 20$ is chosen in our numerical simulation study.

5.5 Two Spacecrafts During Their Formation Flight

Consider the angular velocity tracking and synchronization problem of two spacecrafts during their formation flight. The attitude dynamics of the two rigid axial symmetry spacecrafts can be expressed, in the body-fixed coordinate system, as follows.

$$\begin{aligned} &J_{xi}\dot{\omega}_{xi} + (J_{zi} - J_{yi})\omega_{zi}\omega_{yi} = M_{xi} \\ &J_{yi}\dot{\omega}_{yi} + (J_{xi} - J_{zi})\omega_{xi}\omega_{zi} = M_{yi}\,, \ i = 1, 2, \\ &J_{zi}\dot{\omega}_{zi} + (J_{yi} - J_{xi})\omega_{yi}\omega_{xi} = M_{zi} \end{aligned} \tag{5.47}$$

where ω_{xi}, ω_{yi} and ω_{zi}, $i = 1, 2$, are the roll, pitch and yaw rates, respectively. J_{xi}, J_{yi} and J_{zi}, $i = 1, 2$, represent the moments of inertia about the three axes of the body-fixed coordinate system. M_{xi}, M_{yi} and M_{zi}, $i = 1, 2$, are the applied moments.

The objective of the attitude angular velocity control mission is to design a control law such that the synchronization time of $(\omega_{y1}, \omega_{z1})$ and $(\omega_{y2}, \omega_{z2})$ is minimized, while the tracking of the angular velocities of the two spacecrafts (i.e., $(\omega_{x1}, \omega_{y1}, \omega_{z1})$ and $(\omega_{x2}, \omega_{y2}, \omega_{z2})$) with reference to a desired trajectory is as close as possible.

Let

$$\boldsymbol{x}(t) = [\boldsymbol{x}_1^T, \boldsymbol{x}_2^T, \boldsymbol{x}_3^T]^T \tag{5.48}$$

$$\boldsymbol{u}(t) = [\boldsymbol{u}_1^T, \boldsymbol{u}_2^T, \boldsymbol{u}_3^T]^T \tag{5.49}$$

where

$$\boldsymbol{x}_1(t) = [\omega_{x1}, \omega_{x2}]^T = [x_{1,1}(t), x_{1,2}(t)]^T,\ \boldsymbol{x}_2(t) = [\omega_{y1}, \omega_{z1}]^T = [x_{2,1}(t), x_{2,2}(t)]^T,$$

$$\boldsymbol{x}_3(t) = [\omega_{y2}, \omega_{z2}]^T = [x_{3,1}(t), x_{3,2}(t)]^T,$$

and

$$\boldsymbol{u}_1(t) = [M_{x1}, M_{x2}]^T = [u_{1,1}(t), u_{1,2}(t)]^T,\ \boldsymbol{u}_2(t) = [M_{y1}, M_{z1}]^T = [u_{2,1}(t), u_{2,2}(t)]^T,$$

$$\boldsymbol{u}_3(t) = [M_{y2}, M_{z2}]^T = [u_{3,1}(t), u_{3,2}(t)]^T.$$

Then, the original system dynamics (5.47) can be rewritten as:

$$\dot{\boldsymbol{x}}(t) = \boldsymbol{h}(\boldsymbol{x}(t)) + \boldsymbol{G}\boldsymbol{u}(t) \tag{5.50}$$

where

$$\boldsymbol{h}(\boldsymbol{x}(t)) = \begin{bmatrix} -(J_{z1} - J_{y1})x_{2,2}(t)x_{2,1}(t)/J_{x1} \\ -(J_{z2} - J_{y2})x_{3,2}(t)x_{3,1}(t)/J_{x2} \\ -(J_{x1} - J_{z1})x_{1,1}(t)x_{2,2}(t)/J_{y1} \\ -(J_{y1} - J_{x1})x_{2,1}(t)x_{1,1}(t)/J_{z1} \\ -(J_{x2} - J_{z2})x_{1,2}(t)x_{3,2}(t)/J_{y2} \\ -(J_{y2} - J_{x2})x_{3,1}(t)x_{1,2}(t)/J_{z2} \end{bmatrix} \tag{5.51}$$

and

$$\boldsymbol{G} = \mathrm{diag}(1/J_{x1}, 1/J_{x2}, 1/J_{y1}, 1/J_{z1}, 1/J_{y2}, 1/J_{z2}) \tag{5.52}$$

The initial condition for the state is:

$$\boldsymbol{x}(0) = [0, 0, -0.2, -0.5, -0.8, -1]^T(\mathrm{deg/sec}) \tag{5.53}$$

The system inertia parameters are $J_{x1} = J_{x2} = 350\mathrm{kgm}^2$, $J_{y1} = J_{y2} = 305\mathrm{kgm}^2$ and $J_{z1} = J_{z2} = 300\mathrm{kgm}^2$. The bounds on the control variables are:

$$-10\mathrm{Nm} \le u_{i,j}(t) \le 10\mathrm{Nm},\ \ i = 1, 2, 3;\ \ j = 1, 2. \tag{5.54}$$

The angular velocity command in the x-axis is $\boldsymbol{x}_{1r}(t) = [0, 0]^T(\mathrm{deg/sec})$. $\boldsymbol{x}_2$ and $\boldsymbol{x}_3$ are required to track the trajectory $\boldsymbol{x}_{2r}(t) = [\omega_{yr}(t), \omega_{zr}(t)]^T$ for $t \in [0, 10]$, where $\omega_{yr}(t) = 4.5\cos(0.05\pi t)(\mathrm{deg/sec})$ and $\omega_{zr}(t) = 4.5\cos(0.1\pi t)(\mathrm{deg/sec})$. Thus, the objective function of this problem can be formulated as

$$J(\boldsymbol{u}) = a_0\tau + \int_0^{10} \left\{a_1\|\boldsymbol{x}_1(t) - \boldsymbol{x}_{1r}(t)\|^2 + a_2\|\boldsymbol{x}_2(t) - \boldsymbol{x}_{2r}(t)\|^2 + a_3\|\boldsymbol{x}_3(t) - \boldsymbol{x}_{2r}(t)\|^2\right\}dt \tag{5.55}$$

where τ is the synchronization time of $\boldsymbol{x}_2$ and $\boldsymbol{x}_3$, which is also required to be minimized. The weighting coefficients are chosen as $a_0 = 1$, $a_i = 10^4$, $i = 1, 2, 3$.

We apply the switching synchronization control method, the control parameterization technique and the time scaling transform to solve this optimal synchronization control problem. The original time horizon $[0, 10]$ is mapped into a new time horizon $[0, 1]$ with

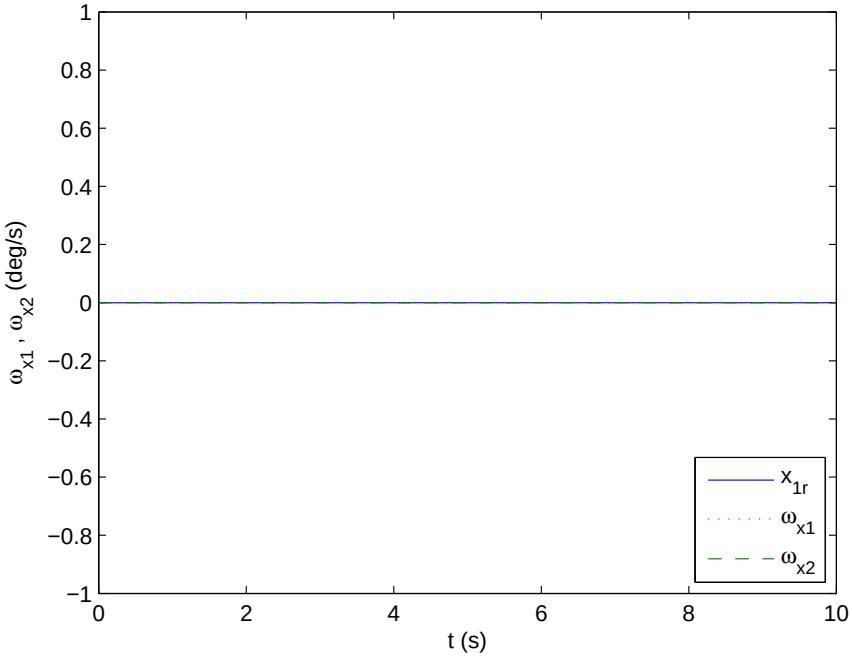

Figure 5.1: Angular velocities ω_{x1}, ω_{x2}.

20 partition points. We map the synchronization time, τ, to the first partition point. The cost function (5.55) is transformed into the form given below.

$$\begin{aligned}\tilde{J}(\tilde{\boldsymbol{u}}^p) = &\int_0^{0.05} \left\{a_0\nu^p + a_1\|\tilde{\boldsymbol{x}}_1 - \tilde{\boldsymbol{x}}_{1r}\|^2 + a_2\|\tilde{\boldsymbol{x}}_2 - \tilde{\boldsymbol{x}}_{2r}\|^2 + a_3\|\tilde{\boldsymbol{x}}_3 - \tilde{\boldsymbol{x}}_{2r}\|^2\right\} ds \\ &+ \int_{0.05}^1 \left\{a_1\|\tilde{\boldsymbol{x}}_1 - \tilde{\boldsymbol{x}}_{1r}\|^2 + a_2\|\tilde{\boldsymbol{x}}_2 - \tilde{\boldsymbol{x}}_{2r}\|^2\right\} ds.\end{aligned} \tag{5.56}$$

The cost function (5.56) is to be minimized subject to the control constraints (5.54) and the following constraints.

$$\tilde{x}_4(1) = 10 \tag{5.57}$$

$$\|\tilde{\boldsymbol{x}}_2(0.05) - \tilde{\boldsymbol{x}}_3(0.05)\|^2 = 0 \tag{5.58}$$

This optimal control problem is solved by using the method detailed in Section 5.4, where the optimal control software, MISER 3.3, is used. The time histories of the system states and controls, in the original time horizon $[0, 10]$, are shown in Figure 5.1 to Figure 5.6. From Figure 5.1 to Figure 5.3, we see that the roll rates of the two spacecrafts are maintained at zero for all the simulation time, the pitch and yaw rates of the two spacecrafts achieve a precise synchronization at $t = 0.1597$sec, and the command trajectory $\boldsymbol{x}_{2r}(t)$ is well tracked. Figure 5.4 to Figure 5.6 depict the time histories of the optimal control inputs. It is easy to see that all the controls operate within their bounds. The time scaling control is shown in Figure 5.7. The tracking and synchronization missions of the spacecraft angular velocities are well accomplished.

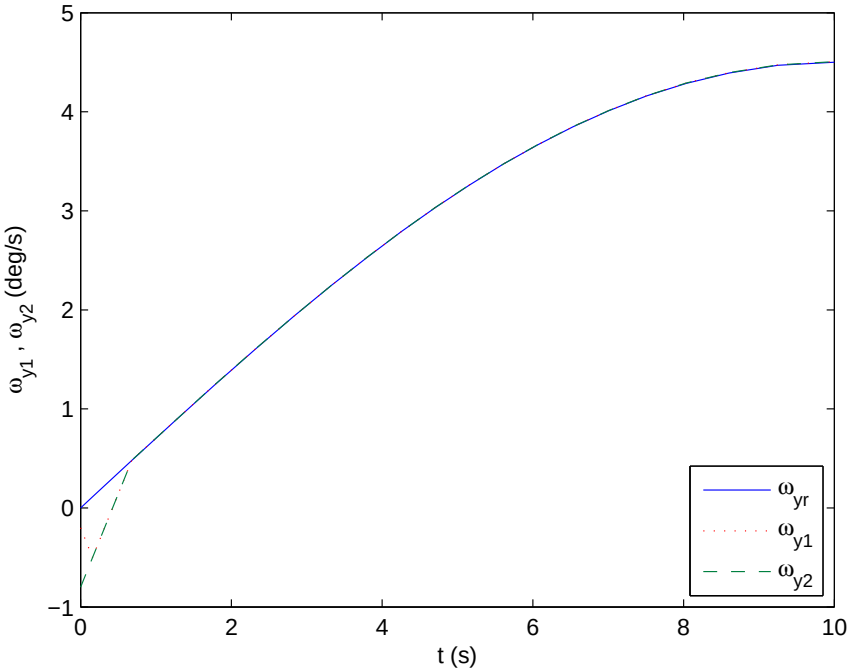

Figure 5.2: Angular velocities ω_{y1}, ω_{y2}.

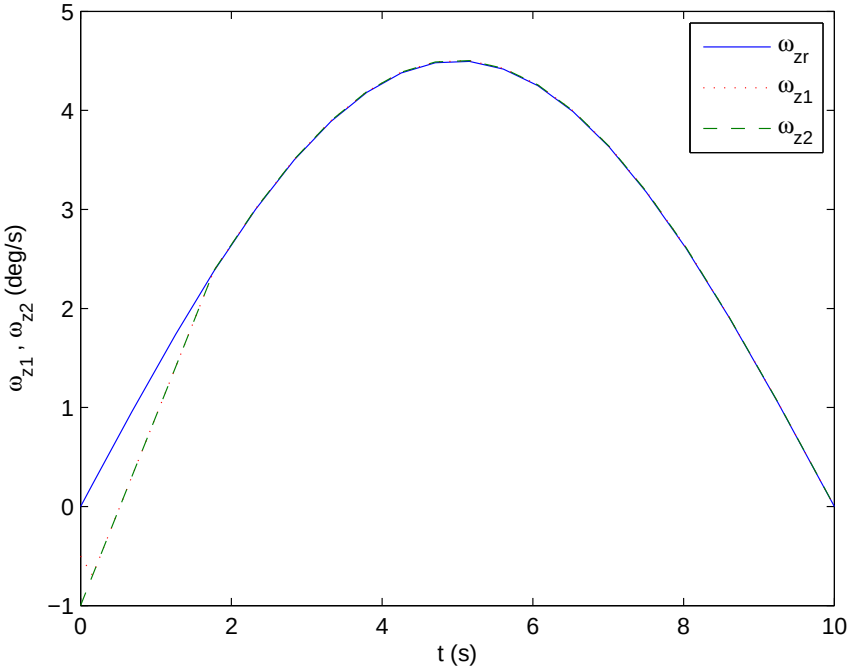

Figure 5.3: Angular velocities ω_{z1}, ω_{z2}.

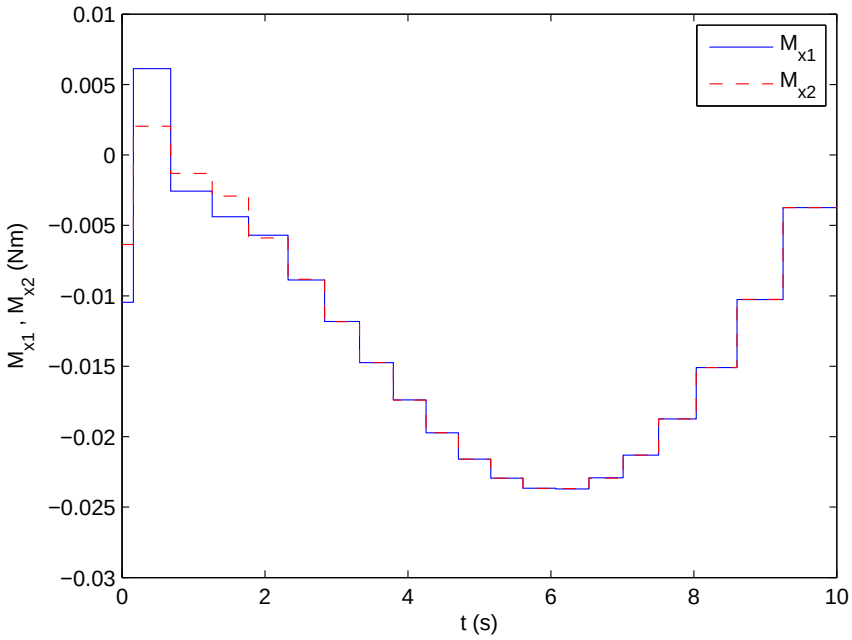

Figure 5.4: Applied moments M_{x1}, M_{x2}.

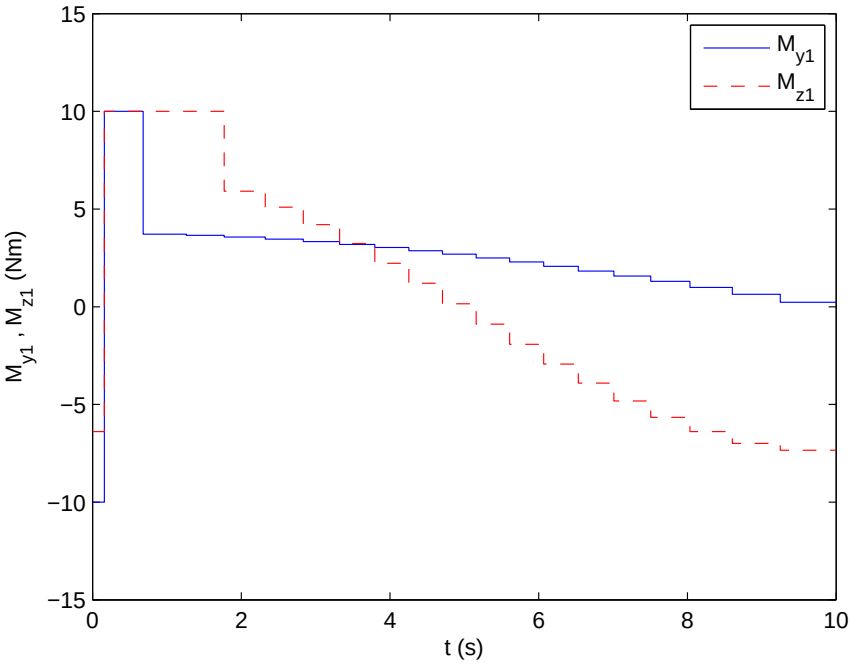

Figure 5.5: Applied moments M_{y1}, M_{z1}.

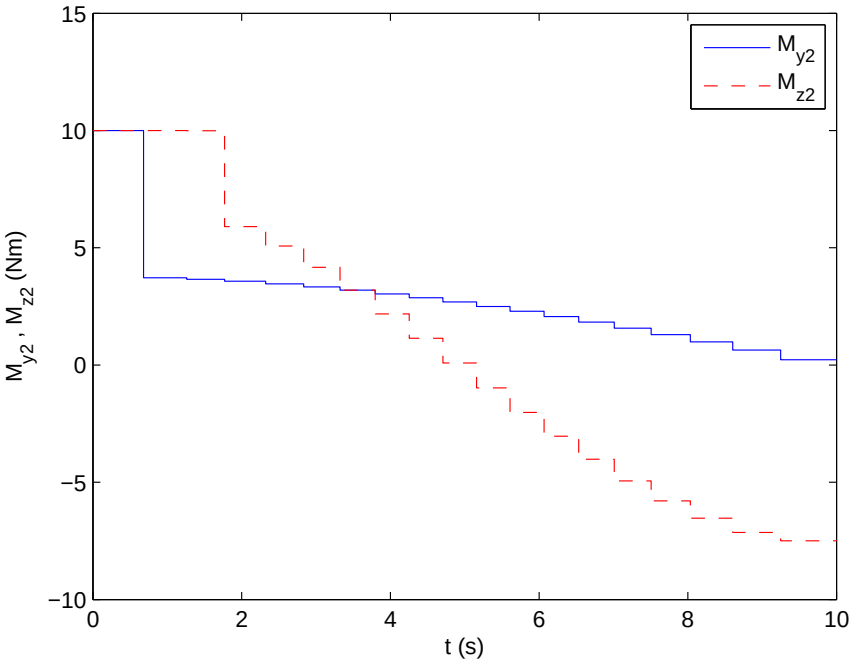

Figure 5.6: Applied moments M_{y2}, M_{z2}.

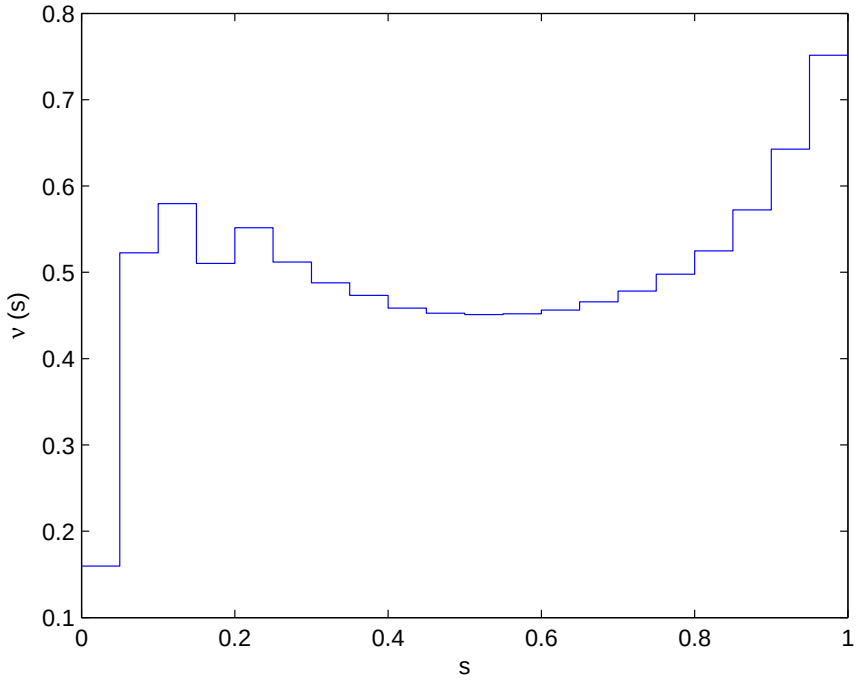

Figure 5.7: Time scaling control ν.

5.6 Conclusion

The tracking and synchronization control problem for a class of nonlinear systems subject to constraints on the controls was studied in this chapter. A new result for constructing a switching synchronization control was obtained. With this result, this nonlinear control problem was stated equivalently as an optimal control problem subject to constraints on the controls and an interior point state equality constraint. By applying the control parameterization technique and the time scaling transform, it was shown that the constrained optimal control problem can be solved as an optimal parameter selection problem. Numerical simulation shows that the proposed method is highly effective.

CHAPTER 6

Finial remarks

6.1 Main contributions of this thesis

In this thesis, we addressed several optimal guidance and control problems of the spacecrafts arising from the study of lunar exploration. We summarize our main contributions below.

In Chapter 2, by introducing three frames, we derived a three dimensional dynamics to describe the motion of the lunar module for the powered descent part with consideration of the moon rotation. The lunar module soft landing was treated as a continuously powered descent process with a constraint on the terminal angle of the module between its longitudinal axis and the moon surface. Then, an optimal guidance law was proposed to realize a precise pinpoint soft landing at the desired landing target. The terminal attitude of the module was restricted to be within a small deviation from being vertical with respect to lunar surface, which ensured the module to stand vertically when it touched down on the moon surface. The fuel consumption and the flight time were also minimized. The optimal guidance law was realized by using the control parameterization method in conjunction with a time scaling transform. By these two methods, the optimal control problem was approximated by a sequence of optimal parameter selection problems and solved by a general purpose optimal control software package, MISER 3.3. An optimal trajectory tracking problem, where a desired trajectory is to be tracked with the least fuel consumption in the minimum time, was also solved with the same approach.

In Chapter 3, we considered the lunar module soft landing problem under some unpredicted situations, such as initial point perturbations. As in Chapter 2, the three dimensional dynamics was utilized to describe the motion of the module. Based on the nonlinear dynamics of the module, we obtained the form of an optimal closed loop control law, where a feedback gain matrix is involved. The feedback gain matrix satisfies a Riccati-like matrix differential equation. Then, it was approximated in terms of the third order B-spline functions. We first solved the optimal control problem as an open loop optimal control problem by using the time scaling transform and the control parameterization method. Then, by virtue of the relationship between the optimal open loop

control and the optimal closed loop control along the optimal trajectory, we presented a practical method to calculate an approximate optimal feedback gain matrix, without having to solve an optimal control problem involving the complex Riccati-like matrix differential equation coupled with the original system dynamics. Simulation results showed that, when the initial point is perturbed, the performance of the feedback control law is much better than that of the open loop control law.

In Chapter 4, we discussed the attitude control problem of a spacecraft driven by DGCMGs system. We derived an exact general mathematical description of spacecraft attitude motion driven by DGCMGs. Based on the mathematical description, we designed a nonlinear feedback control law which can realize the spacecraft large angle attitude maneuver missions. The control law was constructed with the help of the second method of Lynpunov, and the system stability was proved during the design process. The singularity robustness plus null motion steering law was presented which could avoid the internal singularity status. We also proved the Principle of DGCMGs' singularity and analyzed the singular configurations of the orthogonally mounted three DGCMGs and the parallel mounted four DGCMGs. It is also shown that the proposed feedback control law and the SRNM steering law can work well even in the presence of DGCMG failure.

In Chapter 5, we considered a class of nonlinear optimal synchronization control problems subject to control constraints arising from the study of spacecraft formation flight. In this problem, the motions of two distinct objects are required to achieve synchronization at the minimum time while achieving the optimal tracking of a reference target. We provided a rigorous mathematical formulation for this class of optimal control problems and then obtained a new result ensuring the synchronization of the two distinct objects. By using the control parameterization method and a time scaling transform, we developed a computational method for constructing an optimal switching control law under which the motions of the two distinct objects will achieve synchronization at the minimum time while achieving the optimal tracking of a reference target. An angular velocity tracking and synchronization problem during the spacecraft formation flight was formulated and solved by the proposed method.

6.2 Future research directions

In this thesis, we studied the optimal guidance problem of the lunar module soft landing. The optimal descent trajectory was calculated. During the design process, we assumed that the attitude information of the landing module can be obtained directly where the design of the attitude actuators was not considered. In practice, to realize a fast and accurate attitude maneuver of the landing module which requires large output torques, we could use a united attitude control system consisting of the reverse force thrusters and the DGCMGs. The numbers and the configurations of the thrusters and the DGCMGs

should be optimally designed with consideration of the allowable mass allocation and the required system performance. The singularity problem is one of the most crucial problems among the CMG research area. Though the DGCMGs system has simpler singularity configuration compared with the SGCMGs system, it does encounter singularities in some situations. To avoid the singularity status, we shall design an optimal steering law by searching the directions along which the system singularity measure will be maximized. Thus, the CMGs system could be kept as far away as possible from the singularity status. The null motion method could also help the CMGs system to avoid the singularity status in many cases. There are numerous ways to choose the null motions. In this thesis, we used the preferred gimbal angle null motion approach. However, in this approach, a suitable computational method for choosing the preferred gimbal angles under various conditions has not been found yet. Hence, it would be very interesting to design an optimal steering law together with a suitable null motion to realize the maneuver of the CMGs system without encountering any singularities. We could also use the thruster system to help the CMGs to avoid internal singularity status and even withdraw from the external singularities. The study of the optimal attitude control system consisting of the thrusters and the CMGs would be very promising in future research.

Bibliography

[1] J. Ahmed, and D. S. Bernstein, "Adaptive control of double-gimbal control-moment gyro with unbalanced rotor," *AIAA Journal of Guidance, Control, and Dynamics*, vol. 25, no. 1, pp. 105–115, 2002.

[2] N. U. Ahmed, *Elements of finite-dimensional systems and control theory*. Essex: Longman Scientific and Technical, 1988.

[3] S. Arimoto, F. Miyazaki, and S. Kawamura, "Cooperative motion control of multiple robot arms or fingers," in *Proceedings of IEEE International Conference on Robotics and Automation*, Raleigh, pp. 1407–1412, 1987.

[4] G. Avanzini, and D. M. Guido, "A local optimization technique for attitude motion tracking using control moment gyroscopes," *The Journal of the Astronautical Sciences*, vol. 50, no. 2, pp. 213–229, 2002.

[5] N. S. Bedrossian, J. Paradiso, E. V. Bergmann, and D. Rowell, "Redundant single gimbal control moment gyroscope singularity analysis," *AIAA Journal of Guidence, Control, and Dynamics*, vil. 13, no. 6, pp. 1096–1101, 1990.

[6] N. S. Bedrossian, J. Paradiso, E. V. Bergmann, and D. Rowell, "Steering law design for redundant single-gimbal control moment gyroscopes," *AIAA Journal of Guidence, Control, and Dynamics*, vol. 13, no. 6, pp. 1083 1089, 1990.

[7] V. B. Bhatia, *Classical Mechanics: With introduction to Nonlinear Oscillations and Chaos*. Narosa Publishing House, 1997.

[8] P. A. Bliman, "Extension of Popov absolute stability criterion to non-autonomous systems with delays," *International Journal of Control*, vol.73, no. 15, pp. 1349–1361, 2000.

[9] S. Boyarski, and J. Z. Ben-Asher, "Minimum-time reorientation of a two-degree-of-freedom gyroscope," *AIAA Journal of Guidance, Control, and Dynamics*, vol. 18, no. 4, pp. 782–791, 1995.

[10] A. E. Bryson, and Y. C. Ho, *Applied Optimal Control*. London: Taylor and Francis, 1975.

[11] N. D. Christopher, "A optimal guidance law for planetary landing," *AIAA Guidance, Navigation, and Control Conference*, New Orleans LA, pp. 11–13, Aug. 1997.

[12] V. Costanza and P. S. Rivadeneira, "Finite-horizon dynamic optimization of nonlinear systems in real-time," *Automatica*, vol. 44, no. 9, pp. 2427–2434, 2008.

[13] J. Dzielski, D. Rowell, and D. Wormley, "Approach to control moment gyroscope steering using feedback linerization," *AIAA Journal of Guidance, Control, and Dynamics*, vol. 14, no. 1, pp. 96–106, 1991.

[14] R.W. Fang, and J.S. Chen, "A cross-coupling controller using an H_∞ scheme and its application to a two-axis direct-drive robot, *Journal of Robotic Systems*, vol.19, no.10, pp. 483–497, 2002.

[15] B. Farhadinia, K. L. Teo, and R. C. Loxton, "A computational method for a class of non-standard time optimal control problems involving multiple time horizons," *Mathematical and Computer Modelling*, vol. 49, no. 7-8, pp. 1682–1691, 2009.

[16] T. Furukawa, H. F. Durrant-Whyte, and G. Dissanayake, "Time-optimal cooperative control of multiple robot vehicles," in *Proceedings of the 2003 IEEE International Conference on Robotics and Automation*, September 2003.

[17] T. G. Gao, Z. Q. Chen, and Z. Z. Yuan, "Robust finite time synchronization of chaotic systems," *ACTA PHYSICA SINICA*, vol. 54, no. 6, pp. 2574–2579, 2005.

[18] B. Z. Guo and T. T. Wu, "Approximation of optimal feedback control: a dynamic programming approach," *Journal of Global Optimization*, vol. 46, no. 3, pp. 395–422, 2010.

[19] L. Hasdorff, *Gradient optimization and nonlinear control*. New York: John Wiley, 1976.

[20] S. R. Hebertt, "Soft landing on a planet: a trajectory planning approach for the liouvillian model," in *Proceedings of American Control Conference*, pp. 2936–2940, 1999.

[21] X. Y. Huang, D. Y. Wang, "Autonomous navigation and guidance for pinpoint lunar soft landing," in *Proceedings of IEEE International Conference on Robotics and Biomimetics*, Sanya, pp. 1148-1153, 2007.

[22] L. S. Jennings, M. E. Fisher, K. L. Teo, and C. J. Goh, *MISER3 Optimal control software: Theory and user manual*, The University of Western Australia, Perth, July 2004.

[23] L. S. Jennings and K. L. Teo, "A computational algorithm for functional inequality constrained optimization problems," *Automatica*, vol. 26, no. 2, pp. 371–375, 1990.

[24] Y. H. Jia, and S. J. Xu, "Spacecraft attitude control using parallel-gimbaled variable speed control moment gyrosgroup," *Journal of Astronautics*, vol. 24, no. 5, pp. 490–495, 2003.

[25] B. T. John, *Practical methods for optimal control using nonlinear programming*. Society for Industrial and Applied Mathematics, Philadelphia, 2001.

[26] T. Kamano, T. Suzuki, N. Iuchi, and M. Tomizuka, "Adaptive feedforward controller for synchronization of two axes positioning system," *Transactions of the Society of Instrument and Control Engineers*, vol. 29, no. 7, pp. 785–791, 1993.

[27] H. F. Kennel, "Steering law for parallel mounted double-gimbaled control moment gyros-revision A," *NASA TM-82390*, 1981.

[28] H. F. Kennel, "Individual angular momentum vector distribution and rotation laws for three double-gimbaled control moment gyros," *NASA TM X-53696*, 1968.

[29] H. Kenneth, M. Frode, and M. M. Edvall, User's guide for tomlab/scos, *(http://tomopt.com/tomlab/products/socs/)*, 2006.

[30] D. E. Kirk, *Optimal control theory: An introduction*. New York: Dover, 2004.

[31] Y. Koren, "Cross-coupled biaxial computer control for manufacturing systems," *Journal of Dynamic Systems, Measurement, and Control*, vol. 102, no. 4, pp. 265–272, 1980.

[32] S. Krishnant, and S. R. Vadali, "An inverse-free technique for attitude control of spacecraft using CMGs," *Acta Astronautica*, vol. 39, no. 6, pp. 431–438, 1996.

[33] V. Lappas, W. H. Steyn, and C. Underwood, "Design and testing of a control moment gyroscope cluster for small satellites," *AIAA Journal of Spacecraft and Rockets*, vol. 42, no. 4, pp. 729–739, 2005.

[34] H. C. Lee, and G. J. Jeon, "A neuro-controller for synchronization of two motion axes," *International Journal of Intelligent System*, vol. 13,no. 6, pp. 571–586, 1998.

[35] H. W. J. Lee, K. L. Teo, and L. S. Jennings, "On optimal control of multi-link vertical planar robot arms systems moving under the effect of gravity," *Journal of the Australian Mathematical Society—Series B*, vol. 39, no. 2, pp. 195–213, 1997.

[36] H. W. J. Lee, K. L. Teo, and W. Y. Yan, "Nonlinear optimal feedback control law for a class of nonlinear systems," *Neural, Parallel and Scientific Computations*, vol. 4, no. 2, pp. 157–178, 1996.

[37] K. Li, M.A. Mannan, M. Xu, and Z. Xiao, "Electro-hydraulic proportional control of twin-cylinder hydraulic elevators, *Control Engineering Practice*, vol.9, no.4, pp. 367–373, 2001.

[38] R. Li, Y. J. Shi, "A time-fuel optimal control problem of a cruise missile," *The Australian and New Zealand industrial and applied mahtematics journal*, vol. 51, no. 2, pp. 261–276, 2010.

[39] C. Liu, Z. Gong, E. Feng, and H. Yin, "Modelling and optimal control for nonlinear multistage dynamical system of microbial fed-batch culture," *Journal of Industrial and Management Optimization*, vol. 5, no. 4, pp. 835–850, 2009.

[40] H.T. Liu, and J. Shan, "Adaptive synchronized attitude angular velocity tracking control of multi-UAVs," in *Proceedings of American Control Conference*, Portland, pp. 128–133, 2005.

[41] H. T. Liu , and D. Sun, "Uniform synchronization in multi-axis motion control," in *Proceedings of American Control Conference*, Portland, pp. 4537–4542, 2005.

[42] P. Liu, "A new nonlinear optimal feedback control law," *Control Theory and Advanced Technology*, vol. 9, no. 4, pp. 947–954, 1993.

[43] T. C. Liu, W. B. Chubb, S. M. Seltzer, and Z. Thompson, "Optimal control of a variable spin speed CMG system for space vehicles," in *IEEE Conference on Decision and Control including the 12th Symposium on Adaptive Processes*, San Diego, 1973, pp. 722–726.

[44] X. L. Liu, G. R. Duan, K. L. Teo, "Optimal soft landing control for moon lander," *Automatica*, vol. 44, no. 4, pp. 1097-1103, 2008.

[45] R. C. Loxton, K. L. Teo, and V. Rehbock, "Computational method for a class of switched system optimal control problems," *IEEE Transactions on Automatic Control*, vol. 54, no. 10, pp. 2455–2460, 2009.

[46] D.G. Luenberger, "The gradient projection method along geodesics," *Management Science*, vol. 18, no. 11, pp. 620–631, 1972.

[47] K. M. Ma, L. J. Chen, and Z. C. Wang, "Practical design of control law for flight vehicle soft landing," *Missiles and Space Vehicles*, no. 2, pp. 39–43, 2001.

[48] G. Margulies, J. N. Aubrun, "Geometric theory of single-gimbal control moment gyro systems," *The Journal of the Astronautical Sciences*, XXVI, no. 2, pp. 159 191, 1978.

[49] R. B. Martin, "Optimal control drug scheduling of cancer chemotherapy," *Automatica*, vol. 28, no. 6, pp. 1113–1123, 1992.

[50] S. J. Meditch, "On the problem of optimal thrust programming for a lunar soft landing," *IEEE Transaction on Automatic Control*, vol.9, no. 4, pp. 477–484, 1964.

[51] F. Miyazaki, S. Matsubayashi, T. Yoshimi, and S. Arimoto, "A new control methodology toward advanced teleoperation of master-slave robot systems," in *Proceedings of IEEE International Conference on Robotics and Automation*, pp. 997–1002, 1986.

[52] P. Moore, and C. M. Chen, "Fuzzy logic coupling and synchronised control of multiple independent servo-drives," *Control Engineering Practice*, vol. 3, no. 12, pp. 1697–1708, 1995.

[53] A. Muise , and R. J. Bauer, "A comparison of the effectiveness of double and single gimbaled control moment gyroscopes for vibration suppression," *Transactions of the Canadian Society for Mechanical Engineering*, vol. 29, no. 3, pp. 389–402, 2005.

[54] M. Namvar, and F. Aghili, "Adaptive force-motion control of coordinated robots interacting with geometrically unknown environments," *IEEE Transactions on Robotics*, vol. 21, no. 4, pp. 678–694, 2005.

[55] H. S. Oh, and S. R. Vadali, "Feedback control and steering laws for spacecraft using single gimbal control moment gyros," *Journal of the Astronautical Sciences*, vol. 39, no. 2, pp. 183–203, 1991.

[56] J. A. Paradiso, "Global steering of single gimballed control moment gyroscopes using a directed search," *AIAA Journal of Guidance, Control, and Dynamics*, vol. 15, no. 5, pp. 1236–1244, 1992.

[57] S. A. Raymond, J. W. Jewett, *Physics for Scientists and Engineers*. Brooks/Cole., 2004.

[58] V. Rehbock and I. Livk, "Optimal control of a batch crystallization process," *Journal of Industrial and Management Optimization*, vol. 3, no. 3, pp. 585–596, 2007.

[59] S. Richardson, S. Wang, L. S. Jennings, "A multivariate adaptive regression B-spline algorithm (BMARS) for solving a class of nonlinear optimal feedback control problems," *Automatica*, no. 44, pp. 1149–1155, 2008.

[60] D. J. Richie, P. Tsiotras, and J. L. Fausz, "Simultaneous attitude control and energy storage using VSCMGs: theory and simulation," in *Proceedings of the American Control Conference*, Arlington, pp. 3973–3979, 2001.

[61] A. A. Rodriguez, and H. Nijmeijer, "Mutual synchronization of robots via estimated state feedback: a cooperative approach," *IEEE Transactions on Control Systems Technology*, vol. 12, no. 4, pp. 542–554, 2004.

[62] C. M. Roithmayr, "International space station attitude motion associated with flywheel energy storage," *Space Technology and Application*, vol. 504, pp. 454–459, 2000.

[63] M. Romano, and B. N. Agrawal, "Attitude dynamics/control of dual-body spacecraft with variable-speed control moment gyros," *AIAA Journal of Guidance,Control,and Dynamics*, vol. 27, no. 4, pp. 513–525, 2004.

[64] X. G. Ruan, "A nonlinear nuerocontrol scheme for lunar soft landing," *Journal of Astronautics*, vol. 19, no. 1, pp. 35–43, 1998.

[65] H. Schaub, and J. L. Junkins, "Singularity avoidance using null motion and variable-speed control moment gyros," *Journal of Guidance, Control, and Dynamics*, vol. 23, no. 1, pp., 11–16, 2000.

[66] H. Schaub, S. R. Vadali, and J. L. Junkins, "Feedback control law for variable speed control moment gyros," *The Journal of the Astronautical Sciences*, vol. 46, no. 3, pp. 307–328, 1998.

[67] J. Shan, H. T. Liu, and S. Nowotny, "Synchronised trajectory-tracking control of multiple 3-DOF experimental helicopters, *IEE Proc.-Control Theory Appl.*, vol. 152, no. 6, pp. 683–692, 2005.

[68] K. Srinivasan, and P. K. Kulkarni, "Cross-coupled control of biaxial feed drive servomechanisms," *Journal of Dynamic Systems, Measurement, and Control*, vol. 112, no. 2, pp. 225–232, 1990.

[69] D. Sun, "Adaptive coupling control of two working operations in CNC integrated machines," *Journal of Dynamic Systems, Measurement, and Control*, vol.125, no.4, pp. 662–665, 2003.

[70] D. Sun, "Position synchronization of multiple motion axes with adaptive coupling control," *Automatica*, vol. 39, no. 6, pp. 997–1005, 2003.

[71] D. Sun, and J. Mills, "Adaptive synchronized control for coordination of multirobot assembly tasks," *IEEE Transactions on Robotics and Automation*, vol. 18, no. 4, pp. 498–510, 2002.

[72] H. Sun, and G. T. C. Chiu, "Motion synchronization for dual-cylinder electrohydraulic lift systems," *IEEE/ASME Transactions on Mechatronics*, vol. 7, no. 2, pp. 171-181, 2002.

[73] J. M. Tao, J. Y. S. Luh, and Y. F. Zheng, "Compliant coordination control of two moving industrial robots," *IEEE Transactions on Robotics and Automation*, vol.6, no.3, pp. 322–330, 1990.

[74] K. L. Teo, C. J. Goh, and K. H. Wong, *A Unified Computational Approach to Optimal Control Problems*. New York: Longman Scientific and Technical, 1991.

[75] K. L. Teo, L. S. Jennings, H. W. J. Lee, and V. Rehbock, "The control parameterization enhancing transform for constraint optimal control problems," *J. Austral. Math. Soc. Ser. B*, no. 40, pp. 314–335, 1999.

[76] M. Tomizuka, J. S. Hu, T. C. Chiu, and T. Kamano, "Synchronization of two motion control axes under adaptive feedforward control," *Journal of Dynamic Systems, Measurement, and Control*, vol. 114, no. 2, pp. 197–203, 1992.

[77] J. G. Tsao, L. T. Sheu, and L. F. Yang, "Adaptive synchronization control of the magnetically suspended rotor," *System, Dynamics and Control*, vol. 10, no. 2, pp. 239–253, 2000.

[78] Y. Tsuneo, "A steering law for three double-gimbal control moment gyro systems," *NASA TM X-64926*, 1975.

[79] D. G. Tuckness, "Future lunar landing navigation schemes, with emphasis on precision landings," *Journal of the Institute of Navigation*, vol. 41, no. 2, pp. 215–228, 1994.

[80] S. R. Vadali, S. Krishnan, "Suboptimal command generation for control moment gyroscopes and feedback control of spacecrat," *AIAA Journal of Guidence, Control, and Dynamics*, vol. 18, no. 6, pp. 1350–1354, 1995.

[81] S. R. Vadali, H. S. Oh, and S. R. Walker, "Preferred gimbal angles for single gimbal control moment gyros," *AIAA Journal of Guidance, Control, and Dynamics*, vol. 13, no. 6, pp. 1090–1095, 1990.

[82] D. Y. Wang, T. S. Li, and X. R. Ma, "Numerical solution of TPBVP in optimal lunar soft landing," *Aerospace Control*, no. 3, pp. 44–49, 2000.

[83] D. Y. Wang, T. S. Li, H. Yan, and X. R. Ma, "A suboptimal fuel guidance law for lunar soft landing," *Journal of Astronautics*, no. 21, pp. 55–63, 2000.

[84] D. Y. Wang, T. S. Li, H. Yan, and X. R. Ma, "Neuro-optimal guidance control for lunar module soft landing," *Journal of Systems Engineering and Electronics*, vol. 10, no. 3, pp. 22–31, 1999.

[85] L. Y. Wang, W. H. Gui, K. L. Teo, R. C. Loxton and C. H. Yang, "Timedelayed optimal control problems with multiple characteristic time points," *Computation and Industrial Applications*, vol. 5, no. 4, pp. 705–718, 2009.

[86] S. Wang, F. Gao, and K. L. Teo, "An upwind finite-difference method for the approximation of viscosity solutions to Hamilton-Jacobi-Bellman equations," *IMA Journal of Mathematical Control and Information*, vol. 17, no. 2, pp. 167–178, 2000.

[87] S. Wang, L. S. Jennings, and K. L. Teo, "Numerical solution of Hamilton-Jacobi-Bellman equations by an upwind finite volume method," *Journal of Global Optimization*, vol. 27, no. 2-3, pp. 177–192, 2003.

[88] X. Y. Wang, and M. Liu, "Sliding mode control for the synchronization of master-slave chaotic systems with sector nonlinear input," *ACTA PHYSICA SINICA*, vol. 54, no. 6, pp. 2584–2589, 2005.

[89] Z. Wang, J. F. Li, N. G. Cui, and T. Liu, "Genetic algorithm optimization of lunar probe soft landing trajectories," *Journal of Tsinghua University (Science and Technology)*, vol. 43, no. 8, pp. 1056–1059, 2003.

[90] J. Wei, J. P. Yuan, "New algorithm to attitude control for the space station," *Flight Dynamics*, vol. 18, no. 2, pp. 67–69, 2000.

[91] Z. Wu, "Dynamic steering law design for redundant single gimbal control moment gyroscopes," *Journal of Astronautics*, vol. 26, no. 1, pp. 24–28, 2005.

[92] Z. Wu, and W. S. Chou, "Steering law design for SGCMGs taking gimbal servo characteristics into account," *Journal of Beijing University of Aeronautics and Astronautics*, vol. 30, no. 6, pp. 489–492, 2004.

[93] Z. Wu, and H. X. Wu, "Configuration analysis of single gimbal control moment gyroscope systems," *Aerospace Control*, no. 1, pp. 19–27, 1998.

[94] X. N. Xi, G. Q. Zeng, X. Ren, and H. Y. Zhao, *Orbit design of lunar probe*. Changsha: National Defence Industry Press, 2001.

[95] M. Xu, and J. F. Li, "Optimal control of lunar soft landing," *Journal of Tsinghua University (Science and Technology)*, vol. 41, no. 8, pp. 87–89, 2001.

[96] L. F. Yang, and W. H. Chang, "Synchronization of twin-gyro precession under cross-coupled adaptive feedforward control," *AIAA Journal of Guidance, Control, and Dynamics*, vol.19, no.3, pp. 534–539, 1996.

[97] X. Q. Yang, K. L. Teo, and L. Caccetta, *Optimization methods and applications*. Netherlands: Kluwer Academic, 2001.

[98] H. T. Yau, J. S. Lin, and J. J. Yan, "Synchronization control for a class of chaotic systems with uncertainties," *International Journal of Bifurcation and Chaos*, vol. 15, no. 7, pp. 2235–2246, 2005.

[99] H. Yoon, and P. Tsiotras, "Spacecraft adaptive attitude and power tracking with variable speed control moment gyroscopes," *AIAA Journal of Guidance,Control, and Dynamics*, vol. 25, no. 6, pp. 1081–1090, 2002.

[100] J. J. Zhang, "Research on configuration analysis and comparison of SGCMG system," *Chinese Space Science and Technology*, no. 523, pp. 52–56, 2003.

[101] J. J. Zhang, J. S. Li, "Study on Steering Law of Large Spacecraft SGCMG System Based on Fuzzy Decision," *Chinese Journal of Aeronautics*, vol. 14, no. 2, pp. 100–105, 2001.

[102] D. Zhou, "H_∞ synchronization control of linear systems and its application to wafer-retical stage," *Chinese Journal of Mechanical Engineering*, vol. 18, no. 2, pp. 174-178, 2005.

[103] D. Zhou, J. Y. Zhou, "Nonlinear adaptive slewing motion control of spacecraft truss driven by synchronous V-gimbaled CMG precession," *Chinese Journal of Aeronautics*, vol. 20, no. 4, pp. 332–338, 2007.

[104] J. Y. Zhou, and D. Zhou, "Precise modeling and optimal orbit design of lunar modules soft landing," *Journal of Astronautics*, vol. 28, no. 6, pp. 1462–1466, 2007.

[105] W. H. Zhu, "On adaptive synchronization control of coordinated multirobots with flexible/rigid constraints," *IEEE Transactions on Robotics*, vol. 21, no. 3, pp. 520–525, 2005.